Mapping Crop Types in Smallholder Farming Areas using SAR Imagery with Dynamic Time Warping

GETACHEW WORKINEH GELLA

JUNE, 2020

SUPERVISORS:

Dr. ir. W. Bijker
Dr. M. Belgiu

Mapping Crop Types in Smallholder Farming Areas using SAR Imagery with Dynamic Time Warping

GETACHEW WORKINEH GELLA

Enschede, The Netherlands, June, 2020

Thesis submitted to the Faculty of Geo-Information Science and Earth Observation of the University of Twente in partial fulfilment of the requirements for the degree of Master of Science in Geo-information Science and Earth Observation.
Specialization: Geoinformatics

SUPERVISORS:
Dr. ir. W. Bijker
Dr. M. Belgiu

THESIS ASSESSMENT BOARD:
Prof. dr. ir. A. Stein (Chair)
Dr. M. Li (External Examiner, Fuzhou University, China)

ABSTRACT

Crop type related information is very essential for various planning and decision support activities in everyday life especially for early forecast and monitoring of food production. Though smallholder farming areas are profound food producers, mapping crop types is mainly constrained by their inherent characteristics like fragmentation (small farm size), rugged terrain, and presence of thick clouds in the growing season. More importantly, crops mixed dominance of the landscape coupled with fragmented holdings, crops behave different phenological characteristics which mostly constrains conventional mapping techniques for crop type mapping. Therefore, the main objective of this study was mapping crop types using all-weather time-series Synthetic Aperture Radar (SAR) with time-weighted Dynamic Time Warping that accounts for phenological development of crops. The study has used Sentinel-1 dual polarimetry (VV, VH) and TerraSAR-X single polarimetry (HH) images. Basic Registration of Crop Plots (BRP) dataset was used as a reference for training and validation. Obtained imagery was passed through a series of pre-processing operations. As Sentinel-1 imagery has dual polarimetry bands, derived features (Ratio, Modified Radar Vegetation Index, and Dual Polarimetric Soil Vegetation Index) were computed. Additionally, polarimetric decomposition was also undertaken. Within stated broader objective, a detailed analysis was done to know crop-specific responses for incident radar signal, to understand the capability of Time-Weighted Dynamic Time Warping for crop type mapping, implications of using either only backscatter bands and inclusion of derived features and decomposed polarimetric features on mapping accuracy of crops. In addition to these, under broader dynamic time warping, two further model improvement strategies (Variable Time Weight Dynamic Time Warping and Angular Metric for Shape Similarity) were also tested for performance. More importantly, the study has investigated an ensemble classifier that integrates TerraSAR-X and Sentinel-1 classification outputs for synergistic use of both sensing systems for crop type mapping. From these analyses, the study has come up with promising findings that show potentials of SAR imagery with time-weighted Dynamic Time Warping for crop type mapping. It has also clearly demonstrated predictive capabilities of either using dual polarimetry or single polarimetry SAR datasets for mapping crops in smallholder farming areas. Finally, by considering achieved outputs and existing caveats on this study, to refine the findings, further works were also recommended.

Keywords/Phrases: Classification, Crop type, Dynamic Time Warping, SAR, Mapping, Smallholder areas

ACKNOWLEDGMENTS

I want to thank entities who have contributed a lot to the realization of this work. My first heartfelt gratitude goes for my thesis supervisors Dr. ir. Wietske Bijker and Dr. Mariana Belgiu. Starting from the conception of the research problem to completion of this study, they have provided unreserved support, follow-up with encouragement, provision of insightful ideas, and constructive inputs. For me, the lessons I learned during times of regular discussion and through the overall research process were an enriching academic experience. I want to thank the Orange Knowledge Program (OKP) for offering me the fellowship that covers overall costs related to the study and my stay in the Netherlands. I also want to thank the Faculty of Geo-information Science and Earth Observation Science (ITC) Department of Earth Observation Science (EOS) for providing a high-performance computing facility of which all resource-demanding computational works has been done. I want to acknowledge the European Space Agency (ESA) for the provision of Sentinel-1 imagery and open-source SNAP software free of cost. Similar to ESA, my appreciation goes to Airbus Defense GmBH (DLR) for providing TerraSAR-X image as part of the ESA third party mission data access policy. Finally, I want to thank my friend Samson for his unreserved support and encouragement.

TABLE OF CONTENTS

LIST OF ACRONYMS AND ABBREVIATIONS

AAN	Agricultural Area of the Netherlands
ANN	Artificial Neural Network
AMSS	Angular Metric for Shape Similarity
ASAR	Advanced Synthetic Aperture Radar
CNN	Convolutional Neural Network
DDTW	Derivative Dynamic Time Warping
DEM	Digital Elevation Model
DLR	German Aerospace Centre
DPSVI	Dual Polarization SAR Vegetation Index
DTW	Dynamic Time Warping
ESA	European Space Agency
GEE	Google Earth Engine
GPT	Graph Processing Tool
GRD	Ground Range Detected
HH	Horizontally transmitted Horizontally transmitted Polarimetry
KNMI	Royal Netherlands Meteorological Institute
LAI	Leaf Area Index
MRVI	Modified Radar Vegetation Index
NDVI	Normalized Difference Vegetation Index
PA	Producers Accuracy
PDOK	Public Services On the Map
POF	Precise Orbit File
PSP	Phenological Sequence Patterns
SAR	Synthetic Aperture Radar
SITS	Satellite Image Time Series
SLC	Slant Range Single Look Complex
SNAP	Sentinel Application Facility
SRTM	Surface Radar Topographic Mission
SVM	Support Vector Machine
TOPS	Terrain Observation and Progressive Scan
twDTW	time-weighted Dynamic Time Warping
UA	Users Accuracy
USGS	United States Geological Survey
VH	Vertically Transmitted Horizontally received Polarimetry
vtwDTW	Variable Time Weight Dynamic Time Warping
VV	Vertically transmitted Vertically received Polarimetry

LIST OF FIGURES

LIST OF TABLES

1. Introduction

1.1. Justification for Research

Crop type related information is very important for many applications. Annual information concerning cropland and crop type can be used for decision making in areas like food production and security (Sweeney, Ruseva, Estes, & Evans, 2015; Samberg, Gerber, Ramankutty, Herrero, & West, 2016), characterization of cropping intensity (Jain, Mondal, DeFries, Small, & Galford, 2013), soil and water resources research especially erosion modeling (Panagos et al., 2015) and generation of cost-effective information about agricultural production (Tsiligirides, 1998; Carfagna & Gallego, 2005). From regional planning and farm management perspective, this information can be utilized to understand existing crop rotation patterns and to thought respective recommendations for appropriate cropping patterns. More importantly, from an economic point of view, it can serve as input to study farmers cropping preferences with existing agricultural markets, policy, and institutional arrangements. Not only for understanding crop preference, but also crop type acreage information from satellite imagery was used for the estimation of agricultural loss and respective insurance pay-outs for crop damage (ESA, 2017).

Presence of applications areas highly demand crop type information and proliferation of high spatio-temporal satellite imagery, there is a big tendency of mapping specific crops from earth observation imagery. Previous research works have utilized different classification and clustering approaches in a vast majority of optical datasets (Inglada et al., 2015; Belgiu & Csillik, 2018), radar imagery (Kenduiywo, Bargiel, & Soergel, 2016; Bargiel, 2017) and sometimes with a blend of radar and optical data (Kussul et al., 2016; Lussem, Hütt, & Waldhoff, 2016; Santos et al., 2019). From its inherent seasonality and heterogenous phenological cycle, crop type mapping demands time-series image analysis. Taking this into consideration, some studies have tried to map crop types by generating phenological matrices (Zhang et al., 2018), integration of time series spectral data with fuzzy c-means clustering (Heupel, Spengler, & Itzerott, 2018), radar-based Phenological Sequence Patterns (PSP) (Bargiel, 2017). In the recent past, Maus et al. (2016) have utilized time-weighted Dynamic Time Warping (twDTW) for land cover classification to account for the seasonality of landscape features. In a more specific way, Belgiu & Csillik (2018) have investigated the potentials of integrating twDTW with object-based image analysis to map crop types. Though the findings of these studies are promising, still it is not concluded that adopted methods can robustly predict crop types at different landscapes specifically in smallholder farming areas. Mostly, these studies were carried out in geographic regions where individual plot sizes were large or the landscape is uniformly cultivated with one dominant crop type like rice farms which are mostly uncommon in smallholder farming systems. Beyond small plot sizes, smallholder fragmented holdings were predominant in complex terrain. This creates similar cover types to have significantly different spectral characteristics (Lu & Weng, 2007), and backscatter responses for radar imagery (van Zyl, 1993).

There is some progress in mapping the cropland extent (Oliphant et al., 2019; Useya, Chen, & Murefu, 2019). Although previous studies on cropland extent were encouraging, the result of crop type mapping at a well-known smallholder dominated landscape using single date optical imagery sensed in the summer season is reported unsatisfactory (Delrue et al., 2013). A more practical challenge for the utilization of satellite-based high-resolution optical imagery for phenology based crop classification is the prevalence of thick cloud cover. This limits the probability of getting cloud-free frequent observations at each phenological development phases of crops. For example, a study done in the Netherlands has stated that for a satellite with daily observation frequency, the probability of getting cloud-free optical images is only 20% of days in a year (van der Wal et al., 2013). Accurate mapping of crop types in smallholder farming areas demands an account of the phenological development of each crop type within a growing season. For this purpose, all-weather earth observation datasets from radar sensors can provide frequent observations of crop development in the growing season. In addition to these, in spatially mixed cropping system (landscape level) which is more predominant in smallholder farming areas, even similar crops have different phenology resulting from differences in planting date. Under this circumstance, a specific crop at different plots can have different spectral or scattering characteristics based on its phenological development stage. This creates a challenge to classify crop types using single date imagery (Van Niel & McVicar, 2004). Even if it is possible to incorporate multi-temporal imagery across the growing season as a stack of time series, many classification models, fail to account though it is possible to incorporate multi-temporal imagery across the growing season as a stack of time series, they fail to account for phase changes in the time domain (that means shuffling the temporal order of the images does not have any implications on classification accuracy). In the signal processing community, Dynamic Time Warping (DTW) is reported capable of handling this problem. By using an improved version of this model, Belgiu & Csillik (2018) and Csillik, Belgiu, Asner, & Kelly (2019) have classified crop types from optical imagery. Similarly, Li & Bijker (2019) have also classified short cycle vegetables from SAR imagery. Based on these studies, the current study has tried to identify two major issues that need further investigation. The first is on mechanisms of how the difference in planting dates (time lag) of each crop is accounted for in the computation of linear or logistic weight. Secondly, as previous studies were mainly focused on similarity measure based on euclidean distance, other distances like angular distance measures should also be investigated as an alternative approach. Thirdly, the performance of radar images with different spatial resolution and polarization is also an attribute that has received less attention in crop type mapping.

1.2. Research Objectives

2.1.1. General Objective

Based on the justifications provided above, the general objective of the study was mapping crop types in smallholder farming systems using time series Sentinel-1 C-SAR and TerraSAR-X SAR imagery, phenological information, and twDTW classification model.

2.1.2. Specific Objectives

The study was undertaken:

- To investigate radar backscatter responses of dominant crop types in smallholder farming areas
- To map crop types using time-weighted Dynamic Time Warping in smallholder farming areas
- To investigate the impacts of integrating backscatter coefficient with radar vegetation indices and decomposed features on classification performance
- To investigate the implications of accounting for planting date difference on classification performance
- To assess the performance of different distance measures for assessing similarity between crop samples and unlabelled areas.
- To investigate the performance of integrating Sentinel-1 and TerraSAR-X time-series images for crop type mapping in smallholder farming areas

1.3. Research Questions

The study has tried to answer the following research questions.

- What is the backscatter response of different crops across the growing season?
- Can twDTW achieve good results for crop type mapping from time-series SAR images in smallholder farming areas?
- Does adding radar vegetation indices and decomposed polarimetric features improve crop type mapping accuracy?
- Does the incorporation of crop development temporal lag (planting date difference) improve the accuracy of crop type classification?
- Do different distance measures have implications on the accuracy of crop type retrieval?
- Does the integration of Sentinel-1 and TerraSAR-X contribute to the improvement of crop types mapping in smallholder farming areas?

1.4. Scientific Significance

Mapping crops in smallholder farming areas where each plot is planted with different crops that have different phenology and growing period (duration in the field), requires a method that accounts for backscatter or reflectance changes across the growing period. In this aspect, this study has contributed its part by demonstrating potentials of twDTW with Sentinel-1 and TerraSAR-X multitemporal SAR imagery for crop type mapping in smallholder farming areas. Pioneer studies done on the optical time series have tried to use euclidean distance for measuring shape similarity between two temporal sequences. The current study has investigated the performances of other distance measures, which are based on angular or vector distance. Besides, as crops have different phenological phases mainly regulated by their start of the growing season the study has used variable time lags for each crop which is methodically different from its predecessor studies. Furthermore, it has important clues on Sentinel-1 and TerraSAR-X SAR product performance for accurate crop type mapping. Besides the individual performance of TerraSAR-X and Sentinel-1, this study has also investigated the performance of feature-based fusion of results from both image time series using a rule-based ensemble approach. This is mainly a way for synergetic use of medium spatial resolution, dual polarimetry, and frequently observed Sentinel-1 with single polarimetry, high spatial resolution TeraSAR-X time series. From a usability perspective of the methodology proposed in this study could be tested in other study sites and upscaled at the sub-national or national level. Furthermore, it can be operationalized in government offices for updating production statistics, early cultivated area assessment, and forecast of forthcoming food security scenarios.

1.5. Organization of the Report

The overall thesis was organized into six chapters. The introductory part of the report was provided in the preceding chapter. A detailed literature review related to the study was compiled in the second chapter. The methodological construct of the study was provided in the third chapter. Analysis results were presented in the fourth chapter. In chapter five results were discussed with existing scientific work. In chapter six, concluding remarks and some issues that need further investigation were pointed out. In addition to these main sections, the thesis has preliminary sections (acknowledgment, abstract and list of figures and tables), a list of references, and supplementary information with appendices.

2. Related Work

2.1. Dynamic Time Warping: The Concept

Dynamic Time Warping (DTW) is a model that has been studied for a long time for pattern matching in the signal processing and data mining community (Sakoe & Chiba, 1978). It is used to compute the similarity between two sequences using a DTW distance approach. Suppose a database sequence S with length m and a query sequence Q with length n:

$$S = s_1, s_2, s_3, \dots s_m \tag{1}$$
$$Q = q_1, q_2, q_3, \dots q_n$$

To align the two sequences, a matrix D of size m by n is constructed where its elements $D\ (i, j)$ are populated with a distance $d(s_i,\ q_j)$ which is constructed using data points s_i and q_j. To compute the distance (d), either euclidean distance (Berndt & Clifford, 1994), angular distance (Nakamura, Taki, Nomiya, Seki, & Uehara, 2013) or others like derivative distances (Keogh & Pazzani, 2001) can be used. For computation based on single feature or dataset, euclidean distance can be computed as:

$$d = \sqrt{(s_i - q_i)^2} \tag{2}$$

where d is the euclidean distance between two data points s_i and q_i. Euclidean distance computation for multi-dataset computation is presented in Equation 11. The alignment or warping path (P) of two signals is then considered as a set of data points that define the mapping between the two signals S and Q as:

$$P = p_1, p_2, p_3, \dots p_k \tag{3}$$

and the k^{th} element of the warping path can be defined as $p_k = (i, j)_k$ where i and j are an index for aligned data points in S and Q respectively (Fig 1D). This warping path is subjected to constraints of boundary condition, continuity, and monotonicity (Berndt & Clifford, 1994; Keogh & Pazzani, 2001). As there are potentially many paths in a distance matrix D which satisfy these constraints, the optimum alignment is generated by following a path that minimizes the sum of distances (Fig 1C) as:

$$DTW(S, Q) = min \left\{ \sum_{k=1}^{k} p_k \right. \tag{4}$$

As presented in Sakoe & Chiba (1978) and Berndt & Clifford (1994), while keeping the minimal values (valley points) and fulfilling search constraints can be achieved by using a dynamic programming approach by recursively computing a cumulative distance matrix $C_{i,j}$ which is the sum of distance matrix $D_{i,j}$ and minimum of surrounding cumulative distance values as:

$$C_{i,j} = D_{i,j} + min\,\{C_{i-1,j}, C_{i,j-1}, C_{i-1,j-1}\} \tag{5}$$

Taking this principle, for classification and clustering, each element of a larger database is compared with templates of different classes by computing dynamic time warping distance. A final class label will be assigned for an element of a template that yields minimal DTW distance. Specific to satellite image classification, a time series values of a specific variable at a specific location are matched with DTW distance (Maus et al., 2016).

To create an optimum warping path, DTW recursively searches all elements of the distance matrix. This sometimes leads to the possibility of pathological warping when it searches data points away from a diagonal. To prevent this, a global constraint that restricts the maximum search distance from the diagonal has been introduced. Among these, the Itakura parallelogram (Itakura, 1975) and the Chiba band (Sakoe & Chiba, 1978) were the notable ones. The Chiba band restricts the warping path within a rigid user-defined region around the diagonal (Fig 1A) while the Itakura parallelogram flexibly updates within a parallelogram-shaped search distance (Fig 1B) depending on user-defined slope constraint.

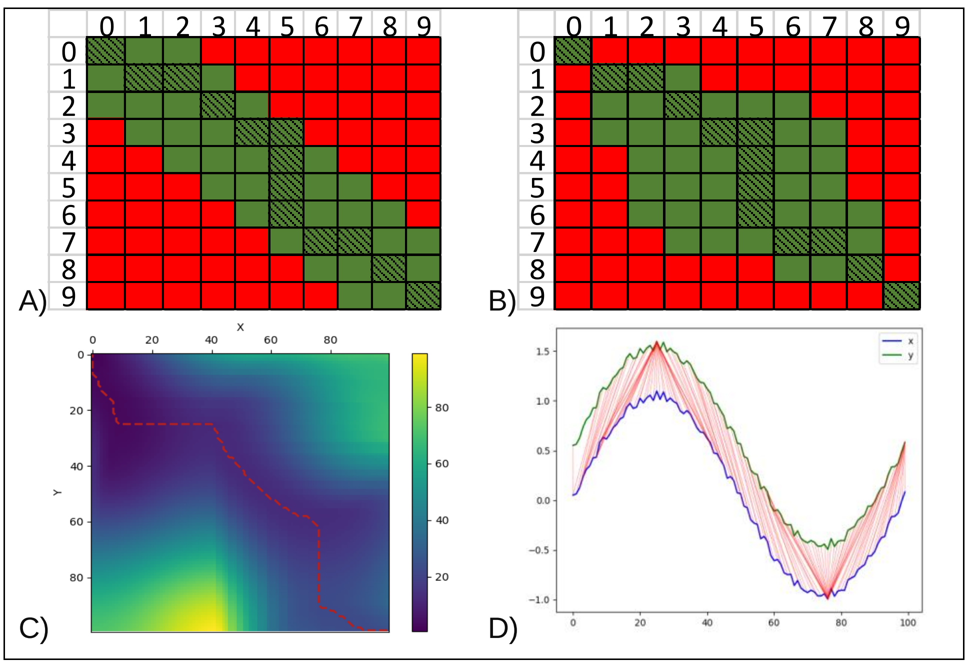

Figure 1: Chiba band (A) and Itakura parallelogram (B) of which green cells indicate allowable search region, diagonally hatched pixels were warping path*; (C)* cumulative cost matrix with red warping path and (D) the mapping between two signals

These global constraints are only looking for the order of data series not the actual time difference between data points. More importantly, it does not account for the temporal distortions within the warping window especially in the existence of missing values and observations taken with irregular time steps. This is most prevalent in Satellite Image Time Series (SITS) with cloud contamination. For some geographic regions, there may not be successive observations with regular time steps. To overcome this phenomenon, Jeong, Jeong, & Omitaomu (2011) have introduced twDTW where rather than putting a rigid warping path, observations within a warping window will be punished with a weight derived from temporal differences of data points. It is primarily intended for reducing misalignment, simplifying computational complexity, and flexibly accounting for the phenological nature of the variable under investigation (Petitjean, Inglada, & Gancarski, 2012). For two data points, the weight is generated as a function of their temporal difference. Points with a larger temporal difference will be punished more than points which have smaller temporal differences. Based on the methodical differences on how to generate the weighting factor, there are families of linear and logistic twDTW. Furthermore, based on the extent of time-based constraints for similarity search, these twDTW versions can also further be divided into a family of an open boundary (Guan et al., 2018) and constrained (Csillik et al., 2019) versions. There is also a family of Derivative Dynamic Time Warping (DDTW) which is mainly based on alignment matching using data points observed before and after a specific time in a sequence (Keogh & Pazzani, 2001). More importantly, some variates also blend original DTW and DDTW with some data transformation methods (Górecki & Łuczak, 2014, 2015).

One of the potentials of DTW for time series sequence matching is its ability to elastically accommodate the phase change in the time domain for signals that have resembling shapes but with different phases (Keogh & Ratanamahatana, 2005). More importantly, despite the euclidean distance which always needs time series of equal length, DTW can handle signals with different lengths. Despite its stated strengths, one of its most noted limitations is its space and time complexity. Having acknowledged existing strategies to speed up DTW like enforcing constraints (Sakoe & Chiba, 1978), abstracting the data and use of indexing strategies, Salvador & Chan (2004) have also tested some strategies that ease model complexity from quadratic to linear time. With the existence of open source cloud computing platforms like Google Earth Engine (GEE), it is believed that this cannot be an enduring problem for the future as there are some studies tried to map cropland extent at regional scale like Oliphant et al. (2019) using Google Earth cloud computing environment.

2.2. Dynamic Time Warping for Satellite Image Classification

Though there are a plethora of studies done in different application domains using DTW, breakthrough research in remote sensing was done by Petitjean, Inglada, & Gancarski (2012) for land cover classification from multi-temporal SITS. The study has reported the potential of DTW for handling cloud contaminated pixels (time series with different length), incorporation of expert domain knowledge for specific phenology by introducing a time-constrained version of the model, and effectively handling the cyclic behavior of some land cover features especially vegetation changes by joint clustering of multi-year imagery. As provided in section 2.1, DTW can efficiently handle time series similarity by shape matching. As one of the improvements in DTW is the introduction of constraints during the creation of temporal alignments like the Itakura parallelogram (Itakura, 1975) and the Chiba band (Sakoe & Chiba, 1978). Though these constraints can limit the maximum similarity search window to prevent some pathological warping, it cannot flexibly account for the seasonality (phase change) of vegetation in the time domain when series with similar lengths have different observation time. To overcome this problem, for time series classification, Jeong et al. (2011) have introduced a weighted version of DTW that optimally balances shape matching and temporal alignment by introducing a weighting factor based on temporal differences of two points in time series. Based on this work, Maus et al. (2016) have investigated the potential of twDTW for land cover classification. Using optical time-series Moderate Resolution Imaging Spectroradiometer (MODIS) imagery, the study has investigated linear and logistic time weights with different temporal lags ranging from 30 to 100 days. From this study, it is concluded that the time-weighted version of the model performs better than the unconstrained version especially for the identification of short cycle land cover classes.

Though Maus et al. (2016) and Petitjean et al. (2012) use DTW for land cover classification, crop types were not mapped independently, but rather in a generic landcover class where all crops were aggregated to cropland. A detailed study by Belgiu & Csillik (2018) has mapped specific crop types by object-based twDTW in some cropland dominated landscapes of Romania, Italy, and the USA. The study has reported that object-based twDTW has achieved better accuracy and relatively shorter computational time than the pixel-based counterpart. Similarly, Csillik, Belgiu, Asner, & Kelly (2019) have investigated a pure object-based DTW which is a time-constrained version of twDTW without time weighting. By comparatively analysing constrained versions with different time lags, purely euclidean distance, and open boundary versions of DTW, the study has shown a better performance of a constrained version of a model to map crop types. The study has also concluded that the utilization of multiple features in classification can improve the accuracy of crop type mapping. Here it should be noted that both time-weighted and constrained versions, the time lags were optimized by trying a series of values. Under the continuum of open boundary DTW, Guan et al. (2018) have implemented a local weighting approach for crop type mapping from MODIS time-series imagery. Accordingly, the study has improved the classification accuracy by 5–7% than the unweighted counterpart of open boundary DTW. Similar to the selection of optimal temporal lag for twDTW, optimal local weighting coefficients are selected by investigating on different values.

Crops can grow in a given landscape either for an extended long period (perennial crops) or for a short duration (seasonal). Seasonal crops especially short-cycle crops like vegetables demand a DTW approach that can handle subsequence matching. In this aspect, a study by Li & Bijker (2019) has employed dynamic time warping with SPRING strategy (Sakurai, Faloutsos, & Yamamuro, 2007) to classify short cycle vegetables in Indonesia using time series Sentinel-1 SAR images. A comparative analysis done by this study has reported that the SPRING strategy is more accurate than the twDTW counterpart.

2.3. Crop Type Mapping using SAR Imagery

The potentials of optical imagery for the provision of biophysical information for different crops is an established reality. On the other hand, the radar signal capability of penetrating the cloud allows monitoring biophysical characteristics in any weather where major crop growth takes place (Liu et al., 2019). Similar to optical imagery, microwave signal from SAR have different responses for vegetation (crops). These responses are changing with changing vegetation characteristics like canopy cover, height, and structure of leaves and branches (Bouman & van Kasteren, 1990a, 1990b). In addition to these, the response also depends on the radar sensing system like frequency and/or wavelength, polarization, and incidence angle (Ulaby, 1975; Skriver, Svendsen, & Thomsen, 1999). Backscattering characteristics that are mostly synchronized with changes in the state of vegetation parameters enable to monitor development of crops and perform time series classification which is the main theme of the current study.

Contrary to optical sensors that have either multispectral or hyperspectral bands in the broader electromagnetic spectrum, one of the limitations of radar sensors is that it is constrained by available polarimetric bands (only co-polarized VV, HH and cross-polarized VH or HV bands). A study carried out in Flevoland, the Netherlands for mapping crop types using single (co-polarized and cross-polarized), dual-polarized, and fully polarimetric data has claimed that fully polarimetric data has yielded better accuracy (Lee, Grunes, & Pottier, 2001). The study has also recommended that as fully polarimetric data is scarce, the combined use of co-polarized HH and VV bands is an alternative option. To overcome this, some derived bands like cross ratios, band differences, and indices were used for crop classification (Sonobe, 2019). More intuitively, when crops grow and canopy structure changes, the scattering characteristics change from surface scattering to double bounce and volumetric scattering. Before the crop grows, the bare soil experiences surface scattering, when the crops grow and their canopy cover is increasing, volumetric scattering is dominant. With increasing crop height, depending on the direction of surface illumination by a radar signal and density of canopy cover, the double bounce is also an inevitable physical phenomenon especially for crops planted in rows. The scattering mechanism is quantitatively estimated by using polarimetric decomposition features. A specific study done on the phenological cycle of rice and respective inherent scattering characteristics has stated similar conclusions (Cheng, Chu, Chen, Yamaguchi, & Lee, 2012). It should be noted that polarimetric decomposition is possible only if the observation is taken either in a dual or quad polarimetric mode which limits the usability of decomposed features only to these observation modes.

Using the SAR sensor's ability to provide imagery at any weather and time as merit, several studies were done to map crops using different classification models. To note some, Support Vector Machine (SVM) for agricultural crop classification (Tan, Ewe, & Chuah, 2011), parallelepiped minimum distance classifier for maize identification (Uppala, Venkata, Poloju, Rama, & Dadhwal, 2016) and, decision tree and Random Forest (RF) for paddy rice detection (Bazzi et al., 2019). Up to this date, the only notable research investigated dynamic time warping with SAR data is a study done for vegetable classification in Indonesia by Li & Bijker (2019).

Depending on features or bands used during the classification of crops, Xu, Zhang, Wang, Zhang, & Liu (2019) have used only backscatter coefficient, while some others like Tan et al. (2011) have utilized only decomposed polarimetric features, and Sonobe (2019) has used backscatter coefficient and decomposed polarimetric features. Regarding the accuracy performance of incorporation of polarimetric decomposed features for accuracy performance, Li & Bijker (2019) have indicated less significant impacts on accuracy while Jiao et al. (2014) have reported accuracy improvements. These differences in output can be attributed to a model used for classification and type of polarimetric decomposition technique. More importantly, crop type classification can also be affected by the selection of optimal sensing dates (Van Niel & McVicar, 2004) which is most challenging for single date image classification.

In SAR based crop type mapping, it is common to see studies that have fused optical with SAR imagery. A specific study by Forkuor et al. (2014) has stated accuracy improvement ranging from 10% to 15% by integrating TerraSAR-X with high-resolution RapidEye imagery. The study has also noted performance differences with different polarizations and classifying pixel-wise and through the use of parcel polygons. Similarly, Kussul et al. (2016) have stated the added benefits of integrating optical Landsat-8 imagery with Sentinel-1 SAR data. Their study has also noted that the incorporation of parcel boundaries for post-classification operations improves the proper classification of crop types. Here because it is not our scope of the study, a review for performance differences on the use of different levels of image fusion is not provided.

2.4. Mapping Crops in Smallholder Farming Areas: Current State and the Gap

Globally smallholder agriculture contributes a profound share of food production (Ricciardi, Ramankutty, Mehrabi, Jarvis, & Chookolingo, 2018) and covers a larger extent of global agricultural land (Lowder, Skoet, & Raney, 2016). Despite their contribution to global food production, they are less mapped especially crop type maps are rarely available. On a national scale, there is some progress, though it is not sufficient. In different parts of the world, studies have tried to map different attributes of smallholder farming areas like retrieval of farm boundary (Persello, Tolpekin, Bergado, & de By, 2019), cropland extent (Oliphant et al., 2019) and agricultural production (Jin, Azzari, Burke, Aston, & Lobell, 2017; Lambert, Traoré, Blaes, Baret, & Defourny, 2018).

From its relevance to various practical applications, there is promising progress in mapping specific crop types in smallholder farming areas using different Earth Observation (EO) products. Accordingly, Hall et al., (2018) have tried to map Maize crop in complex topography using a high-resolution image obtained from a drone by an object-oriented image classification technique. Though their study is capable from a technical perspective, the utility of such experiments in the vast majority of smallholder farming areas could be constrained by technology and cost. Xie, Zhang, & Xue (2019) have also investigated high-resolution Gaofen-1 images with different Convolutional Neural Network (CNN) architectures. The classification accuracy of their work is relatively better than the random forest classification. Both studies have tried to map crops from single date optical imagery. This raised a critical question of how to optimally select imaging dates to account for heterogeneous crops in a landscape to map both short cycle and long cycle crops together. In areas where cloud cover is a prevalent phenomenon, even this poses an enduring limitation for transferability issues of strategies developed in other landscapes. While high resolution images can have a potential to account farm level fine spatial details, it is essential to raise their feasibility for mapping in terms of cost which is mostly impractical for mapping at wider geographic extent. Hence, looking for open source tools, geoprocessing workflows and datasets is an option. In this regard, Useya & Chen (2019) have tried to map cropping patterns in smallholder farming areas using time series Sentinel-1 images which are freely accessible while Stratoulias et al. (2017) have presented a notable contribution on open source-based geoprocessing workflows for mapping crops in smallholder farming areas using raw high-resolution images.

Although the above-mentioned studies have reported promising findings it is difficult to compare reported accuracies as studies were carried out at different geographic areas, with different datasets and different classification models. The common denominator of these studies is that they have acknowledged some of the existing bottlenecks for appropriately mapping smallholder farming areas like small farm size, the complexity of the terrain, landscape-level heterogeneous cropping patterns, irregular boundaries, and the existence of thick clouds in the growing season. More importantly, almost all studies failed to account for the seasonality of cropping patterns in smallholder farming areas. Even studies that are based on time-series observations, beyond extracting features from time-series stack of images, phenological development of crops is less represented in classification models. In an account of this problem, Li & Bijker (2019) have done significant contributions for mapping vegetables using time series Sentinel-1 SAR imagery of which this study is based.

A few studies dedicated to the identification of irrigated crops in the winter season have reported that optical imagery and/or integration of both optical and radar provides accurate crop acreage retrieval (Kussul et al., 2016). Even in areas where there is a good chance of obtaining cloud-free optical imagery during a growing season, integration of radar imagery in crop type classification has brought improvements in classification accuracy (Forkuor et al., 2014). The fusion of SAR time-series images that have a relatively coarse temporal resolution but fine spatial resolution with time-series images that have a coarser temporal resolution but fine spatial resolution is a domain less investigated for crop type mapping.

Most crop type classification studies, especially those dedicated to implementing time-series radar data, were carried out in areas where either field size is large enough (Lopez-Sanchez, Ballester-Berman, & Hajnsek, 2011;

Kussul et al., 2016; Whelen & Siqueira, 2018) or homogenous crops, such as rice, were planted in a vast region (Son, Chen, Chen, & Minh, 2018). Under these circumstances, the level complexity to map crop types can be minimal. This is mostly less probable in smallholder farming systems in developing countries where small and fragmented farm plots were predominant (Vanlauwe et al., 2014). In fragmented landscapes, different crops can be cultivated in heterogenous order at different times in a growing season. These heterogeneous crops can have different growth stages and respective responses for incident radar signal (Wang, Magagi, & Goita, 2016). Furthermore, within fragmented farming areas, different crops can have also similar phenology which further amplified the complexity of mapping crops in smallholder farming areas. To account for these, some studies like Ghazaryan et al. (2018) and Heupel et al. (2018) have tried to incorporate phenological information to map specific crop types.

Whether it was done on radar only or integration of radar with optical data, there is no common procedure on how to map crop types. To this end, studies like Ndikumana, Minh, Baghdadi, Courault, & Hossard, (2018) have adopted one stage classification approach where specific crop types were considered as a land cover class while others like Mandal et al. (2018), Whelen & Siqueira, (2018), and Li & Bijker (2019) have followed a two-stage classification approach where cropland is firstly separated from other land cover classes and followed by mapping of specific crop types. Even though not common, there is also an iterative or a sequential and a decision tree-based classification strategy (Bargiel, 2017). These were done either by using polarimetric information or integration of polarimetry with derived texture, shape, and ratio products (Tso & Mather, 1999; Jiao et al., 2014; Valcarce-Diñeiro, Arias-Pérez, Lopez-Sanchez, & Sánchez, 2019).

Crop type mapping was done by using different classification algorithms and procedures. To note some, Maximum Likelihoods (Tso & Mather, 1999; Chen Liu, Shang, Vachon, & McNairn, 2013), twDTW (Li & Bijker, 2019), Deep Neural Networks (Ndikumana et al., 2018), Decision Tree (Valcarce-Diñeiro et al., 2019), Boosted Decision Tree/Random Forest (Gao, Zribi, Escorihuela, Baghdadi, & Segui, 2018; Son et al., 2018), SVM (Gao et al., 2018; Son et al., 2018), Convolutional Neural Networks (Wang, Sun, Phillips, Zhao, & Zhang, 2018) and object-oriented classification (Jiao et al., 2014). For the generation of classification statistics, parcel/plot based approaches were more accurate than pixel-based mechanisms (Tso & Mather, 1999). The utility of parcel-based statistical approaches is mostly constrained by the availability of agricultural parcel boundaries at mapping areas.

In general, this study is different than reviewed studies in terms of: (i) geographic region (which is mainly focused on smallholder farming areas), (ii) investigation of different approaches for distance measure computation used for sequence matching, (iii) implementation of innovative approaches regarding the definition of the time lag for the defining time weight, (iv) and integration of medium spatial resolution Sentinel-1 with fine spatial resolution TerraSAR-X imagery.

3. Research Methods

3.1. Study Area

The study site is situated in 6º 45' 39" to 7º 3' 29" Longitude and 52º 15' 5" to 52º 21' 33" Latitude. As presented in Figure 2, it is located in the eastern Netherlands, Overijssel province.

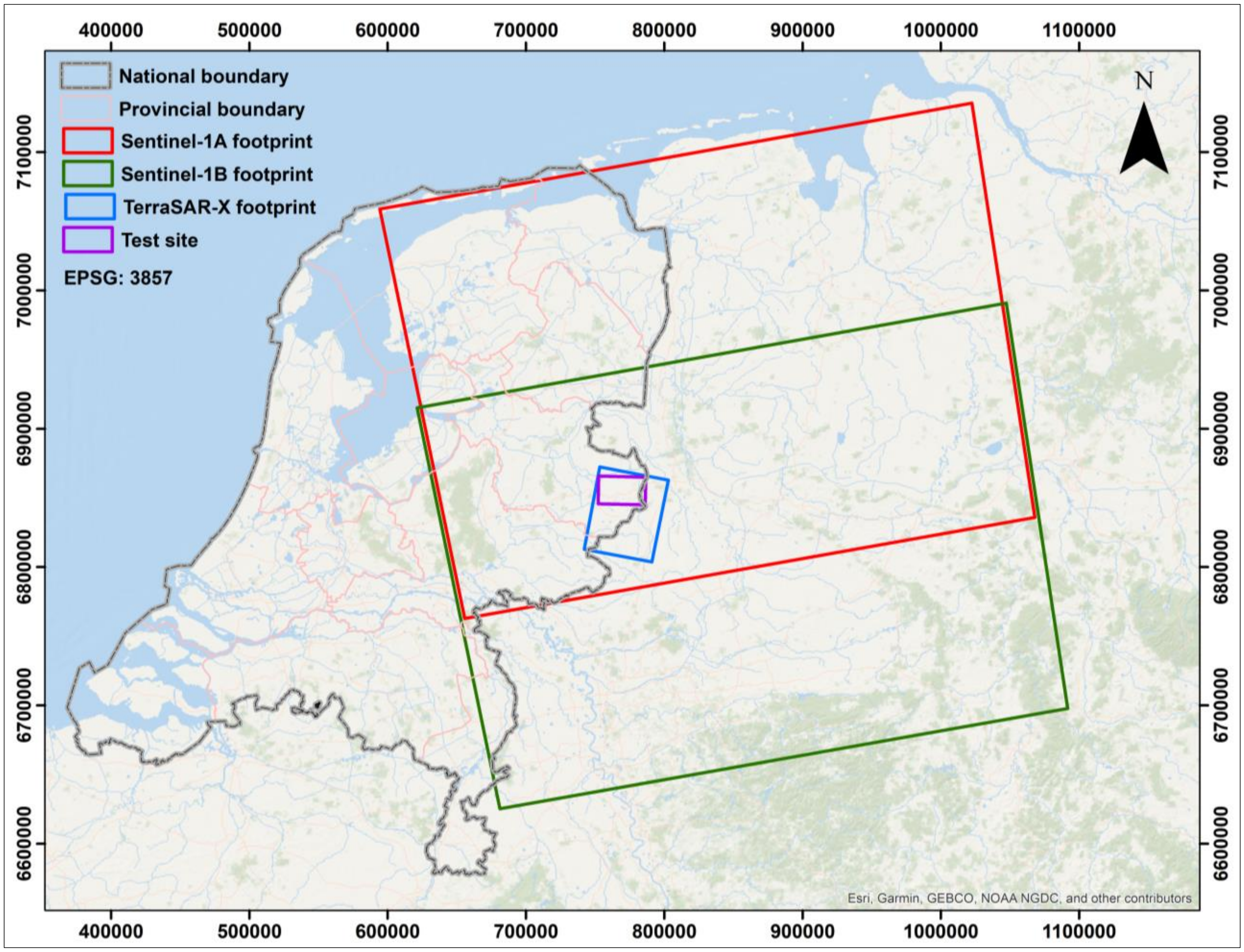

Figure 2: Study site map with satellites footprint (Source: Compiled from AAN, DLR, and ESA (Section 3.2 for detail information))

Analysis results from long-term meteorological observations indicate that the mean monthly total precipitation of the study site is not greater than 125 mm/month in the rainy season with the annual total reaching from 650 to 1000 millimeters (Fig. 3A). The mean minimum monthly temperature falls below the freezing point in January (Fig. 3B). The mean monthly maximum temperature peaks in July. Except for some crops, major crop production takes place from February to the end of September. In the study site, both monthly mean minimum and maximum temperature follow a similar pattern. Governed by available moisture supply and temperature, potential, evapotranspiration follows a similar pattern with a mean monthly maximum temperature, where it peaks in July with a monthly total of around 120 mm/month.

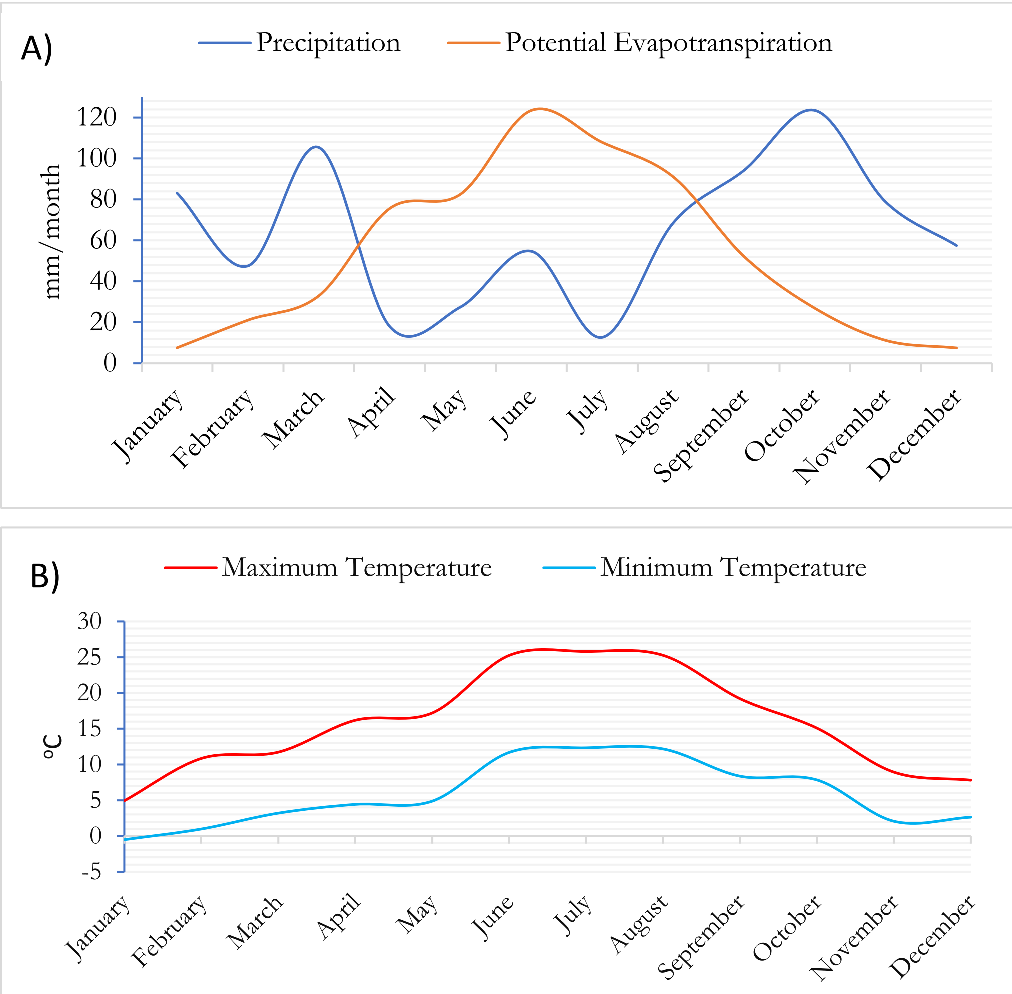

Figure 3: Long-term climatic variables (A) total monthly precipitation and total potential evapotranspiration, (B) mean monthly minimum and maximum temperature. Source: Computed from the Royal Netherlands Meteorological Institute (KNMI), Twente Station (*https://www.knmi.nl/nederland-nu/klimatologie/daggegevens*).

The Netherland is known for its farm plots which are well planned with relatively regular shape and larger size, which is resulted from past rural land consolidation interventions (van den Noort, 1987; van den Brink & Molema, 2008). Though this is a nationwide general trend, the specific study site still possesses irregular, relatively small and fragmented holdings where crops dominate the landscape in a mixed pattern. For this study, it is believed that, though not a perfect replica, the site can be a suitable representative site for smallholder farming areas to further replicate the results of this study elsewhere. The study site is mainly dominated by Maize (*Zea mays*) both for human consumption and animal feed, followed by Potato (*Solanum tuberosum*) production. In addition to these dominant crops, Wheat (*Triticum aestivum*) and Barley (*Hordeum vulgare*) which both grow in summer and winter seasons, Triticale (*Triticosecale*), Rye (*Secale cereal*), vegetables and ornamental plants were grown in the study area. These crops have a different calendar (Figure 4).

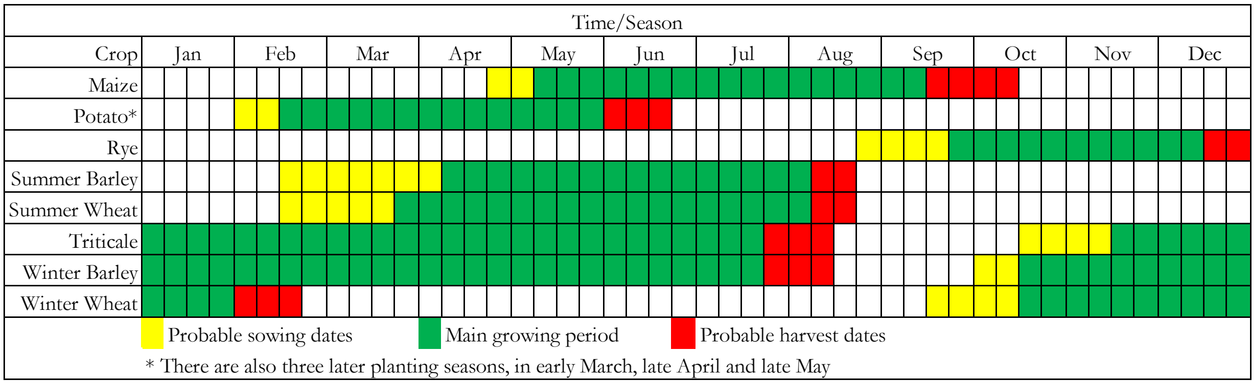

Figure 4: Dominant crops calendar. Source: Compiled from Ruud, Gerard, & Leendert, (n.d.), Darwinkel & Zwanepol (1997), Osman, Bueren, Berg, & Van (2005) and Brink et al. (2008)

3.2. Data

The study has mainly used time-series dual polarimetry Sentinel-1 and Single polarimetry TerraSAR-X SAR datasets. A detailed description of the Sentinel-1 mission was provided in Torres et al. (2012). As Sentinel-1 SAR Ground Range Detected (GRD) data are not suitable for polarimetric decomposition, Slant Range Single Look Complex (SLC) data was used to look into inherent scattering characteristics of different crops across the growing season by polarimetric decomposition. The dataset was accessed from the European Space Agency (ESA) Sentinel Data Hub (https://scihub.copernicus.eu/dhus/#/home). As provided in Table 1, similar to Sentinel-1, TeraSAR-X SLC data with strip map sensing mode was obtained from Airbus as part of the ESA third party mission data access policy (DLR, 2020). A detailed description of TerraSAR-X image products was provided in Roth (2003).

Table 1: Selected metadata for used SAR images

Attribute	Sentinel-1	TerraSAR-X
Polarization	Dual polarimetry (VV, VH)	Single Polarimetry (HH)
Orbit direction	Descending	Descending
Band (frequency)	C band (5.405 GHz)*	X band (9.65 GHz)*
Spatial resolution**	5 by 20 meters	1.2 by 3.3 meters
Sensing mode	Interferometric Wide Swath (IW)	Strip Map (SM)
Incidence angle	29° to 46°	20° to 45°

* This is central frequency of the band
** In range and azimuth direction respectively

Images were selected by considering the growing season of most dominant crops in the study site (Figure 4). The temporal distribution of both datasets is provided in Figure 5. As Sentinel-1 image is accessible free of cost and frequent observations were available, its temporal period starts before the sowing dates of most dominant summer crops. This is mainly from the intension to understand changes in backscattering characteristics before and after crop growth across the growing season. For TerraSAR-X, as access quota is only limited for 15 image scenes, the imaging date was determined to start at a season where sown crops start vegetative growth. This is mainly done after a thorough evaluation of Sentinel-1 backscattering characteristics across the growing season.

Figure 5: Temporal distribution of Sentinel-1 and TerraSAR-X scenes (Appendix 1 for specific dates of each image)

In addition to SAR data, for model training and validation, we have used Basic Registration of Crop Plots (BRP) for the year 2018 which is similar for the year we have imagery for both Sentinel-1 and TerraSAR-X. This dataset contains parcel boundaries that are based on the Agricultural Area of the Netherlands (AAN) linked with specific crops grown or any kind of agricultural land utilization in the specified year. The dataset is publicly available in Public Services On the Map (PDOK) website (https://www.pdok.nl/). For terrain correction of SAR images, 1 arc-second Surface Radar Topographic Mission (SRTM) Digital Elevation Model (DEM) was accessed from the United States Geological Survey (USGS)(https://urs.earthdata.nasa.gov).

3.3. Data Pre-processing

Sentinel-1 SAR data is accessed as an SLC format. The SLC dataset contains amplitude and phase data in a complex number format (ESA, 2013) with its original azimuth and range resolution. Before the actual ingestion of the dataset into the intended model, time-series images have passed three main pre-processing phases. These were the generation of backscatter coefficient, derivation of secondary products (cross ratios and radar indices), and computation of decomposed polarimetric features.

For the generation of surface backscattering coefficient, a downloaded time series dataset was firstly subjected to orbit correction. This was because Sentinel-1 orbit information provided with an image on the flight is not precise, so it was corrected by downloading the Precise Orbit File (POF) from ESA, which is within 3 centimeters accuracy. Sentinel-1 SAR is sensed with Terrain Observation and Progressive Scan (TOPS) with successive sub-swaths and bursts within each sub-swath (De Zan & Guarnieri, 2006). As the study site is situated only within two sub-swaths, part of a sub-swath that has a spatial intersection with a study site was split using the Sentinel-1 TOPS split function. After the split operation, to suppress radiometric irregularities like sensor noise and antenna gain from obtained SAR data (El-Darymli, McGuire, Gill, Power, & Moloney, 2014), radiometric calibration was done using Equation 6 (Miranda & Meadows, 2015). As there are drop lines between successive bursts, these were removed by using TOPS deburst operation. After these operations, individually processed sub-swaths were merged to create a wider sub-scene. As it was known that, the terrain has significant impacts on radar backscatter by creating shadows, layovers, and foreshortening (Kropatsch & Strobl, 1990), the Range Doppler Terrain Correction was done by using Shuttle Radar Topography Mission (SRTM) elevation as terrain 3-D representation. After terrain correction, suppression of speckle-noise is applied by using an improved Lee Sigma filter with a window size of 7 pixels and sigma 0.9 (Lee et al., 2009). Detected, terrain corrected and radiometrically calibrated backscattering coefficient was converted to a decibel scale for both polarizations (VV, VH) as using Equation 7 as provided in Miranda & Meadows (2015).

$$\sigma_{VV}^{o} = \frac{DN^2}{A_{\sigma}^2} \tag{6}$$

$$\sigma_{vv_{db}}^{o} = 10 \log_{10} \sigma_{VV}^{o} \tag{7}$$

where σ_{VV}^{o} is the vertically co-polarized sigma nought or backscatter coefficient and for cross-polarized counterpart the symbol becomes σ_{VH}^{o} by simply replacing the subscripts, DN is observed digital number/signal, A_{σ}^2 is the radar cross-section and $\sigma_{vv_{db}}^{o}$ is a backscatter coefficient in the decibel unit for both VV and VH polarizations.

As processing the whole scene is computationally demanding, part of the scene only covering the study site is extracted by using a boundary polygon in a well-known text (wkt) format. Some steps to generate the backscatter coefficient and the respective application logic of these procedures was provided in a recent publication by Filipponi (2019).

Following the generation of backscatter coefficients for both polarisations, secondary products were generated as follows. Firstly, cross-ratio between co-polarised (VV) and cross-polarised (VH) backscatter coefficients was computed as:

$$CR = \frac{\delta_{HV}^{o}}{\delta_{VV}^{o}} \tag{8}$$

where CR is cross-ratio.

To account for phenological growth development of crops in the classification process, time-series modified Radar Vegetation Index ($mRVI$) was generated as presented in Czuchlewski, Weissel, & Kim (2003) as:

$$mRVI = \frac{4\delta_{HV}^{o}}{\delta_{HV}^{o} + \delta_{VV}^{o}} \tag{9}$$

where $mRVI$ is Modified Radar Vegetation Index

As supplementary for MRVI and cross-ratio, Dual Polarization SAR Vegetation Index (DPSVI) was computed following Periasamy (2018) as:

$$DPSVI = \frac{\delta_{VH}^{o}\left[(\delta_{VV(max)}^{o}\delta_{VH}^{o} - \delta_{VV}^{o}\delta_{VH}^{o} + {\delta_{VH}^{o}}^{2}) + (\delta_{VV(max)}^{o}\delta_{VV}^{o} - {\delta_{VV}^{o}}^{2} + \delta_{VH}^{o}\delta_{VV}^{o})\right]}{\sqrt{2}\delta_{VV}^{o}} \quad (10)$$

where $\delta_{VV(max)}^{o}$ is the maximum co-polarized backscatter coefficient value in the whole scene. As the radar signal is sensitive to surface moisture, especially to the presence of surface water (Joseph, van der Velde, O'Neill, Lang, & Gish, 2010), DPSVI can better differentiate water and crop surface (Periasamy, 2018), so it could have the potential to differentiate vegetated cropland and moist or flooded surface in the growing season.

In addition to the generation of backscatter coefficient, cross ratios, and radar vegetation indices, to account for inherent surface scattering characteristics which are changing with crop development, polarimetric decomposition features were computed from SLC data. Before actual polarimetric decomposition, as an intermediate step, a dual polarimetric coherence matrix (commonly known C2 matrix) was generated as described in Shan, Wang, Zhang, & Chen (2011). Using the computed dual coherent polarimetric matrix, decomposition was undertaken by using Entropy, Anisotropy, and Angle ($H - A - \alpha$) decomposition through analysis of coherent polarimetric matrix as provided in Nasirzadehdizaji et al. (2019) for crop height study. This decomposition model is selected for its suitability to accommodate dual-polarized SAR datasets like Sentinel-1 SAR while other models were mostly suitable for Quad-Pol SAR data. With changing surface roughness and canopy propagation, Entropy (H), Alpha (A) and Angle (α) values were changing (Cloude & Pottier, 1997).

As its sensing strategy is different from Sentinel-1 IW mode, pre-processing approaches for TerraSAR-X are not the same. Accordingly, the obtained SSC data set is calibrated for radiometric irregularities and subsequently sigma nought is generated, multi-looking is done to focus the detected signal. Similar to Sentinel-1 SAR, existing speckle noise is filtered using refined Lee sigma filter and finally, it was geocoded using SRTM DEM where terrain corrected backscatter was generated for HH polarization.

Finally, all processed datasets were arranged to suit DTW input-output structure in a 4-dimensional array, with an order of dimensions (number of features, number of bands per feature, rows, and columns). Overall pre-processing of time-series images was done by integrating the Sentinel Application Facility (SNAP) engine Graph Processing Tool (GPT)(ESA, 2018) on Python scripting environment.

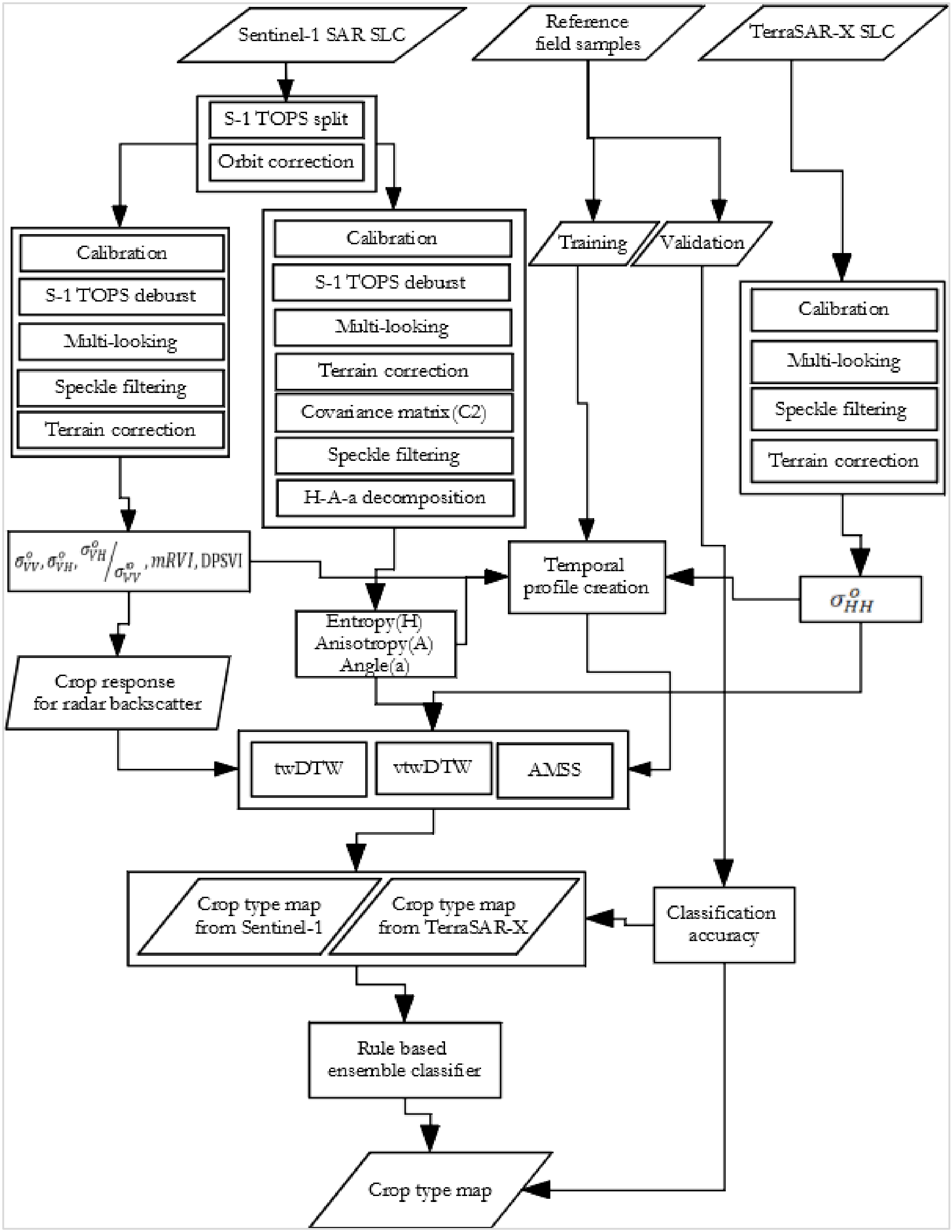

Figure 4: Analytical framework of the study

3.4. Sampling and Creation of Temporal Profiles

For training the model and validation of classification outputs, the study has utilized polygons from the BRP dataset. To select these reference samples, a two-stage sampling strategy was followed. At the first stage, sample polygons were selected using a stratified random sampling approach using crop types as strata. From each crop type (stratum), 20 polygons were selected on a random basis. For a crop that has less than 20 polygons, all parcels were included in the sample. The sample size is mainly decided by considering the existing uniformity of terrain and agroecology in the study site, which is considered not significantly affect the variability of crop phenology. More importantly, as it can be understood from studies like Belgiu & Csillik (2018) and Csillik et al. (2019), rather than the size of samples, the main issue which should be taken into consideration while working on DTW is the appropriate selection of representative or informative crop samples for temporal profile creation. As it was known, random sampling does not guarantee spatial representativeness as samples picked at a random basis can be at close locations. This causes spatial clustering of samples and is inefficient for selecting samples that can well represent a spatially heterogenous object or phenomena in a given geographic region (Dobbie, Henderson, & Stevens, 2008). To control spatial autocorrelation while keeping randomness, a neighborhood/distance constraint was imposed for each crop sample. Accordingly, for each polygon, the minimal distance to the nearest neighbor was computed. Then, within each stratum (specific crop sample), samples were sorted with computed minimal distance in descending order where the first $n*$ polygons were taken. Here it should be noted that within a single polygon, there might be significant variations in the backscatter coefficient which is attributed to differences in surface and subsurface soil moisture, crop development as a factor of variations in soil fertility management. To account for this, at the second stage, from each selected sample polygons, random samples that are proportionate with polygon areal extent were picked from the polygon as final training pixels (Appendix 2A for algorithmic procedure and Appendix 1C for distribution of points within training polygons). To validate classification output, centroid points of all polygons from the whole parcel data set is taken. This yields a dense number of points that are fairly distributed within a study site.

After the preparation of training samples, the temporal profile of each crop is generated using training crop samples and pre-processed SITS. From each crop type in classification samples, values were extracted from SITS which brings an array of values with dimensions of the number of layers and number of specific crop samples. These were converted to a vector of temporal profile by using the median values of all locations. The median statistic is opted because of its robustness for outliers, ability to fairly represent all values in the set especially when the observation has a skewed distribution. Smoothing (filtering) done at the spatial domain cannot completely remove noise from SITS in a temporal domain. As per this, aggregated feature values can experience abrupt changes emanated from either the radar system or interaction of signal with sensing media and object itself. To suppress this noise in one way and to generate a temporal profile that accounts for the smooth and continuous phenological development of crops, smoothing at the temporal domain was done by using Savitzky-Golay smoothing (Savitzky & Golay, 1964). The Savitzky-Golay filter was chosen for its capability of preserving the structure of time series especially the positions of local minima and maxima while

[*] is number of polygons selected from each crop type

smoothing unnecessary fluctuations. Smoothing of NDVI using Savitzky-Golay for phenological studies was investigated by Chen et al. (2004) and was reported effective in suppressing noise from times series satellite imagery. The overall implementation procedure of sampling and generation of a temporal profile is provided in Algorithm 1 (Appendix 2A).

3.5. Classification and Accuracy

To achieve the first objective, from pre-processed multi-dimensional features, a backscatter signature was extracted from locations where crop samples were taken. Samples were taken from the centroid of farm plots that we assume the backscatter signatures were purely the responses from the specific crop. As samples for specific crops were selected from different locations, its backscatter signatures were aggregated by using median statistics. To create smooth temporal profiles representing crop development, aggregated values were smoothened by the Savitzky-Golay filter. Then the response of backscatter signature across the phenological change of crops was assessed by using 2-D graphical plots. This is from the theoretical and empirical evidence that surface backscatter characteristics could be highly associated with vegetative growth and vegetation physical characteristics (Vreugdenhil et al., 2018). More importantly, the dynamics of decomposed polarimetric features were also assessed across the growing season to look into changes in inherent scattering characteristics of crops with vegetative development. Not only assessing scattering characteristics across the season, but outputs from this analysis were also used for specifying optimal temporal window where crop temporal profiles have the best separability.

For the second objective, a crop type classification was done using only the backscatter coefficient dataset. For the third objective, image classification is done by integrating the backscatter coefficient with derived indices and features from $H-A-\alpha$ decomposition. For classification, the study has used twDTW (Jeong et al., 2011).

As twDTW compares 1-D sequences of time series, firstly representative temporal profile for major crop types was generated from processed images on field sample locations. Time series picked from each pixel location were also smoothed by the Savitzky-Golay filter (Savitzky & Golay, 1964). This is mainly to suppress noise and create a smooth phenological pattern and create a comparable series with smoothed temporal profiles. Each crop temporal sequence was matched with a time series of observations in each pixel using the twDTW cost distance matrix.

The first procedure in twDTW is the computation of the distance matrix between SITS at a given pixel location and a temporal profile of a specific crop. As per this, for SITS with a series length of M and specific crop temporal profile with length N, a distance matrix D with sizes of M by N is computed as given in Equation 11.

$$D[i,j] = tw_{i,j} \sqrt{\sum_{i,j=1}^{M,N} \left(SITS_i - TPF_j\right)^2} \tag{11}$$

where $D[i,j]$ are the distance at row i and column j, $SITS_i$ is satellite image time series at specific pixel location at time i, j, TPF_j is the temporal profile of specific crop at time j, and $tw_{i,j}$ is weight factor that accounts for the absolute differences of times i and j, which can be of either linear or logistic weight. For the current study, a logistic weight was used. It was computed by using Equation 11 as:

$$w_{i,j} = \frac{1}{1 + e^{-\alpha(|T_i - T_j| - \beta)}} \tag{12}$$

where T_i is the time for observation in SITS at i^{th} position in a time series, T_j is the time for observation in the temporal profile at j^{th} position, β is the maximum time lag for the warping window to search for a match that is constant for all crops, and α is a user-defined constant to control the steepness of the slope. As stated by Maus et al. (2016) and Belgiu & Csillik (2018), optimal α and β values were hyper-tuned by using a set of user defined values in a grid search strategy.

A warping path (Eq. 3 & 4) is computed with constraints of continuity, monotonicity, and boundary conditions (Sakoe & Chiba, 1978). This can be achieved by using a dynamic programming approach by computing cumulative cost distance matrix C with sizes of M by N which recursively follows the minimum sum of distances (valley) (Eq. 13 & 14):

$$C_{i,j} = D_{i,j} + \min\{D_{i,j-1}, D_{i-1,j}, D_{i-1,j-1}\} \tag{13}$$

which is further subjected to the following constraint.

$$C_{i,j} = \begin{cases} D_{i,j} \ if \ i,j = 1 \ and \ j = 1 \\ D_{i,j} + C_{i-1,1} \ if \ j = 1 \ and \ 1 < i \leq M \\ D_{i,j} + C_{1,j-1} \ if \ i = 1 \ and \ 1 < j \leq N \end{cases} \tag{14}$$

From cumulative cost matrix distance, the optimal similarity/dissimilarity between two different time series observations is equivalent to a pixel value at the position of $C_{M,N}$. To label a pixel with specific crop type, recursively minimum warping distances were computed for each crop. Following a 1-Nearest Neighbour (1-NN) classification approach, a pixel takes a crop type label that has the lowest twDTW distance, compared to other crops. Overall model formulations and mechanisms to include multi-dimensional Satellite Image Time Series (SITS) for twDTW classification are provided in Csillik, Belgiu, Asner, & Kelly (2019), Li & Bijker

(2019), Maus, Câmara, Appel, & Pebesma (2019) and Petitjean et al. (2012). Specific to this study, twDTW was adopted using the procedures presented in Algorithm 2 (Appendix 2B).

For the fourth objective, an innovative improvement was applied on twDTW by accounting for the characteristics of smallholder farming systems. The first is changes in time constraints. Previous studies like Maus et al. (2016) and Belgiu & Csillik (2018) have utilized twDTW for land cover classification and crop type mapping respectively with linear and logistic time weights together with a maximum time lag constraint which is similar for all crop/cover classes. As known, crops at a given landscape can have specific phenology and different planting time dates at the start of the growing season. For example, Figure 4 shows that there are significant variations in the start of the growing season for dominant crops. Accordingly, by accounting for the phenology of specific crops in the study area, the current study has investigated logistic time weights with a varied maximum time lag (constraint) for each specific crop type (hereafter vtwDTW), which is different from previous studies. Accordingly, the weight factor is reformulated as:

$$w_{i,j} = \frac{1}{1 + e^{-\alpha(|T_i - T_j| - \beta_k)}} \tag{15}$$

where β_k is the maximum time lag for specific crop k in the temporal profile and the remaining parameters were kept similar with twDTW counterpart parametrizations. The specific algorithmic procedure adopted for this model is provided in Algorithm 3 (Appendix 2C).

For the fifth objective, a new approach for the computation of time series similarity measure was implemented. To account for the sensitivity of radar backscatter for terrain variations and surface soil moisture, the Angular Metric for Shape Similarity (AMSS) (Nakamura et al., 2013). Rather than computing similarity distances using euclidean distance at a specific data point in a series, it computes a vector between consecutive data points and computes angular distance. Contrary to twDTW and vtwDTW counterparts, for the AMSS, the magnitude of vectors between consecutive data points is more important than the individual data points at a specific time. Accordingly, for specific temporal profile P with length M and SITS S at a specific pixel location (i, j) with length N, the first step is the creation of a series of vectors with length M-1 and N-1 composed of a vector of points with consecutive time.

$$PV = ((P_2 - P_1), (P_3 - P_2), (P_4 - P_3), (P_M - P_{M-1})) \tag{16}$$

$$SV = ((S_2 - S_1), (S_3 - S_2), (S_4 - S_3), (S_N - S_{N-1}))$$

As it considers consecutive points, the model is robust for spatial variability and noise in the image. Following the creation of vectors of consecutive data points, cosine distance matrix (AS) with the size of $M - 1$ and $N - 1$ was computed as:

$$AS_{i,j} = 1 - \frac{\overrightarrow{PV_i}.\overrightarrow{SV_j}}{\|\overrightarrow{PV_i}\|\|\overrightarrow{SV_j}\|} \tag{17}$$

As our dataset is composed of multidimensional SITS, the computation is extended as:

$$AS_{i,j} = 1 - \frac{\sum PV_{i,k}SV_{j,k}}{\sqrt{\sum(PV_{i,k})^2}\sqrt{\sum(SV_{j,k})^2}} \tag{18}$$

where k is a feature or observable both in SITS and temporal profile sorted with a similar order. On the computation of the cumulative similarity matrix, by recursively following the minimum similarity points (valley) as follows:

$$AC_{i,j} = min\begin{cases} AC_{i-1,j-1} + 2AS_{i,j} \\ AC_{i-2,j-1} + 2AS_{i-1,j} + AS_{i,j} \\ AC_{i-1,j-2} + 2AS_{i,j-1} + AS_{i,j} \end{cases} \tag{19}$$

where AC is an angular distance cumulative cost matrix. During the recursion, $AC_{1,1}$ is assigned a value of $AS_{1,1}$ and to accommodate out of bound recursions of $AC_{0,0}$ and $AS_{0,0}$ $i = 0 \,\&\, j >= 0$ and $j = 0 \,\&\, i >= 0$ is assigned a value of ∞. As indicated in original literature in Sakoe & Chiba (1978), and further used in Nakamura et al. (2013) where the recursion picks maximum value, for distance values nearby the diagonal (more temporally aligned), more weight is provided by multiplying with a weight of two and the algorithm follows one symmetric slope constraint. The current study picks the minimum in the recursion as cosine distance is used instead of cosine similarity. It should be noted that smaller cosine distances indicates higher similarity and it should not be confused with cosine similarity in which smaller values indicate more dissimilarity between observations or specific vectors of data points. The remaining procedures of warping were undertaken by following the valley and the final class assignment was done for a crop that has a minimum sum of cosine distances. The specific implementation of the procedure is provided in Algorithm 4 (Appendix 2D).

For the last objective, a new classification output was generated by a rule-based ensemble approach using classification outputs from Sentinel-1 and TerraSAR-X. To do this, firstly user and producer accuracy of each crop from each dataset were normalized into a single accuracy by using a weighted sum approach as provided in Equation 20:

$$\begin{aligned} A_{c,s} &= wa * UA_{c,s} + w * PA_{c,s} \\ A_{c,t} &= wa * UA_{c,t} + w * PA_{c,t} \end{aligned} \tag{20}$$

where $AC_{c,s}$ and $A_{c,t}$ is normalized accuracy for a specific crop at Sentinel-1 and TerraSAR-X classified images respectively, UA and PA are users and producer accuracy respectively, and wa is a weighting factor for each accuracy. For the current study an equal weighting approach was adopted that for UA and PA, a value of 0.5

was used. Then to co-register classified maps, classification output from Sentinel-1 is re-projected to TerraSAR-X pixel spacing using the nearest neighbor approach. Resampling of Sentinel-1 output is opted to prevent unnecessary information loss if TerraSAR-X is upscaled to Sentinel-1 pixel spacing and to fully utilize spatial information of TerraSAR-X. Based on computed normalized accuracy and resampled image, to create a new crop type the following rule was established (Eq. 21) as:

$$E[i,j]_c = \begin{cases} S[i,j]_c \mid T[i,j]_c \quad if \quad S[i,j]_c = T[i,j]_c \\ S[i,j]_c \quad if \quad A_{c,s} > A_{c,t} \\ T[i,j]_c \quad if \quad A_{c,s} < A_{c,t} \end{cases} \qquad (21)$$

where $E[i,j]_c$ is a crop type map label in a map classified by rule-based approach, $S[i,j]_c$ is crop type label in Sentinel-1, and $T[i,j]_c$ is a TerraSAR-X counterpart all at i^{th} row and j^{th} column.

After the overall classification procedure, all classified images were checked for accuracy using validation points prepared at steps presented in Section 3.4 of the report. To do this, using the spatial location of the validation points, crop type labels were extracted from the classified image. This brings a column of classified and reference crop labels from which all accuracy performance metrics were generated. Following procedures presented in Congalton (1991) user, producer, and overall classification accuracies were computed.

4. Results

4.1. Crop Specific Responses for Radar Signal

Dominant crops in the study site have a different response for incoming radar signals. This variation is across different crop types and polarization bands. As indicated in Figure 6A, for the co-polarized VV polarization band, the backscatter coefficient has shown a decreasing trend up to the first weeks of May. Starting from the first weeks of May, the backscatter coefficient for Maize and Potato abruptly starts to increase from below -11 dB and reaches to around -10.5 dB at the end of June. From the end of June to almost the first weeks of August, it has shown an almost constant trend and then starts to drop. Winter Wheat and Winter Barley follow almost a decreasing pattern up to the end of May. This is mainly because of a similar growing season and similar physical characteristics of the crops. Starting from July, Winter Barley backscatter continues to drop but contrary to this Winter Wheat backscatter has shown an increasing trend and reaches to -10 dB in October. This can be attributed to either replanting of short-season crops after the first harvest or regeneration of grass and weeds at the farm after the first harvest. On cross-polarized Sentinel-1 VH polarization (Figure 6B), except differences in magnitudes, up to the end of April, all crops experience decreasing backscatter characteristics. Starting from the first weeks of May, Potato and Maize crops follow a similar increasing pattern with scattering characteristics they show on VV polarization. Though they follow a similar pattern (shape), backscattering from Potato is higher than Maize. Starting from the first weeks of May, backscatter from Winter Barley starts to drop and reaches below -19 dB in the first weeks of July. After that, it shows a minor reduction. Having major shape similarity with Winter Barley, Winter Wheat backscatter has also decreased until the mid of June. After this time, contrary to Winter Barley, it has experienced an increasing trend. Despite the expected reduction in the backscatter coefficient of Winter Wheat, it increases with a similar pattern of its summer counterpart. Except for minor differences, Triticale and Rye follow a similar pattern. Mainly this indicates that these crops have almost similar plant vegetative structure and canopy characteristics.

In the TerraSAR-X co-polarized HH band (Figure 6C), except for small variations in the amount of backscatter signal, until the end of April, all crops experience a similar backscattering pattern in terms of shape. Within this period, there is a strong variability of the backscatter coefficient. This could be attributed to the sensitivity of the HH signal for surface roughness emanated from tillage during field preparation. After the end of April, dominant crops follow three distinct categories. In the first category, Maize and Potato follow an almost similar pattern. They show minor differences starting in May. Their profile is almost similar from May to the end of June. After the start of July, there is a minor deviation where Potato backscatter is greater than Maize backscatter. The second category is mainly comprised of summer grains (Summer Wheat and Summer Barley) with Triticale and Rye that have experienced a similar pattern. A third cluster, Winter Wheat and Winter Barley, has scattered a minimal backscatter coefficient which has a reversed trend with Maize and Potato.

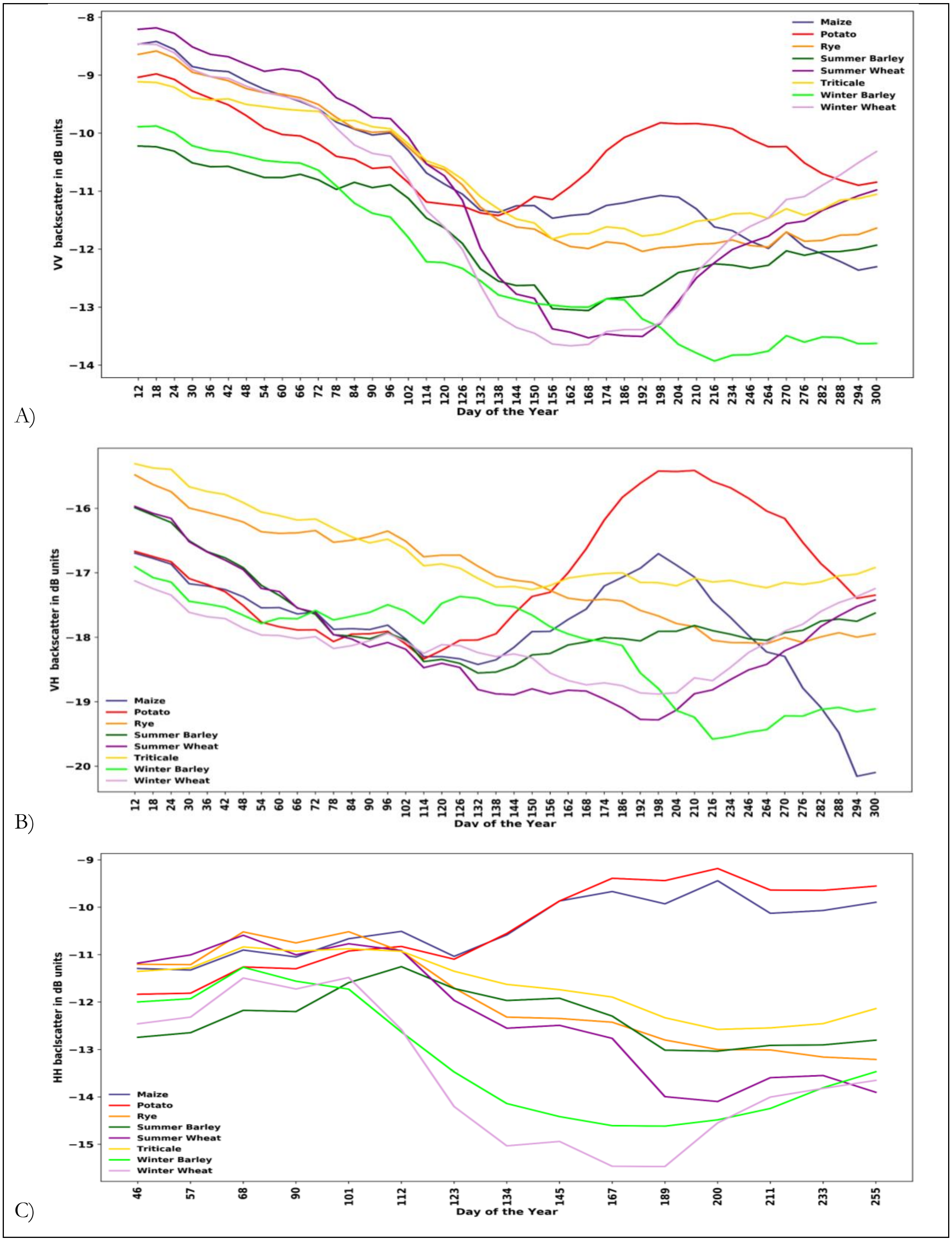

Figure 6: Crop specific responses for SAR signal (A) and (B) Sentinel-1 VV and VH respectively; (C) TerraSAR-X HH

4.2. Crop Type Map Using Time-Weighted Dynamic Time Warping

Results from Sentinel-1 (Table 2) using twDTW shows that it yields an overall accuracy of 67.48%. Concerning the predictive performance of specific crop types, Maize crop has better user and producer accuracy. Though it has relatively better user and producer accuracy, it has also shown strong confusion with Potato. From classified grain crops, Winter Wheat experiences strong confusion with Rye, Triticale, and Summer Barley where classified Winter Wheat is committed from these crops. The classifier optimally identifies Winter Wheat from Potato with almost no confusion. Similarly, as indicated in Figure 7A, the model (twDTW) has shown the dominance of Maize crop in the landscape followed by Potato. In comparison to reference plots from PDOK (Appendix 3D), results from this classification (Fig. 9A) approach are promising.

Table 2: Accuracy results from twDTW using Sentinel-1 VV+VH and TerraSAR-X

Sentinel 1 VV+VH										
	Reference									
Crop	Maize	Potato	Rye	Summer Barley	Summer Wheat	Triticale	Winter Barley	Winter Wheat	Sum	UA
Maize	789	10	3	4	0	0	0	2	808	97.65
Potato	135	37	0	4	1	1	0	0	178	20.79
Rye	18	0	1	1	0	2	0	0	22	4.55
Summer Barley	58	2	1	6	1	5	0	0	73	8.22
Summer Wheat	14	0	1	4	2	1	0	1	23	8.70
Triticale	23	1	7	5	1	5	0	0	42	11.90
Winter Barley	23	1	7	3	3	9	4	0	50	8.00
Winter Wheat	12	0	21	8	5	12	3	13	74	17.57
Sum	1072	51	41	35	13	35	7	16	1270	
PA	73.60	72.55	2.44	17.14	15.38	14.29	57.14	81.25		
Overall accuracy	67.48									
TerraSAR-X										
Crop	Maize	Potato	Rye	Summer Barley	Summer Wheat	Triticale	Winter Barley	Winter Wheat	Sum	UA
Maize	290	13	5	3	1	5	0	0	317	91.48
Potato	573	32	4	2	2	3	0	0	616	5.19
Rye	13	0	7	0	0	2	0	1	23	30.43
Summer Barley	57	3	0	11	3	6	0	0	80	13.75
Summer Wheat	27	2	5	9	2	3	0	1	49	4.08
Triticale	100	1	3	6	2	10	0	1	123	8.13
Winter Barley	5	0	5	1	1	1	3	0	16	18.75
Winter Wheat	7	0	12	3	2	5	4	13	46	28.26
Sum	1072	51	41	35	13	35	7	16	1270	
PA	27.05	62.75	17.07	31.43	15.38	28.57	42.86	81.25		
Overall accuracy	28.98									

Classification result from the TerraSAR-X co-polarized HH band has yielded an accuracy performance of only 28.98%, which is much smaller than the performance achieved from its dual polarimetric (VV, VH) Sentinel-1 counterpart. As indicated in Table 2, there is a strong confusion between Maize and Potato crops followed by Triticale and Summer Barley. Relative to other crops, this classification approach has effectively separated Potato from Winter Wheat and Winter Barely. Contrary to the results from Sentinel-1, the model overpredicts Potatoes and extremely underpredict Maize. As indicated in Figure 7B, the model predicts Potato as the most dominant crop and it is wrongly populated within a landscape. Additionally, even classified Maize crops were mixed with Potato. As can be seen from the spatial plot (Fig. 7B), Potato and Maize crops were mixed within a single parcel.

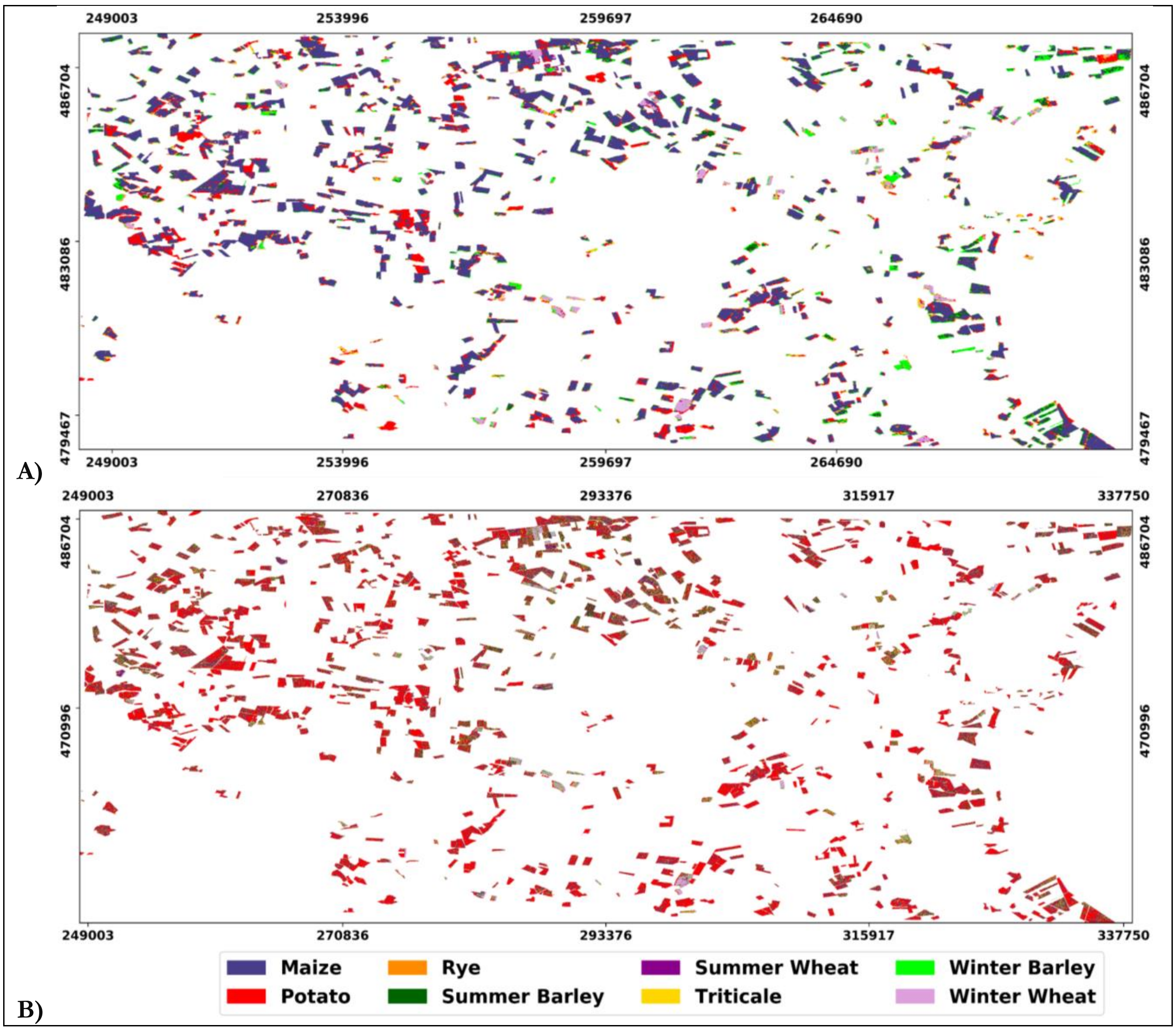

Figure 7: Crop type maps from twDTW using (A) Sentinel-1 VV+VH (B) TerraSAR-X HH polarimetry

4.3. Accuracy using Derived Indices and Decomposed Features

As indicated in Table 3, the inclusion of generated features from polarimetric bands (Ratio, mRVI, and DPSVI) has resulted in a minor improvement on overall accuracy and moderately improves user accuracy and producer accuracy of Rye, Summer Wheat, and Summer Barley and producer accuracy of Maize. As per this, the producer accuracy of Maize, Rye, and Summer Barley is increased from 73.60%, 2.44% and 17.14% to 77.05%, 7.32%, and 20.0% respectively while Rye, Summer Barley, Winter Barley, and Winter Wheat user accuracy is improved from 4.55%, 8.22%, 8.0% and 17.57% to 8.11%, 11.29%, 8.52%, and 23.53% respectively. The overall accuracy has also shown an improvement of around 2.0%. The spatial distribution of crops presented in Figure 8A indicates that similar to results obtained from VV+VH backscatter, Maize and Potato are predicted as dominant crops.

Table 3: Classification from Sentinel-1 backscatter, derived indices and decomposed features using twDTW

Input	**Sentinel-1 (Backscatter coefficient + derived indices)**									
					Reference					
Crop	Maize	Potato	Rye	Summer Barley	Summer Wheat	Triticale	Winter Barley	Winter Wheat	Sum	UA
Maize	826	23	3	2	0	2	0	0	856	96.50
Potato	111	22	0	6	1	1	0	0	141	15.60
Rye	30	0	3	2	1	1	0	0	37	8.11
Summer Barley	42	1	2	7	3	7	0	0	62	11.29
Summer Wheat	8	0	1	5	2	1	0	4	21	9.52
Triticale	36	3	8	6	1	5	0	0	59	8.47
Winter Barley	13	1	7	4	3	10	5	0	43	11.63
Winter Wheat	6	1	17	3	2	8	2	12	51	23.53
Sum	1072	51	41	35	13	35	7	16	1270	
PA	77.05	43.14	7.32	20.00	15.38	14.29	71.43	75.00		
Overall Accuracy		69.45								
Input	**Sentinel-1 (backscatter coefficient + derived indices + decomposed features)**									
Crop	Maize	Potato	Rye	Summer Barley	Summer Wheat	Triticale	Winter Barley	Winter Wheat	Sum	UA
Maize	438	18	2	4	0	1	0	0	463	94.60
Potato	148	8	1	2	3	2	0	0	164	4.88
Rye	53	0	5	2	1	6	0	1	68	7.35
Summer Barley	35	3	2	0	1	1	1	1	44	0.00
Summer Wheat	99	2	12	7	3	4	1	8	136	2.21
Triticale	37	2	1	2	0	2	0	0	44	4.55
Winter Barley	95	4	11	14	4	15	3	0	146	2.05
Winter Wheat	167	14	7	4	1	4	2	6	205	2.93
Sum	1072	51	41	35	13	35	7	16	1270	
PA	40.86	15.69	12.20	0.00	23.08	5.71	42.86	37.50		
Overall accuracy		36.61								

Inclusion of decomposed polarimetric features from $H - A - \alpha$ decomposition together with backscatter coefficient and derived radar indices has provided an overall accuracy of 36.61% (Table 3) which is far lower than overall accuracy results obtained by using only polarimetric bands and polarimetric bands with generated indices which are 67.48% and 69.45% respectively (Table 2).

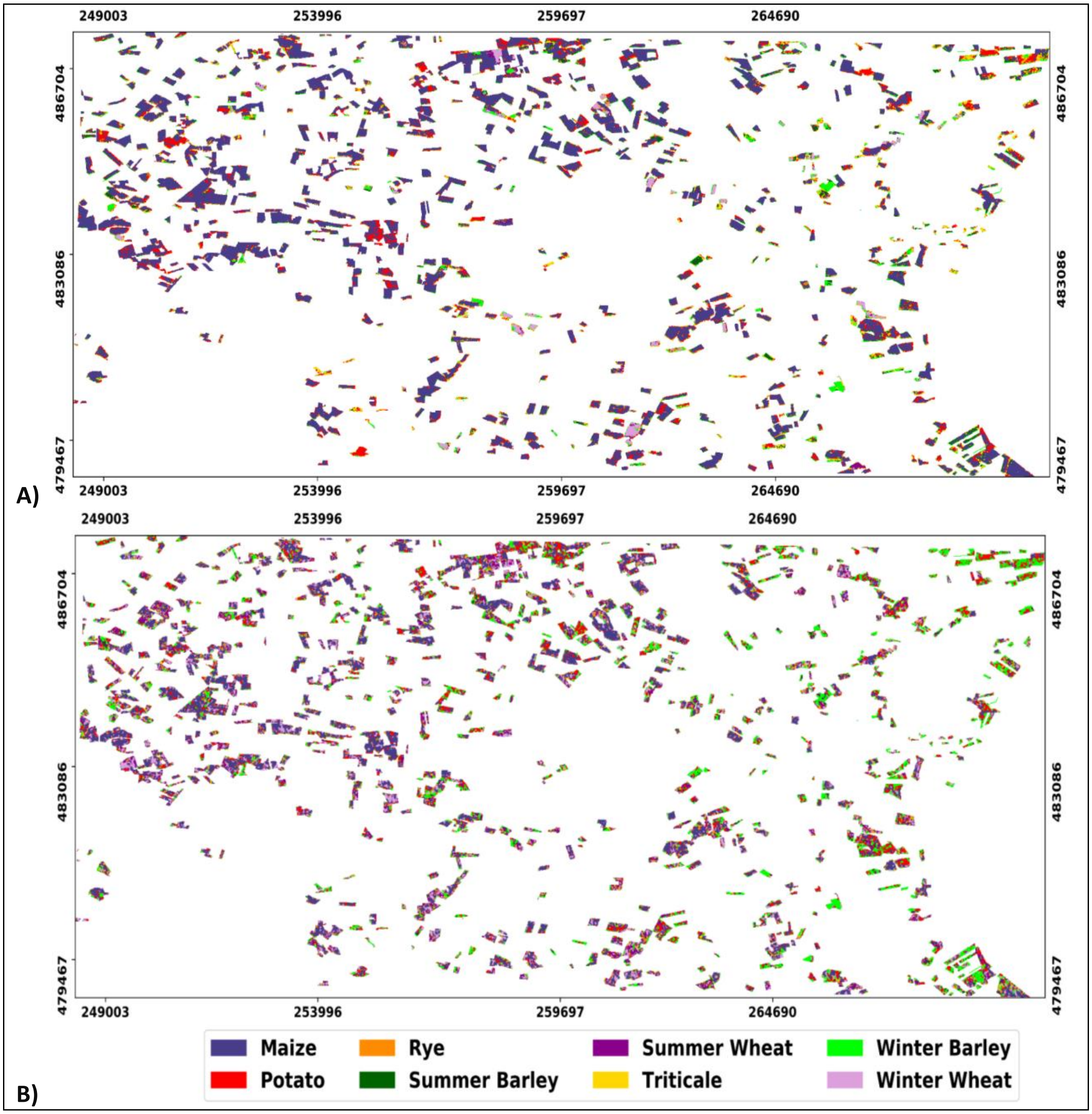

Figure 8: Crop type map from Sentinel-1 VV+VH with (A) derived indices and (B) Derived indices and $\boldsymbol{H} - \boldsymbol{A} - \boldsymbol{\alpha}$ features using twDTW

One situation which is also consistent with this classification strategy is strong confusion between Maize and Potato. In contrast to other classification approaches presented in Tables 2 and 3, with this classification approach which is done using twDTW with the inclusion of backscatter and decomposed features, Maize has shown strong confusion with Winter Wheat, Winter Barley, and Rye. Concerning the crispness and within-class stability of classified crops, the spatial plot presented in Figure 12 indicates that within Maize crop fields, the presence of other misclassified crop types yielded a noisy feature on classified maps. Furthermore, on this classification approach, Winter Wheat was also overpredicted and populated within other classes.

4.4. Crop Type Map Using Variable Time Dynamic Time Warping

Rather than using a single temporal lag during computation of logistic time weight, the application of crop-specific temporal lag per crop by accounting dominant crops calendar has yielded comparable results with twDTW outputs. As shown in Table 4, the classifier (vtwDTW) using Sentinel-1 backscatter has yielded an overall accuracy of 56.85%. Potato has shown a producer accuracy of 80.39% followed by Winter Wheat, Maize, and Winter Barley which is 75.0%, 59.98%, and 57.14% respectively. From a user accuracy, it can be evident that the model overpredicts Potato that from a total of predicted 315 Potato points only 41 were correctly predicted and the remaining 258 points were potato fields followed by Summer Barley and Winter Wheat. Similar to the twDTW counterpart, on outputs of vtwDTW, Rye crop is strongly confused with Winter Wheat. As shown in Figure 9A, similar to classification results obtained from the twDTW model (Table 2 & Figure 7A), with vtwDTW, Maize, and Potato crops dominate the landscape.

When input datasets were replaced by time series TerraSAR-X HH polarimetric bands, the overall accuracy for vtwDTW is lower than a classification approach that takes Sentinel-1 dual polarimetry bands (VV + VH) counterpart (Table 4). Similar to other classification approaches, there is still a strong mixing between Potato and Maize. When the results of Table 4 are compared with Table 2 which is the output from twDTW using TerraSAR-X HH backscatter, the result from vtwDTW is almost comparable. As indicated in Table 4, this classification approach also underpredicts Maize that from 1072 reference points, only 283 points correctly coincided with predicted points. Additionally, as shown in Figure 9B, this classification approach has overpredicted Potato though Mazie is the dominant crop in reference dataset (Appendix 1B).

Table 4: Accuracy from Sentinel-1 VV+VH and TerraSAR-X HH polarimetry using vtwDTW

Reference										
Input	**Sentinel-1 Polarimetry (VV +VH) bands**									
Crop	Maize	Potato	Rye	Summer Barley	Summer Wheat	Triticale	Winter Barley	Winter Wheat	Sum	UA
Maize	643	6	2	1	0	0	0	0	652	98.62
Potato	258	41	2	7	1	2	0	4	315	13.02
Rye	5	0	1	1	0	1	0	0	8	12.5
Summer Barley	124	2	3	15	1	9	1	0	155	9.68
Summer Wheat	10	0	1	1	2	0	0	0	14	14.29
Triticale	12	1	5	3	1	4	0	0	26	15.38
Winter Barley	11	1	6	1	3	8	4	0	34	11.76
Winter Wheat	9	0	21	6	5	11	2	12	66	18.18
Sum	1072	51	41	35	13	35	7	16	1270	
PA	59.98	80.39	2.44	42.86	15.38	11.43	57.14	75.00		
Overall Accuracy		56.85								
Input	**TerraSAR-X HH**									
Crop	Maize	Potato	Rye	Summer Barley	Summer Wheat	Triticale	Winter Barley	Winter Wheat	Sum	UA
Maize	283	11	5	4	1	5	0	0	309	91.59
Potato	590	34	4	2	2	3	0	0	635	5.35
Rye	14	0	6	0	0	2	0	2	24	25
Summer Barley	32	4	1	13	2	7	0	0	59	22.03
Summer Wheat	43	1	7	6	3	3	0	1	64	4.69
Triticale	97	1	2	6	2	9	0	1	118	7.63
Winter Barley	4	0	4	1	1	2	3	0	15	20
Winter Wheat	9	0	12	3	2	4	4	12	46	26.09
Sum	1072	51	41	35	13	35	7	16	1270	
PA	26.4	66.67	14.63	37.14	23.08	25.71	42.86	75.0		
Overall accuracy		28.58								

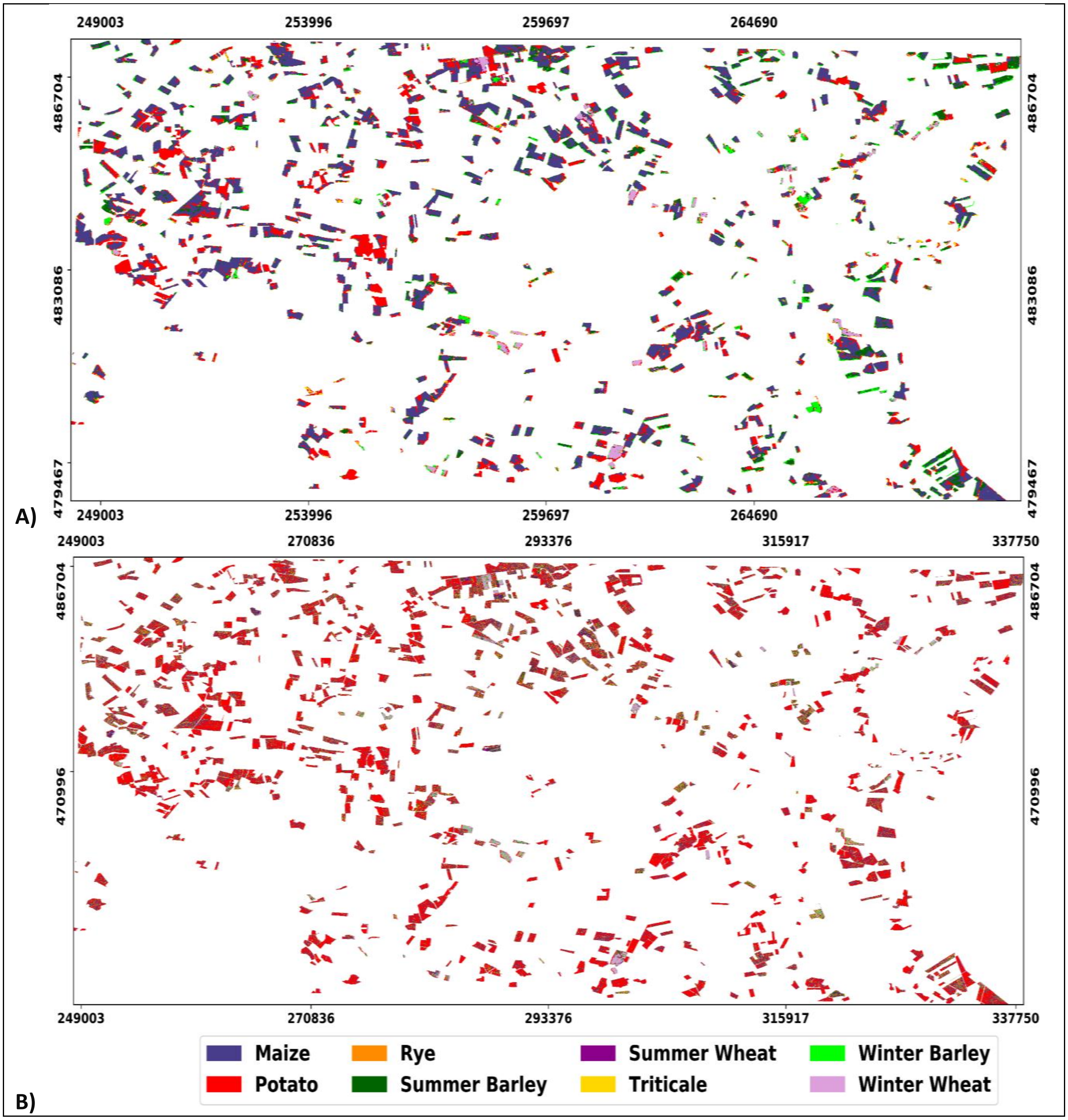

Figure 9: Crop type maps from vtwDTW using (A) Sentinel-1 VV+ VH and (B) TerraSAR-X HH backscatter

4.5. Crop Type Map Using AMSS

Instead of using Euclidean distance for dynamic time warping distance computation, implementing angular distance has not improved the crop type prediction accuracy of the model. As presented in Table 5, Angular Metric for Shape Similarity (AMSS) using Sentinel-1 VV+VH bands has yielded an overall accuracy of 37.5%.

The model extremely underpredicts Maize and overpredicts Potato. It has also significantly underpredicted winter crops. The Maize crop is highly confused with Potato. Relative to its twDTW and vtwDTW counterparts, with this classification model, Maize crop is highly confused with Rye crop. As shown in Figure 10A, Rye crop is spread all over the landscape where it is mixed within Maize crops. This yields a noisy crop type map. With a similar classification approach, when the input image was replaced with time-series TerraSAR-X HH backscatter, the overall classification output is only 10.63% which is far lower from its Sentinel-1 counterpart. In its worst case, it extremely omits Maize crop where its producer accuracy reaches to 8.96%. It made a false inclusion of a large amount of Maize to Potato class followed by Summer Wheat which can be evidenced from the confusion matrix (Table 5). Almost all Maize plots were dominated by Summer Wheat and Potato followed by Winter Wheat (Fig. 10B).

Table 5: Classification accuracy from AMSS with Sentinel-1 VV+VH and TerraSAR-X HH

Sentinel-1 VV+VH										
Input	**Reference**									
	Maize	Potato	Rye	Summer Barley	Summer Wheat	Triticale	Winter Barley	Winter Wheat	Sum	AU
Maize	406	17	6	6	1	3	1	0	440	92.27
Potato	359	29	3	8	2	6	0	0	407	7.13
Rye	110	1	5	1	1	0	0	1	119	4.20
Summer Barley	12	1	0	3	2	0	0	0	18	16.67
Summer Wheat	83	1	9	7	3	15	2	5	125	2.4
Triticale	36	0	0	3	0	4	0	1	44	9.09
Winter Barley	66	1	18	7	4	7	4	9	116	3.45
Winter Wheat	0	1	0	0	0	0	0	0	1	0.0
Sum	1072	51	41	35	13	35	7	16	1270	
PA	37.87	56.86	12.2	8.57	23.08	11.43	57.14	0		
Overall accuracy		35.75								
Input	**TerraSAR-X HH**									
	Maize	Potato	Rye	Summer Barley	Summer Wheat	Triticale	Winter Barley	Winter Wheat	Sum	UA
Maize	96	4	2	1	1	1	0	3	108	88.89
Potato	423	20	10	5	3	8	3	5	477	4.19
Rye	15	0	1	1	1	4	0	0	22	4.55
Summer Barley	83	1	4	4	1	6	0	3	102	3.92
Summer Wheat	245	16	6	16	6	7	1	2	299	2.01
Triticale	107	3	4	3	1	4	0	0	122	3.28
Winter Barley	14	0	4	1	0	2	2	1	24	8.33
Winter Wheat	89	7	10	4	0	3	1	2	116	1.72
Sum	1072	51	41	35	13	35	7	16	1270	
PA	8.96	39.22	2.44	11.43	46.15	11.43	28.57	12.5		
Overall accuracy		10.63								

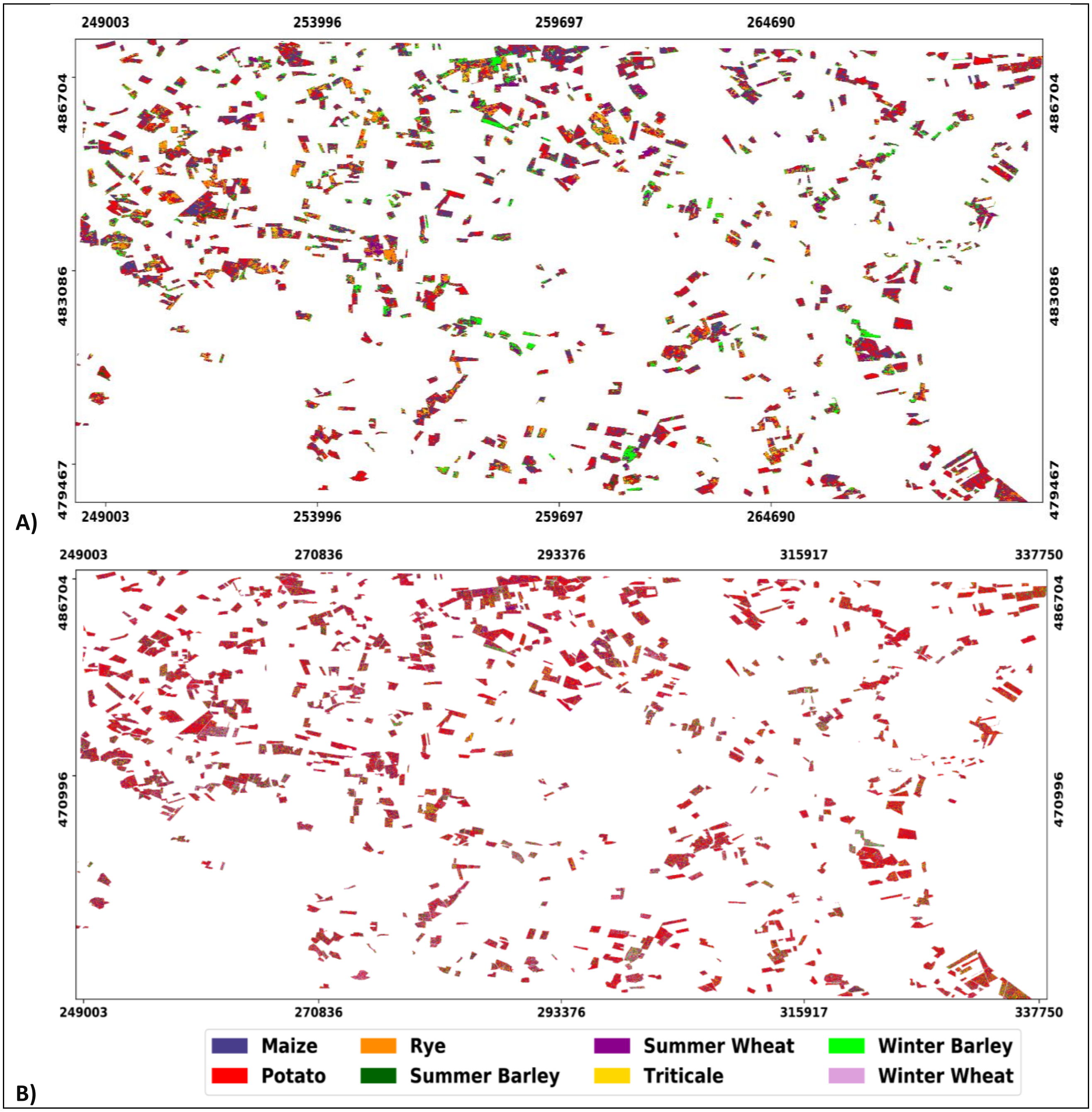

Figure 10: Crop type maps from AMSS using (A) Sentinel-1 VV+VH and (B) TerraSAR-X HH backscatter

4.6. Crop Type Mapping from Combined Sentinel-1 and TerraSAR-X Imagery

By applying a rule-based ensemble classifier on crop type maps obtained from twDTW, crop type prediction was improved than results obtained from TerraSAR-X and Sentinel-1 alone. As presented in Table 6, an ensemble classifier from twDTW has yielded an overall accuracy of 77.09% which is almost greater than all classifiers done without integrating both datasets (Table 7 for comparison with others). The model has also reduced the level of confusion between Maize and Potato crop to a certain degree. The error of omission and commission was also reduced for Maize where it has resulted in 84.51% and 94.47% of producer and user accuracy respectively. For Potato crop, though its producer accuracy is relatively improved, its user accuracy is still minimal which was caused by its confusion with Maize and Summer Barley. There is also a strong confusion between winter grains (Triticale, Rye, Winter Wheat, and Winter Barley). Among available grains, Rye has relatively better user accuracy and Winter Barley has better producer accuracy. As indicated in Figure 11A, an ensemble classifier from twDTW has provided more homogeneous classified crop fields than individual classification outputs obtained from a similar model.

Similar to the ensemble twDTW counterpart, an ensemble classifier from vtwDTW has resulted in a classification accuracy significantly better than individual outputs from Sentinel-1 and TerraSAR-X alone. As given in Table 6, an ensemble classifier has brought an overall classification accuracy of around 69.69%. Except for minor deviations in level of accuracy, the pattern of confusion between Potato and Maize and confusion among Winter grains is almost similar to the twDTW counterpart. The model also shows more overprediction of Potato than an ensemble classifier from twDTW. This can also be clearly seen in Figure 11B where Potato plots populate the landscape in the results of the vtwDTW ensemble classifier more than is the case for twDTW (Fig. 11A).

The ensemble classifier from AMSS has achieved overall accuracy which is significantly higher than individual Sentinel-1 and TerraSAR-X classification results from the same classification approach. As indicated in Table 12, the classifier resulted in an overall accuracy of 51.81%. Relative to ensemble counterparts of twDTW and vtwDTW classification approaches, an ensemble AMSS has resulted in lower user and producer accuracy. Concerning the level of improvement achieved when implementing a rule-based ensemble classifier, AMSS has resulted in more improvement than twDTW and vtwDTW counterparts. Compared to ensemble versions of twDTW and vtwDTW within boundary confusion of crops was higher in AMSS (Fig. 11C).

Table 6: Classification accuracy from rule-based ensemble classifiers using Sentinel-! And TerraSAR-X

Model					**twDTW**					
					Reference					
Crop	Maize	Potato	Rye	Summer Barley	Summer Wheat	Triticale	Winter Barley	Winter Wheat	Sum	UA
Maize	906	12	14	13	2	10	0	2	959	94.47
Potato	108	36	1	3	1	1	0	1	151	23.84
Rye	1	0	5	0	0	0	0	1	7	71.43
Summer Barley	5	0	0	9	1	4	0	0	19	47.37
Summer Wheat	22	2	3	5	4	1	0	0	37	10.81
Triticale	13	0	1	2	1	6	0	1	24	25.00
Winter Barley	17	1	10	2	2	11	6	4	53	11.32
Winter Wheat	0	0	7	1	2	2	1	7	20	35.00
Sum	1072	51	41	35	13	35	7	16	1270	
PA	84.51	70.59	12.20	25.71	30.77	17.14	85.71	43.75		
Overall accuracy		77.09								
Model					**vtwDTW**					
Crop	Maize	Potato	Rye	Summer Barley	Summer Wheat	Triticale	Winter Barley	Winter Wheat	Sum	UA
Maize	811	7	12	12	1	7	0	1	851	95.30
Potato	211	41	2	3	1	1	0	4	263	15.59
Rye	4	0	5	0	0	0	0	1	10	50.00
Summer Barley	3	1	0	9	1	3	0	0	17	52.94
Summer Wheat	15	1	4	2	4	7	1	0	34	11.76
Triticale	21	0	1	5	1	4	0	1	33	12.12
Winter Barley	6	1	10	2	3	11	5	3	41	12.20
Winter Wheat	1	0	7	2	2	2	1	6	21	28.57
Sum	1072	51	41	35	13	35	7	16	1270	
PA	75.65	80.39	12.20	25.71	30.77	11.43	71.43	37.50		
Overall accuracy		69.69								
Model					**AMSS**					
	Maize	Potato	Rye	Summer Barley	Summer Wheat	Triticale	Winter Barley	Winter Wheat	Sum	UA
Maize	622	32	12	13	3	13	2	6	703	88.48
Potato	221	13	0	3	0	4	1	0	242	5.37
Rye	107	4	8	3	2	1	0	1	126	6.35
Summer Barley	57	1	4	6	3	5	0	1	77	7.79
Summer Wheat	20	0	1	3	2	2	0	0	28	7.14
Triticale	28	1	6	3	2	5	1	1	47	10.64
Winter Barley	15	0	8	4	1	3	2	7	40	5.00
Winter Wheat	2	0	2	0	0	2	1	0	7	0.00
Sum	1072	51	41	35	13	35	7	16	1270	
PA	58.02	25.49	19.51	17.14	15.38	14.29	28.57	0.00		
Overall accuracy		51.81								

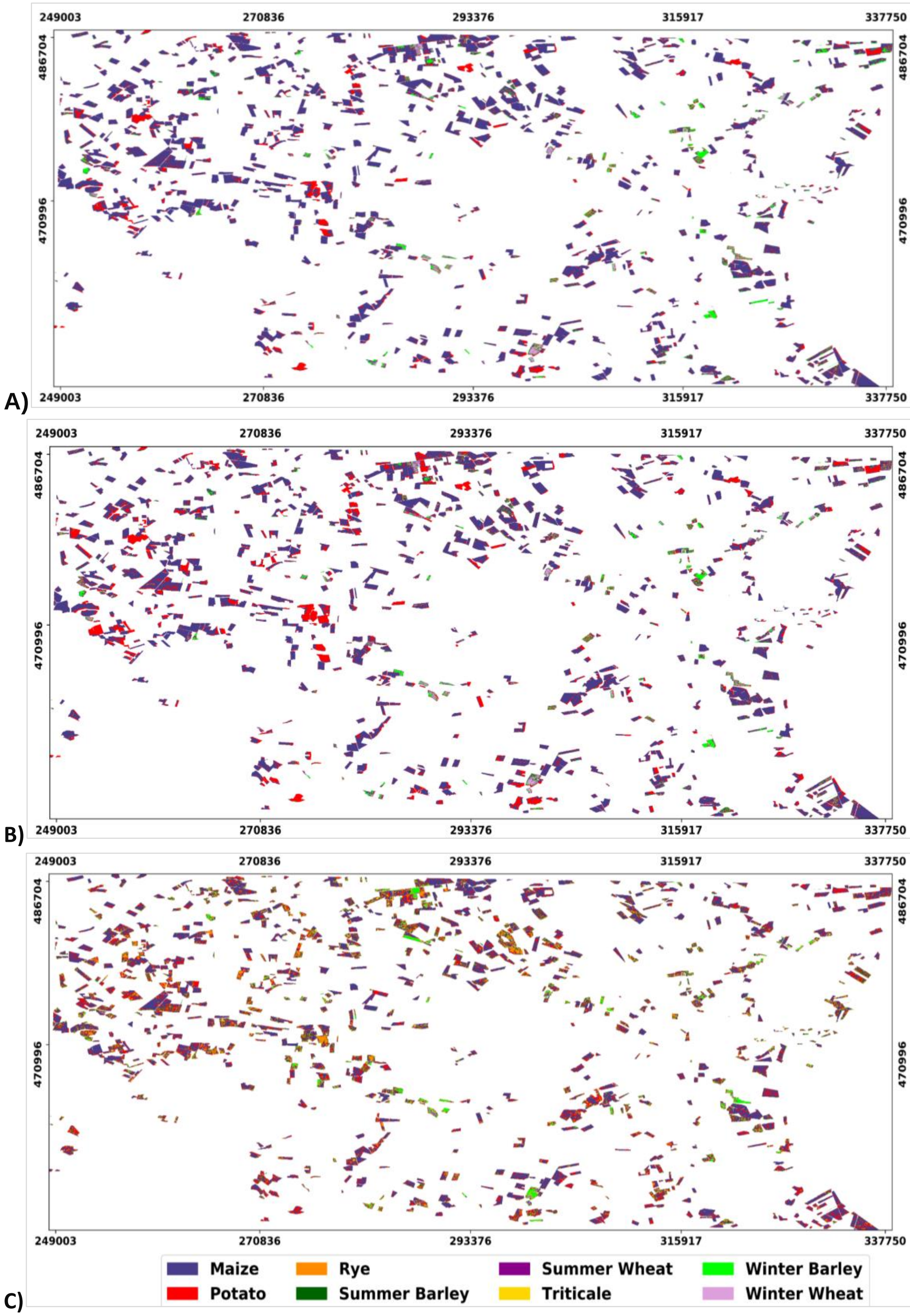

Figure 11: Crop type maps from ensemble classifiers of (A) twDTW (B) vtwDTW and (C) AMSS

Table 7: Summary of user, producer and overall accuracy for all models and classification approaches

Model	twDTW				twDTW		twDTW		vtwDTW				AMSS				Ensemble twDTW		Ensemble vtwDTW		Ensemble AMSS	
Input	Sentinel-1 VV+VH		TerraSAR-X HH		Sentinel-1 VV+VH + Indices		Sentinel-1 (VV+VH) + Indices + Decomposed		Sentinel-1 VV+VH		TerraSAR-X HH		Sentinel-1 VV+VH		TerraSAR-X HH		Both		Both		Both	
Accuracy	UA	PA	UA	PA	UA	PA	UA	PA	UA	PA	UA	PA	UA	PA	UA	PA	UA	PA	UA	PA	UA	PA
Maize	97.7	73.6	91.5	27.1	96.5	77.1	94.6	40.9	98.6	60.0	91.6	26.4	92.3	37.9	88.9	9.0	94.5	84.5	95.3	75.7	88.5	58.0
Potato	20.8	72.6	5.2	62.8	15.6	43.1	4.9	15.7	13.0	80.4	5.4	66.7	7.1	56.9	4.2	39.2	23.8	70.6	15.6	80.4	5.4	25.5
Rye	4.6	2.4	30.4	17.1	8.1	7.3	7.4	12.2	12.5	2.4	25.0	14.6	4.2	12.2	4.6	2.4	71.4	12.2	50.0	12.2	6.4	19.5
Summer Barley	8.2	17.1	13.8	31.4	11.3	20.0	0.0	0.0	9.7	42.9	22.0	37.1	16.7	8.6	3.9	11.4	47.4	25.7	52.9	25.7	7.8	17.1
Summer Wheat	8.7	15.4	4.1	15.4	9.5	15.4	2.2	23.1	14.3	15.4	4.7	23.1	2.4	23.1	2.0	46.2	10.8	30.8	11.8	30.8	7.1	15.4
Triticale	11.9	14.3	8.1	28.6	8.5	14.3	4.6	5.7	15.4	11.4	7.6	25.7	9.1	11.4	3.3	11.4	25.0	17.1	12.1	11.4	10.6	14.3
Winter Barley	8.0	57.1	18.8	42.9	11.6	71.4	2.1	42.9	11.8	57.1	20.0	42.9	3.5	57.1	8.3	28.6	11.3	85.7	12.2	71.4	5.0	28.6
Winter Wheat	17.6	81.3	28.3	81.3	23.5	75.0	2.9	37.5	18.2	75.0	26.1	75.0	0.0	0.0	1.7	12.5	35.0	43.8	28.6	37.5	0.0	0.0
Overall Accuracy	67.5		29.0		69.5		36.6		56.9		28.6		35.8		10.6		77.1		69.7		51.8	

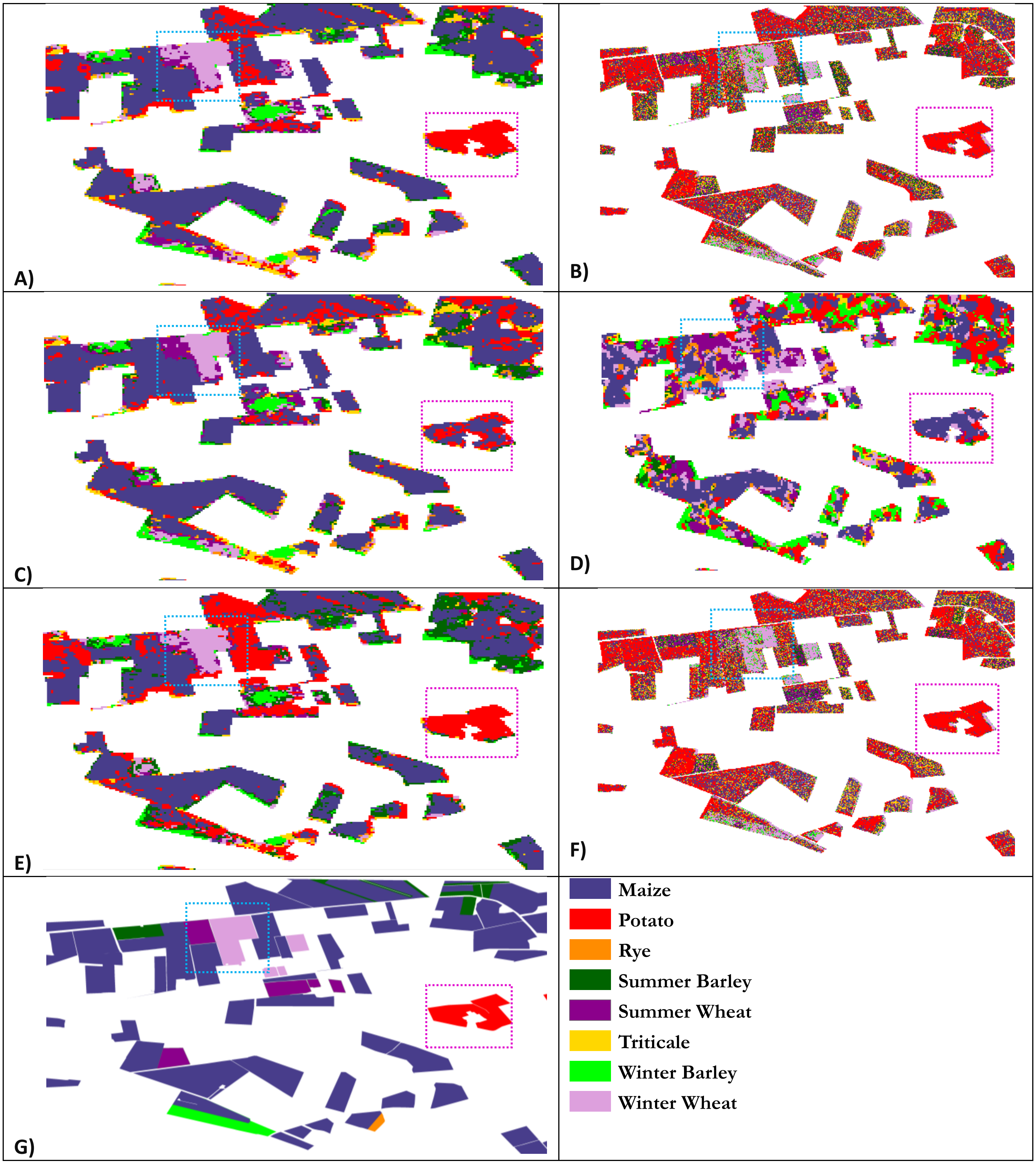

Figure 12: Subsets of analysis results from twDTW using (A) Sentinel VV+VH, (B) TerraSAR-X HH, (C) Sentinel VV+VH + Indices (D) Sentinel-1 VV+VH + Indices + Decomposed; and analysis results from vtwDTW using (E) Sentinel VV+VH, (F) TerraSAR-X HH; and (G) Reference polygons from BRP

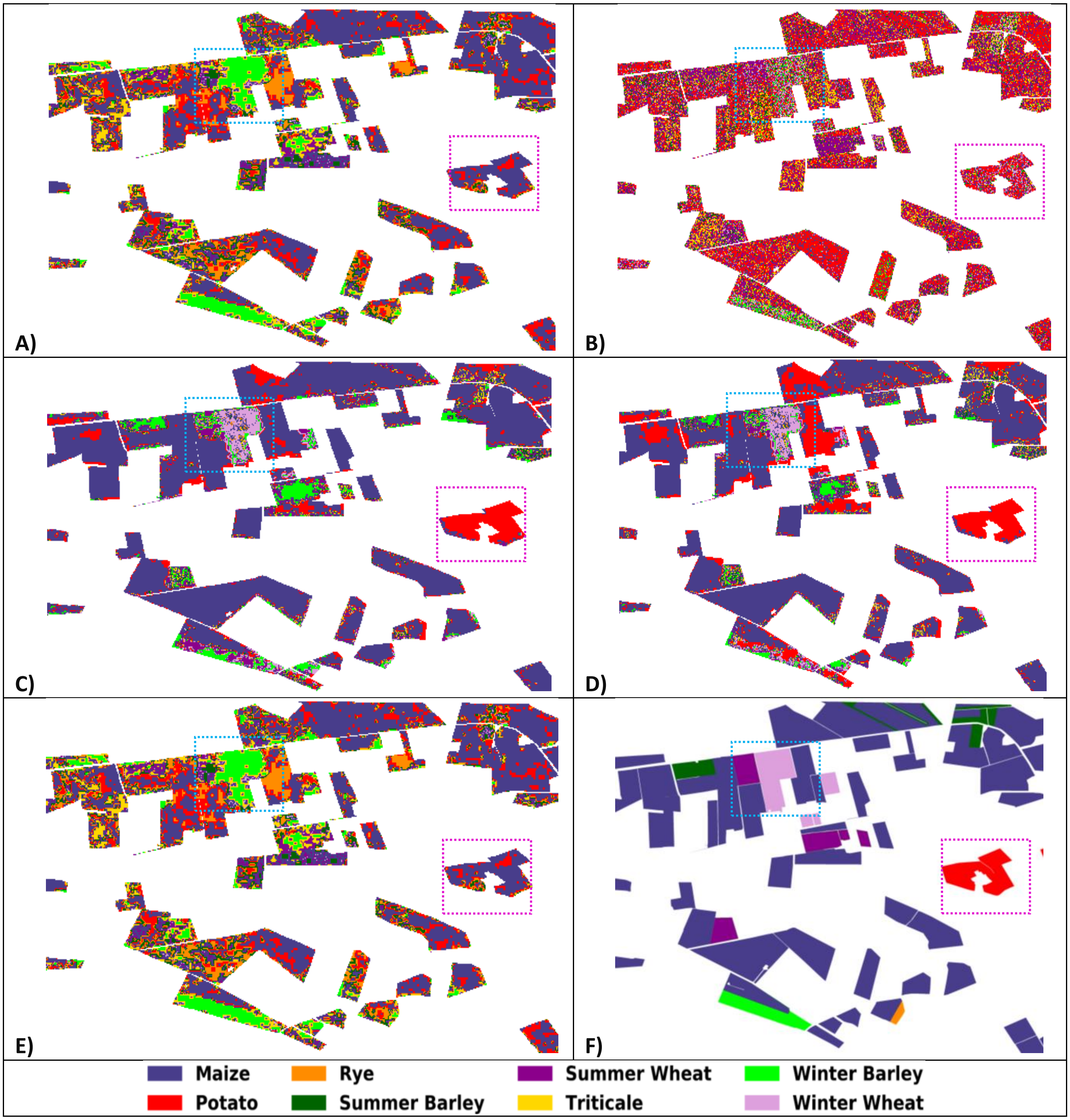

Figure 13: Subsets from AMSS using (A) Sentinel-1 VV+VH and (B) TerraSAR-X HH; and analysis results from ensemble classifiers (C) twDTW, (D) vtwDTW, and (E) AMSS; and (F) Reference polygons from BRP

In both Figures 12 and 13, dotted blue rectangles indicate performance of different models in a more complex areas dominated with summer and winter wheat with Maize crops while pink dotted rectangles indicates their performance in areas that have only Potato crop.

5. Discussion

5.1. How do crops respond to the SAR signal?

One of the identifiable patterns in the backscatter response of crops is the profile of Maize and Potato. From early January to the end of April the two crops experience a decreasing backscatter. This is the season where field preparation is the main activity for summer crops. The variability of backscatter before the emergence of these crops can be attributed to surface roughness resulting from tillage operation during field preparation (Mc Nairn & Brisco, 2004). As indicated in Figure 4, the end of April and early May is the probable sowing season of Maize and Potato where these crops start sprouting. As crop leaves and stalks can better scatter than bare surfaces, the backscatter coefficient starts to increase (Ferrazzoli et al., 1992). Regeneration of vegetation converts the scattering mechanism from the surface to double bounce scattering. The backscatter increases up to some point and then starts to diminish. As investigated by Macelloni, Paloscia, Pampaloni, Marliani, & Gai (2001) when LAI of broad leave crops increases, their backscatter increases to some point. Similarly, Liao et al., 2018 have reported that vegetation cover (FVC) has also responded positively to the backscatter coefficient for a crop to cover up to 75% of the surface. Not only the LAI but also the crop height can have a similar role for the state backscatter coefficient. As indicated in Nasirzadehdizaji et al. (2019), when the Maize height increases, its sensitivity to the backscatter coefficient increases as well up to the points when at a later stage the sensitivity is insignificant and even backscatter coefficient starts to drop. In both Sentinel-1 VV + VH and TerraSAR-X (HH) bands, Potato backscatter is greater than Maize backscatter. Though both crops have broad leaves, the geometry and density of leaves for both crops are not the same. Maize crop experience relatively regular, less dense, and either vertically or horizontally oriented leaves governed by its development, whereas Potato has randomly oriented, densely covering the surface which can scatter more incident energy than Maize from its full canopy. This result supports experimental findings reported by Khabbazan et al. (2019) that the Potato scattering is more intense than Maize counterpart across the growing period. It is reported that Sentinel-1 VV polarization can penetrate Maize canopies that it is sensitive for under canopy surface soil moisture (El Hajj, Baghdadi, Bazzi, & Zribi, 2019). This interaction of the radar signal with a moist surface can result in less return of incident radar signal to the sensor.

It should also be noted that Maize and Potato crops are planted in rows. Both Potato and Maize can completely cover the surface with dense leaves but maximum scattering is higher for Potato than for Maize. Row orientation of crops to radar look direction can affect radar signal return (Batlivala & Ulaby, 1976). Accordingly, by putting an assumption as rows could be parallel oriented with the longest side of the farm plot, backscatter differences among farm plots with different orientation angels both for Maize and Potato crops were also examined. Results from sample plots have indicated that there were no major differences in radar signal return from farm plots of a similar crop with different orientation angle (Appendix 3B).

Contrary to Maize and Potato, Summer Wheat and Summer Barley experience a decreasing backscatter until a point where Maize and Potato backscatter start to fall. This is mainly, attributed to the similarity of geometry and orientation of leaves. As a detailed study done by Macelloni et al. (2001) demonstrated, the backscattering coefficient of crops with narrow dimension and vertically oriented leaves, e.g. Wheat and Barley, starts to drop as soon as their leaf area index start to increase. The drop in return signal from narrow-leaf crops during plant development was also contributed by crop height. A detailed study by Sonobe, Tani, Wang, Kobayashi, & Shimamura (2014) using the TerraSAR-X band has reported the significant inverse relationship of Winter Wheat height and backscattering coefficient from its surface. As indicated in Figures 6A and 6B, after a continuous decrease in the backscatter signal, there is an abrupt increase in Summer Wheat and Summer Barley. This is mainly because as leaves become dry, shrink in dimension, reduced water content resulted in scattering from the stem and even from the surface. Contrary to this, winter grains Rye, Triticale, Winter Wheat have shown increasing backscatter in the summer season. This is mainly because the harvest of crops from the field can switch electromagnetic interaction to surface scattering. Instead of an expected increase in the backscattering coefficient like Winter Wheat, Winter Barley has shown a diminishing trend. This can be attributed to the existence of surface moisture, replanting of short-cycle crops after harvest, and or regeneration of weeds and grasses in the field which foster absorption of an incoming radar signal. More importantly, the backscatter difference in Winter Wheat and Winter Barley may be related to the residue and residue soil moisture after harvest (Mc Nairn, Duguay, Boisvert, Huffman, & Brisco, 2001) and subsequent tillage operations if there are any (Mc Nairn & Brisco, 2004). A clearer pattern is observed in the TerraSAR-X HH temporal profile (Fig. 6C). At the start, there is a strong variability of the backscatter coefficient which can be attributed to surface roughness from tillage and soil moisture which relatively affects the TerraSAR-X HH band (Aubert et al., 2011). After April, winter crops experience a slightly increasing pattern while summer crops have relatively higher backscatter but which is slowly decreasing. Crops that have similar leaf structure and orientation can only be identified if their growing season is different. The main issue here that should be taken into consideration is that for DTW, rather than separability of crops in the feature space, separability in terms of shape matters more. That is why the shape similarity of Maize and Potato temporal profiles create confusion on classification.

5.2. Performance of Dynamic Time Warping for crop type mapping in smallholder farming areas

As indicated in Tables 2 and 7, accuracy results from Sentinel-1 polarimetry bands (VV+VH) are higher than for TerraSAR-X single polarimetry (HH) bands using twDTW. It is clear from these results that, dual polarimetric data can yield better prediction than single polarimetry for crop types mapping in smallholder farming areas. The confusion matrix tables in both classification strategies show a strong mixing between Maize and Potato. As parametric classifiers' performance mainly depends on the separability of generated signatures at the feature space, DTW and its variates mainly depend on shape separability of generated temporal profiles. As depicted in Figures 6A and 6B, the temporal profiles of Maize and Potato are better separable in Sentinel-1 VV and VH bands in terms of its amplitude, but the separability of their temporal profile in TerraSAR-X HH band (Fig. 6C), is very poor. Even from May 12 to June 3, their temporal profile was quite similar. This creates a strong confusion of the two crops in classifiers that use backscatter from TerraSAR-X HH polarization as an input.

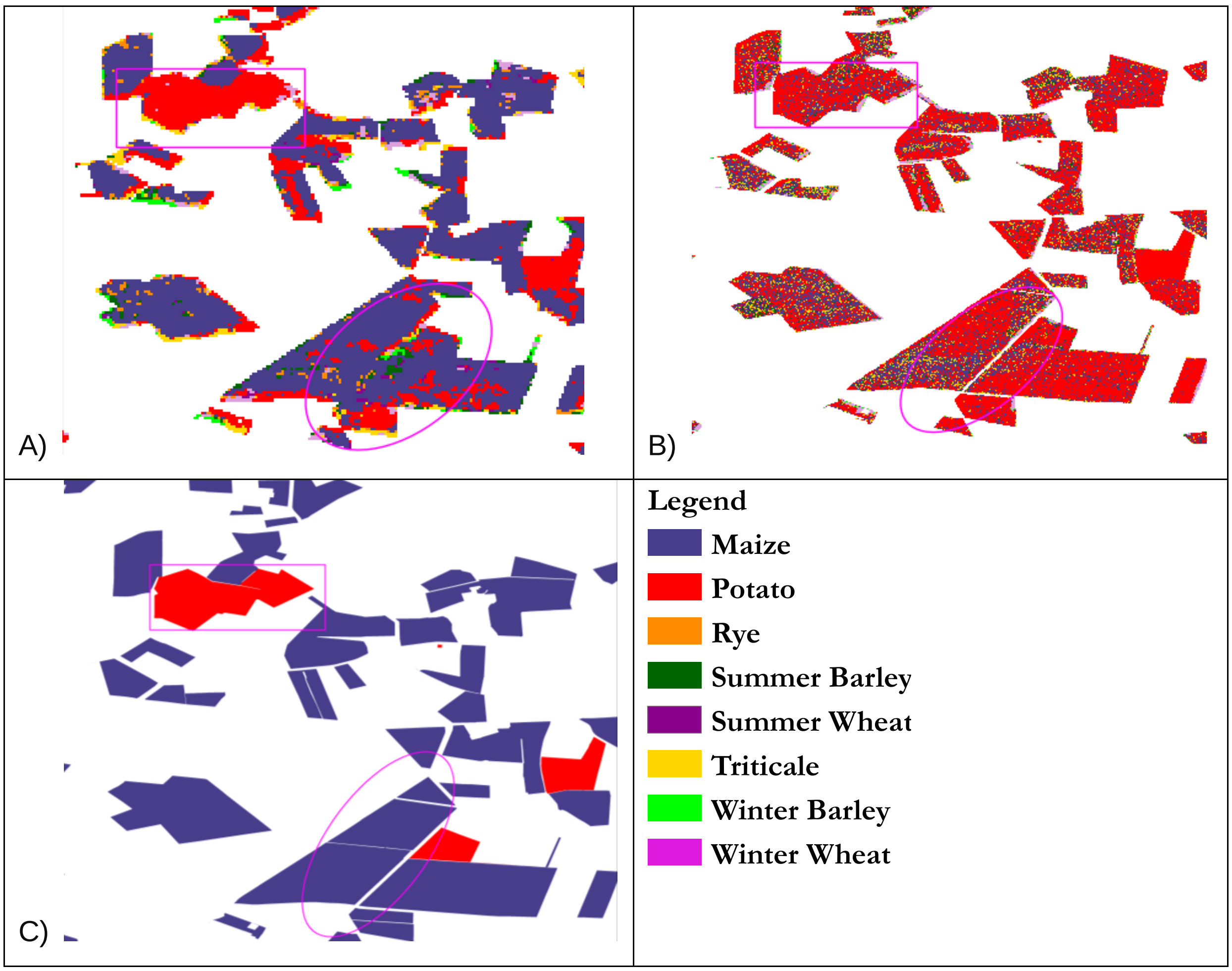

Figure 14: Subset of classification outputs from twDTW (A) Sentinel-1 (VV+VH), (B) TerraSAR-X HH and C) Reference polygons from AAN

The subset of classified images from twDTW (Figure 14) using Sentinel-1 and TerraSAR-X indicates that strong within polygon mixing is more prevalent on the classification map from TerraSAR-X than on that from Sentinel-1 (see also Figs. 12 & 13 to compare with other classifiers). Though the performance of Sentinel-1 is better than TerraSAR-X for twDTW at the current study, the accuracy reports from both Sentinel-1 and

TerraSAR-X images were much lower than those of other studies using time series optical images (Belgiu & Csillik, 2018; Csillik et al., 2019). Despite the fact that these studies come up with better classification accuracies than the current study, two things should be taken into consideration. First, the authors have utilized optical datasets, which can be subjected to varying cloud cover depending on the location. Second, their test sites were not dominated by smallholder farming areas where the level of complexity is fairly different. The only frame of reference to compare the results of the current study from twDTW using SAR imagery in the smallholder farming area is Li & Bijker (2019) where they have classified short cycle vegetables in Indonesia. Their result using SPRING strategy is better than the performance of the current study. Though it was not implemented on a family of DTW classifier, a comparable study in terms of the utilized dataset was done by Danilla, Persello, Tolpekin, & Bergado (2017) using different classification models in Flevoland, the Netherlands. Accordingly, reported overall accuracies from their study using SVM, RF and Convolutional Neural Networks (CNN) were lower than accuracies of this study. It should be noted that after classification, they have done post-processing smoothing to augment accuracy which is not done in the current study for a reason. Their study has also noted the existence of strong confusion of crops that have a similar physical structure: e.g. Summer cereals with Winter cereals and Potatoes with Beets. This agrees with the findings of the current study. It should also be noted that their study is tested in a newly developed farming area with regular and fairly large farm plots which are a less complex area than the current study site.

In both classification strategies, except for Potato and Maize, most crops have a relatively small amount of user and producer accuracy. As validation samples were taken proportionate to existing polygons, there is an imbalance between dominant crops (Maize, Potato) and cereals. By speculating that smaller user and producer accuracy could be attributed to the class imbalance in validation samples, the effect of this imbalance was further analyzed. Accordingly, the accuracy implications of some sample balancing strategies such as Minority Oversampling (MOS), Synthetic Minority Oversampling (SMOTE), Adaptive Synthetic Minority Oversampling (ADASYN) and SMOTE followed with cleaning using Tomek links (SMOTETomek) were investigated. Results (Appendix 3E) indicated that the creation of synthetic samples results in moderate improvement in user accuracy without any changes in producer accuracy. These results have also come up with a trade-off of reducing overall accuracy. After claiming similar results, rather than increasing the number of the samples representing the minority classes, Yang & Boryan (2019) have recommended the selection of proportionate samples during the training phase for good accuracy performance. Though class imbalance has an impact on prediction accuracy of less frequent classes (Waldner, Fritz, Di Gregorio, & Defourny, 2015) at the training phase, it was strongly argued that DTW is robust to class imbalance if it is supported with an appropriate sampling strategy to select training samples (Dau et al., 2018). As the current study has implemented a two-stage sampling technique where stratified sampling is part of the sampling process, spatial and scattering characteristics of each crop are well represented. As a matter of fact, every classification model is not always sensitive to class imbalance. For example, Ustuner, Sanli, & Abdikan (2016) have reported the robustness of different models for class imbalance. In their study, RF and Artificial Neural Network (ANN) were found sensitive while SVM is too robust for class imbalance. It was concluded that if land cover classes were naturally overlapping, managing class imbalance may not always bring significant classification accuracy improvements (Bogner, Seo, Rohner, & Reineking, 2018).

Though image smoothing (speckle reduction) in the spatial domain is done using improved Lee sigma filter, still there exists a strong variation of backscatter in the spatial domain which can confuse the classifier. This is mainly prevalent in the TerraSAR-X image time series. Taking this into consideration, the other two pre-processing approaches that can properly handle significant within plot backscatter irregularities were also investigated. The first is the segmentation of TerraSAR-X images using Mean Shift segmentation (Comaniciu & Meer, 2002). The second one was a direct replacement of the values of each pixel within a given boundary by the mean backscatter value of a parcel. Both procedures were followed by the generation of temporal profile and subsequently classification. From these analyses, two major outcomes were realized. First, they improve the overall accuracy of up to 10% (Appendix 3D). The second one was that these strategies have reduced within polygon mixing of crop types where it yields within polygon homogenous maps (Appendix 3C). In general, results from these strategies shows that integration of segmentation strategy as part of the pre-processing operation can provide better results than findings obtained based on the pixel-wise analysis. This can be useful especially in areas where there is a possibility of getting dual or quad-pol polarimetric images with a high spatial resolution like TerraSAR-X and RADARSAT. For the current study, further analysis has also been done to check whether the confusion or mixing of these crops has any spatial pattern. The result of the uncertainty analysis has indicated the absence of any distinct spatial pattern (Appendix 3A). Accordingly, the mixing is random in space and that the confusion may mainly be attributed to crop-related attributes rather than to any other biophysical variables like soil moisture and soil type or topography.

5.3. Did the inclusion of radar indices and decomposed features improve accuracy?

This question is mainly answered by using Sentinel-1 datasets as TerraSAR-X has only one polarimetry band (HH). The results presented in Table 3, have revealed that the inclusion of derived features (Ratio, mRVI, DPSVI) from dual polarimetry VV +VH bands has resulted in minor improvements to a range of 2.0%. Though not for a model with DTW variates, a study done by Lee et al. (2001) has stated that inclusion of polarimetric phase differences (ratio) between co-polarized and cross-polarized bands does not improve classification accuracy. This is because it is not as strong as the difference (ratio) between co-polarized VV and HH bands. Blaes et al. (2006), in a study dedicated to the investigation of the sensitivity of ratio between VV and VH bands for Maize crop monitoring, has indicated that ratio band in C-SAR imagery immediately stagnates when the

LAI is above some point and it is recommended to use this feature to monitor the emergence of Maize as it is sensitive at a seedling phase of crops. Contrary to derived indices, the inclusion of polarimetric features from $H - A - \alpha$ decomposition did not improve accuracy and even it has degraded classification accuracy of the classifier. Similar to this, Li & Bijker (2019) have also reported that the inclusion of decomposed polarimetric features from Sentinel-1 did not improve the mapping accuracy of vegetables in smallholder farming areas of Indonesia. This is mainly because the decomposition is not fully polarimetric. Therefore, it cannot completely characterize the inherent scattering characteristics of crops. A study by Ji & Wu (2015) has stated that dual polarimetry images either in HH+HV or VV+VH are not capable of efficiently identifying surface and multiple (volumetric) scattering characteristics as they lack one co-polarized band either HH or VV based on cross-polarized configuration.

In addition to the nature of utilized polarimetric bands, smaller accuracy levels can also be related to crop vegetative characteristics. Different crops that have similar geometry and leaf morphology like Wheat, Barley, and Triticale in one cluster and Maize and Potato in other clusters are responding similarly to the incident SAR signal. Therefore, decomposed features for the crops under similar leaf category have similar inherent scattering characteristics, so decomposed features are less likely to add any improvement in classification accuracy. As discussed in Section 5.1, the scattering mechanism of a specific crop type starts from the surface to double bounce and immediately turns to volumetric scattering where backscatter saturates for a long period as LAI, canopy cover, and crop height peaks. A study dedicated to using compact polarimetry with power decomposition by Kumar, Mandal, Bhattacharya, & Rao (2020) has firmly supported this argument. Accordingly, for a Cotton crop that is planted in rows for an extended period, surface and volumetric scattering dominate almost with an equal share of contribution for total scattering, whereas in case of sugar cane, volumetric scattering is the dominant one. Here it can be argued that polarimetric decomposition can be used for identification of target features from its inherent scattering characteristics (like surface from standing tree or standing tree from crops) but in time series domain, many targets can have similar scattering characteristics for an extended period if other factors remain constant (a specific crop after it fully covers the surface towards its harvest or annual trees with matured biomass).

5.4. Did accounting for changes in planting dates improve accuracy?

It is strongly believed that crops complex phenology governed by planting date should be accounted for during classification. Accordingly, variable time lag was used for computation of logistic time weight and subsequent classification (Appendix 2C for algorithmic procedure). As per this, the analysis results presented in Table 4 for Sentinel-1 (VV+VH) and TerraSAR-X HH band were promising but lower than the twDTW counterpart. Here some conditions might limit the performance of vtwDTW. The first one is related to the correct representation of crop calendars (planting dates). Crop calendar utilized for this study is compiled from the literature that is more or less generic and there may be some deviations with specific study plots. The second one is related to crops that have double or triple cropping season. These crops can create inconsistency (like Potato as presented in Figure 4, which calls for a further detailed experimental study that records each phenological event of a crop within a growing period. Thirdly, as presented in Figure 4, crops that have similar leaf structures have also almost a similar growing period. This creates a complete confusion on the separability of their scattering profile in the temporal domain.

5.5. Did changing distance measure improve classification accuracy?

To investigate a DTW approach with an angular distance measure reported in the signal processing community, AMSS for Sentinel-1 and TerraSAR-X SITS was tested. Results presented in Tables 5 have shown that the performance of AMSS is relatively much lower than the original version of twDTW and vtwDTW. As stated in a detailed study by Nakamura et al. (2013), though AMSS is insensitive for outliers in the data series, it is not performing very well for each dataset. Accordingly, from 21 datasets tested in their study, it has performed best for only 10 datasets with varied accuracy. With little modification of the AMSS shape similarity computation procedure, Choi & Kim (2018) have reported outstanding performance of the model for gesture recognition as compared with other DTW variates. Except for an unpublished article by Teke & Yardımcı (2019), which reported excellent performances of AMSS for crop type mapping using the Sentinel-2 and Landsat 8 dataset, there is no study to compare results of the current study done either using optical or radar imagery. Though full parametrization of the model is not provided in methodological part of the study, the current study has also tested a different DTW distance computation method which mainly follows an ensemble approach of distance computation with non-isometric data transformation presented in Górecki & Łuczak (2014) and a more detailed companion study by Górecki & Łuczak (2015). The results from this approach using the TerraSAR-X HH dataset (Appendix 3F) were not better than overall accuracy from AMSS. More importantly, it was realized that, as an ensemble approach undergoes a series of data transformations and computations of many distances, it is computationally demanding especially for optimal selection of hyper parameters.

5.6. Did integrated use of Sentinel-1 and TerraSAR-X improve accuracy?

Among all three classification models investigated (twDTW, vtwDTW, and AMSS), the rule-based ensemble classifier, which integrates individual classification results from both Sentinel-1 and TerraSAR-X has yielded the best results. The level of improvement is much pronounced in AMSS followed by vtwDTW which relatively showed the performance almost comparable with the original twDTW counterpart. Ensemble classifier has also moderately reduced within polygon mixing of crops than using either only Sentinel-1 or TerraSAR-X (Figs. 12 and 13). An ensemble version of twDTW has yielded more homogenous crop fields (Fig.15 and Fig 19A for a detailed subset view). There are two reasons why the ensemble model outperformed the other two individual approaches. The first is the classifier favors a crop type from the classified map with a better user and producer accuracy which adds robustness for a model. The second is it benefits from the synergy of high spatial resolution TerraSAR-X with single polarimetry and repeatedly observed dual polarimetry Sentinel-1 images that have dual polarimetric bands.

By considering results from backscatter responses of crops for SAR signal presented in Section 4.1 and consecutive discussions provided in section 5.1, three of the models (twDTW, vtwDTW, and AMSS) were rerun by merging grains growing in winter season to class 'Winter grains' and grains growing in summer season to a class 'Summer grains' while leaving Potato and Maize as individual classes. Classification results presented in Table 8 indicates that merging the crops with similar leaf structure, morphology, and growth pattern within a similar season has improved the classification accuracy. Beyond improvements in overall classification accuracy, merging of grains has resulted in more homogenous crop fields than individual outputs. As indicated on subset maps (Fig 19), merging of crops with similar leaf structure from twDTW is more comparable with reference polygons. As indicated in Figures 16-18, Maize is predicted as a dominant crop in the landscape followed by Potato, similar to proportions that exist in reference polygons.

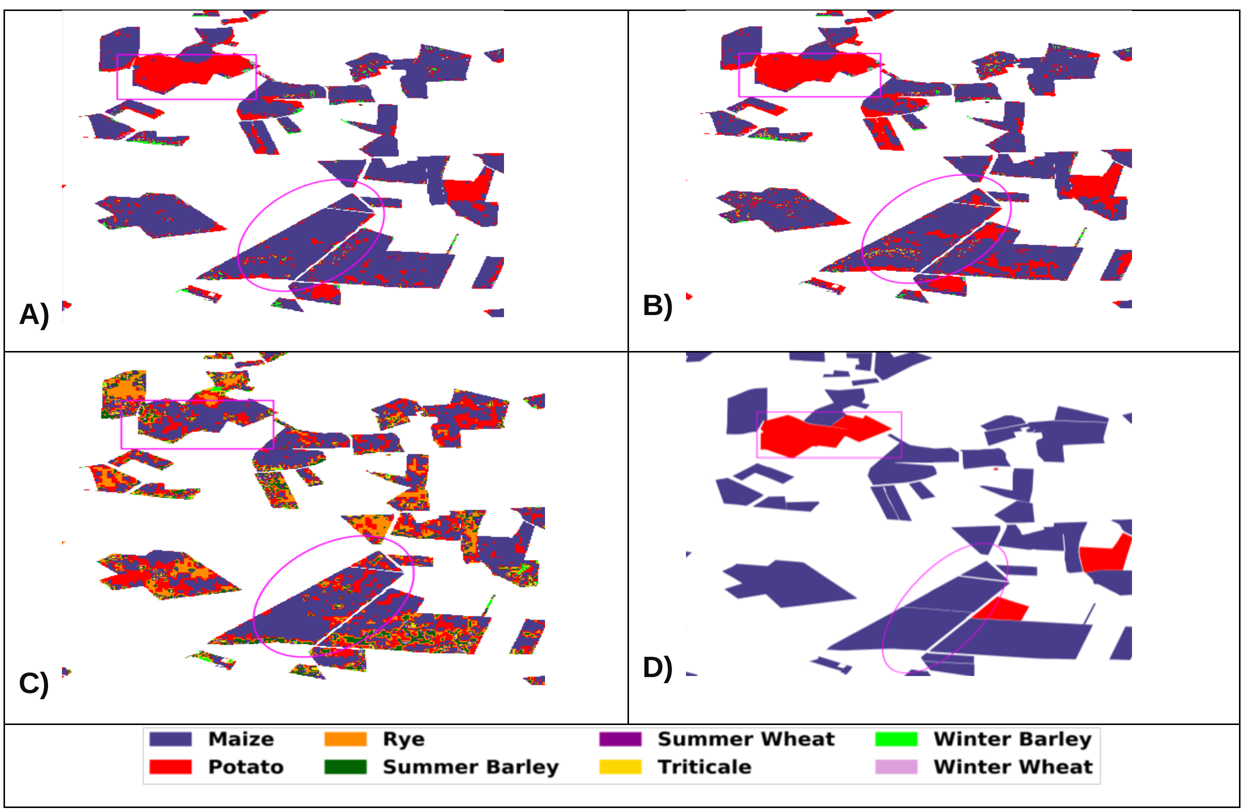

Figure 15: Subsets from ensemble classifiers (A) twDTW, (B) vtwDTW (C) AMSS and (D) Reference plots

Similar to the current study, a study done by Hütt & Waldhoff (2018) using dual polarimetric TerraSAR-X data with RF classifier has also reported better performance of their model after merging crops growing in winter season to generic class "Winter grains". The authors reported an improvement in the overall classification accuracy from 75% to 95%. Using TerraSAR-X spotlight data, Bargiel & Herrmann (2011) have adopted a hierarchical classification approach where the merging of crops with similar leaf structures provided better overall classification accuracy at test sites located in Germany and Poland. Firstly, they have classified landcover features into broad-leafed and fine-leafed classes. Following that, fine-leafed vegetation was further classified into grains and non-grains. Grains were also further refined into Winter and Spring grains. The authors have also found out that the confusion of fine-leaved grains with non-grain fine-leafed hedge grass has reduced overall accuracy in one test site. More importantly, the study has also demonstrated the benefit of treating crops with similar leaf structure into clusters than classifying individual crops for improved classification accuracy.

Table 8: Classification accuracy after merging winter and summer grains

Model	twDTW		vtwDTW		AMSS	
Crop type	PA	UA	PA	UA	PA	UA
Maiz	84.51	94.47	75.65	95.30	58.02	88.48
Potato	70.59	23.84	80.39	15.59	25.49	5.37
Summer Crops	39.58	33.93	33.33	31.37	29.17	13.33
Winter Crops	62.63	59.62	57.58	54.29	48.48	21.82
Overall Accuracy	80.55		72.83		54.88	

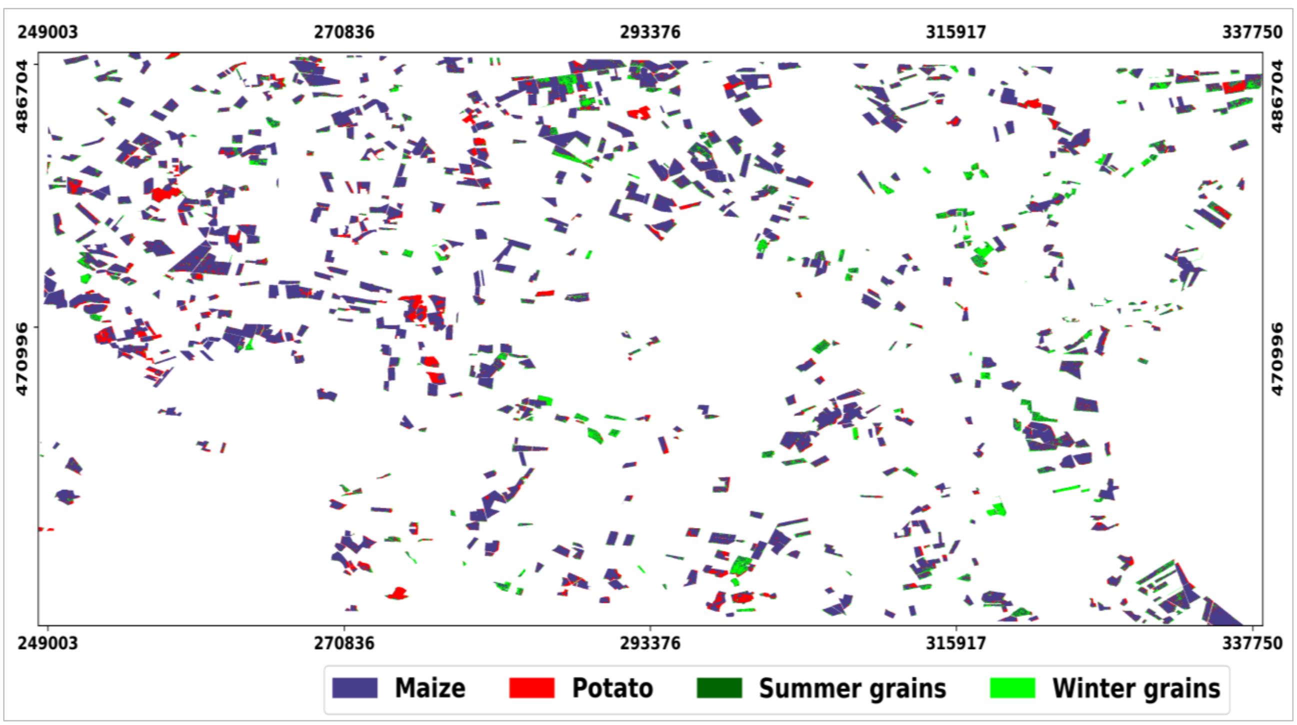

Figure 16: Crop type maps after merging grains from twDTW

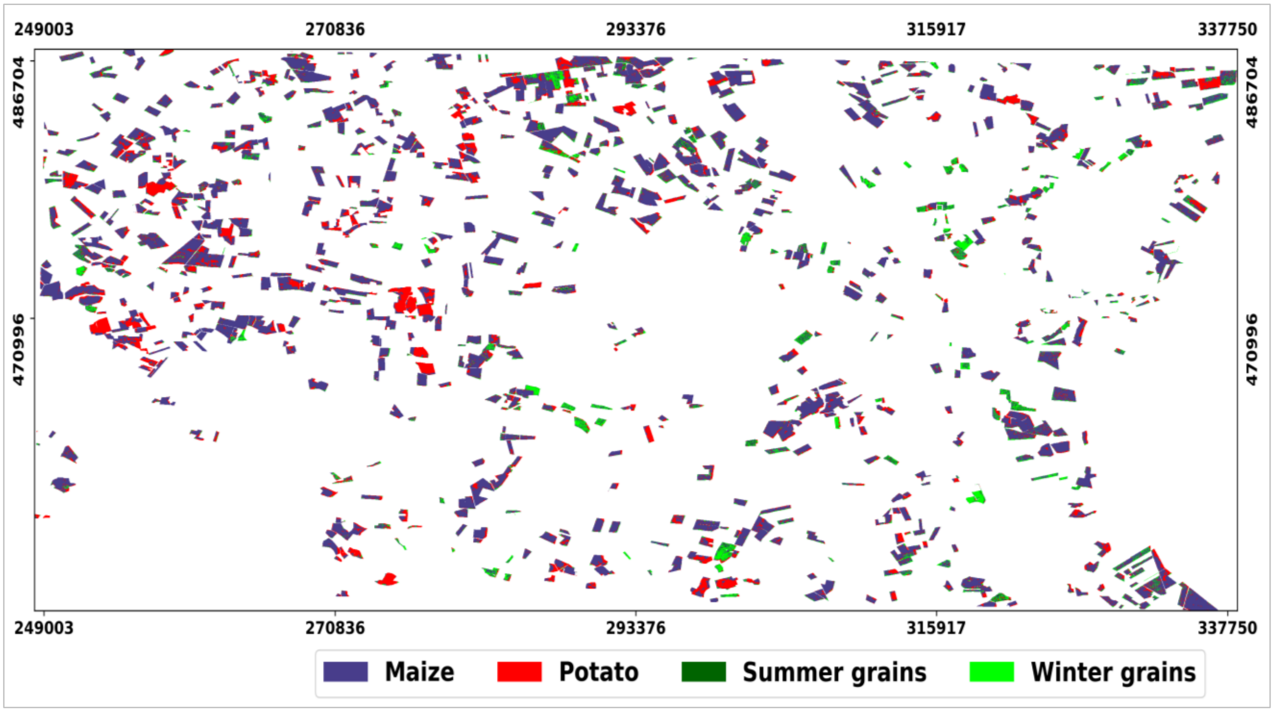

Figure 17: Crop type maps after merging grains from vtwDTW

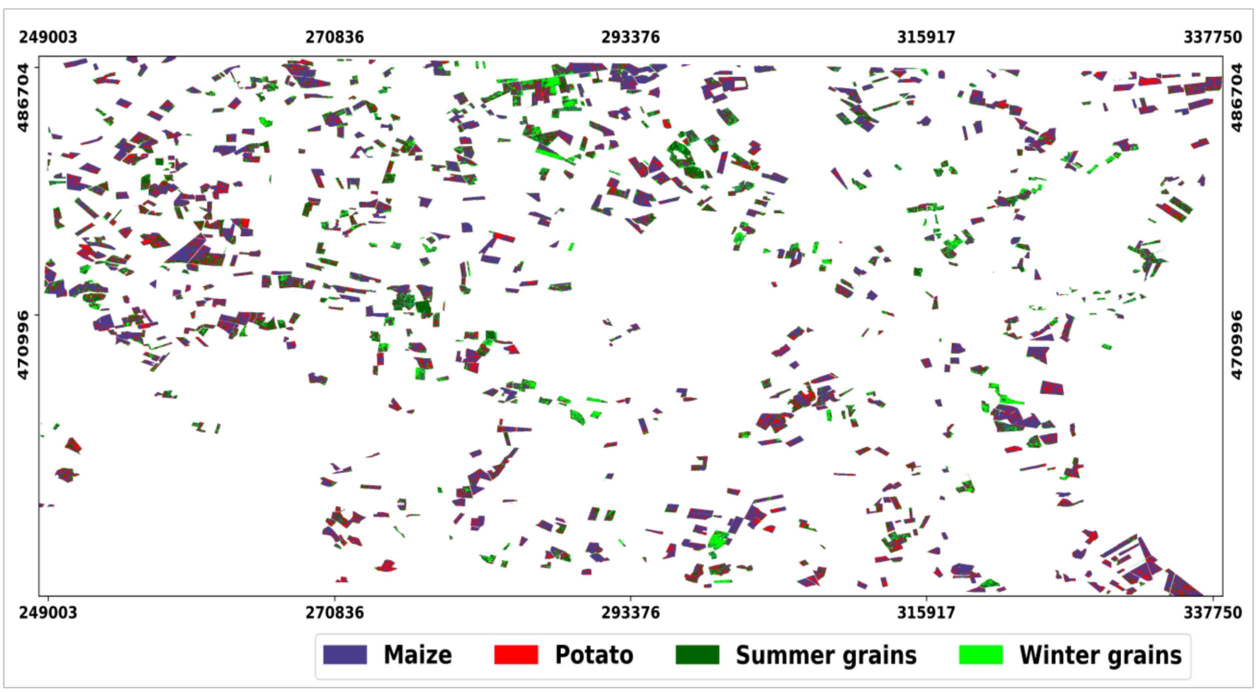

Figure 18: Crop type maps after merging grains from AMSS

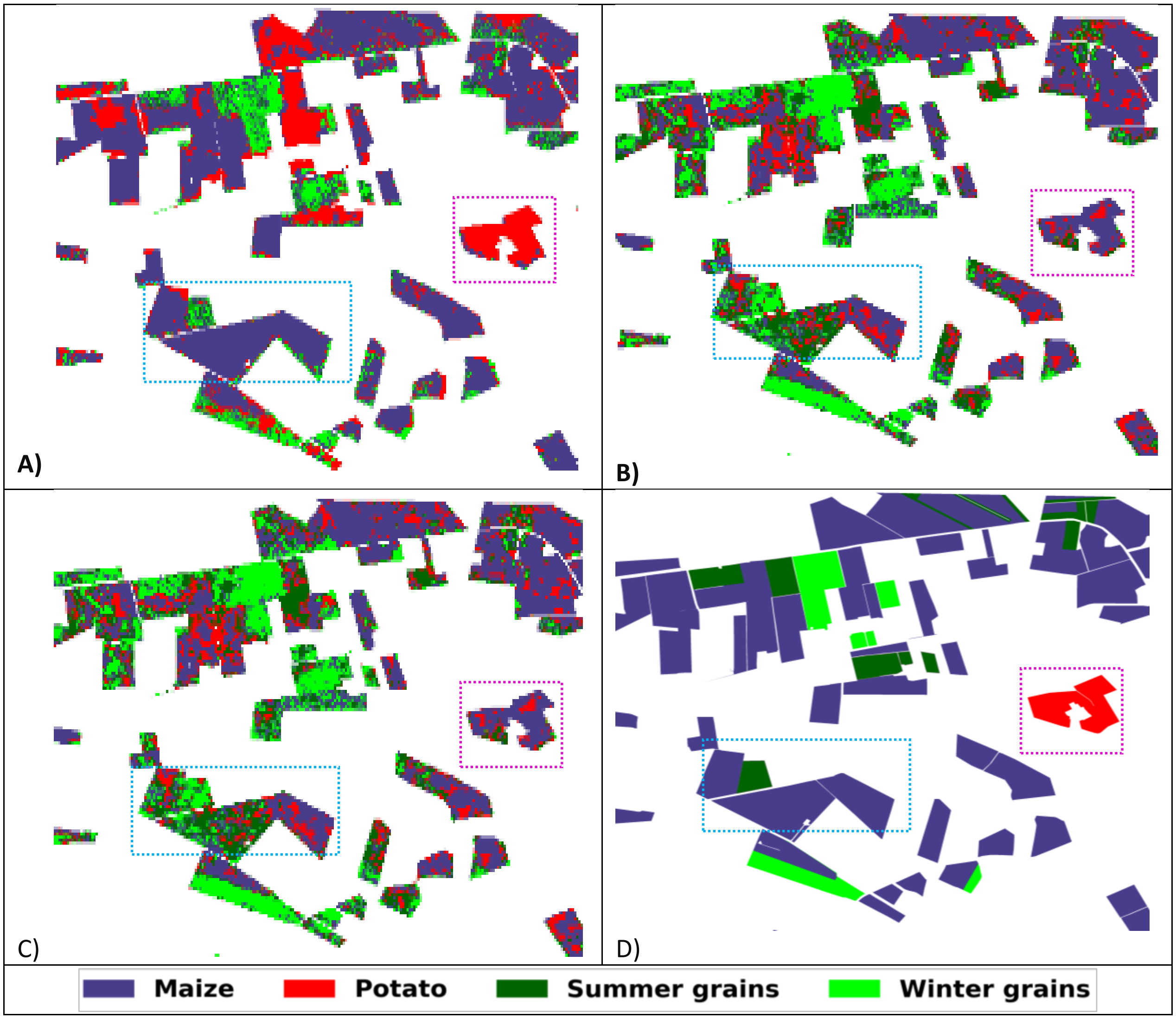

Figure 19: Subset crop type maps from merging of Similar grains (A) twDTW, (B) vtwDTW (C) AMSS and (D) Reference polygons from AAN; Dotted blue and pink rectangles indicate performance of models in Maize and Potato dominated areas respectively

6. Conclusions and Further Work

6.1. Conclusions

This study was dedicated to mapping crop types in smallholder farming areas using Sentinel-1 dual polarimetric and TerraSAR-X single polarimetric image time series using twDTW and some of its variates. Based on the undertaken analysis and discussion the following conclusions were drawn. In general, this study has investigated the potentials of SAR imagery for crop type mapping using twDTW. From the analysis of temporal profiles of dominant crops throughout their growing period, their responses for incident radar signal is different. Crops that have similar leaf structures and grow in a similar season have comparable backscattering temporal profiles. This creates confusion for classifiers which are mainly based on shape similarity of temporal profiles like twDTW, a model investigated by the current study. The twDTW has predicted dominant crop types in smallholder farming areas. The classification accuracy strongly varies between dual polarimetric Sentinel-1 time-series images and single polarimetric TerraSAR-X image time series. Dual polarimetric Sentinel-1 has performed better than single polarimetric TerraSAR-X for mapping crops. The inclusion of multi-polarization images has provided a better possibility of separating crop types using SAR data. Contrary to images sensed in the optical domain with multi and hyperspectral bands, radar image is sensed with either single, dual, or quad polarimetric mode, its number of bands per scene is limited. To overcome this limitation, the analysis of various derived vegetation indices and decomposed polarimetric features was considered in this work. The addition of radar vegetation indices and the polarimetric ratio has provided a small improvement in classification accuracy. Further inclusion of decomposed polarimetric features has resulted in classification accuracy lower than results obtained from original polarimetric bands and included vegetation indices. To account for the complex phenological pattern of crops in smallholder farming areas caused by the differences in the start of the growing period (planting date), a fixed time lag of twDTW is converted into variable time lag. The obtained result was comparable with those obtained by the twDTW. This study proved that the integrated use of Sentinel-1 dual polarimetric data and TerraSAR-X at object level has yielded better classification results than using the datasets alone. Integration approaches followed in this study can be ideal prototype research for areas where there is no frequent observation of high spatial resolution with fully polarimetric mode. By considering the strong confusion of crop temporal profile observed for crops with similar leaf structure and temporal growth patterns, merging of these crops into Winter and Summer grains has further improved the overall classification accuracy. This does not mean the study is free of limitations which calls for further work.

6.2. Future Work

To further refine the results and benefit from the potentials of the SAR image time series, the following issues could be further considered.

- The study has utilized ANN datasets for training and validation of the model. Except for the qualitative evaluation of the geometry of the polygon with OpenStreet Map, its attribute quality is not checked. Therefore, further studies should incorporate either mechanism on attribute quality checking or the use of reference datasets from field-based observations.
- This study proved that Sentinel-1 dual polarimetry outperformed TerraSAR-X single polarimetry (HH) for crop type mapping. A further study that incorporates either dual or quad polarimetry from TerraSAR-X or other datasets should also be investigated. This provides an opportunity to do polarimetric decomposition from high-resolution radar images for characterizing inherent scattering mechanisms.
- For vtwDTW, the crop calendar for this study is compiled from the literature. This could be more generic and there might be some deviations from the specific study site. To draw more robust conclusions on this model, further experimental study that incorporates field-based measurement of crop calendar i.e. record of major phenological events, and other parameters like surface and subsurface soil moisture.
- Smallholder farming areas are dominant in a different part of the globe especially in developing countries with various agro-ecologies. To test the robustness of the model at different landscapes, the transferability of the proposed classification model should also be tested at different smallholder farming areas.
- Accuracy results reported in this study were computed on the classified image without post-classification smoothing. This is mainly because smoothing can eliminate small and fragmented crop polygons that it causes unnecessary information loss. Some post-classification smoothing strategies that account prior class probabilities should also be done with caution.

References

Aubert, M., Baghdadi, N., Zribi, M., Douaoui, A., Loumagne, C., Baup, F., … Garrigues, S. (2011). Analysis of TerraSAR-X data sensitivity to bare soil moisture, roughness, composition, and soil crust. *Remote Sensing of Environment*, *115*(8), 1801–1810. https://doi.org/10.1016/j.rse.2011.02.021

Bargiel, D. (2017). A new method for crop classification combining time series of radar images and crop phenology information. *Remote Sensing of Environment*, *198*, 369–383. https://doi.org/10.1016/j.rse.2017.06.022

Bargiel, D., & Herrmann, S. (2011). Multi-temporal land-cover classification of agricultural areas in two European regions with high resolution spotlight TerraSAR-X data. *Remote Sensing*, *3*(5), 859–877. https://doi.org/10.3390/rs3050859

Batlivala, P. P., & Ulaby, F. T. (1976). Radar look direction and row crops. *Photogrammetric Engineering and Remote Sensing*, *42*(2), 233–238.

Bazzi, H., Baghdadi, N., El Hajj, M., Zribi, M., Minh, D. H. T., Ndikumana, E., … Belhouchette, H. (2019). Mapping paddy rice using Sentinel-1 SAR time series in Camargue, France. *Remote Sensing*, Vol. 11. https://doi.org/10.3390/RS11070887

Belgiu, M., & Csillik, O. (2018). Sentinel-2 cropland mapping using pixel-based and object-based time-weighted dynamic time warping analysis. *Remote Sensing of Environment*, *204*, 509–523. https://doi.org/10.1016/j.rse.2017.10.005

Berndt, D., & Clifford, J. (1994). Using dynamic time warping to find patterns in time series. *Workshop on Knowledge Knowledge Discovery in Databases*, *398*, 359–370. Retrieved from http://www.aaai.org/Papers/Workshops/1994/WS-94-03/WS94-03-031.pdf

Blaes, X., Defourny, P., Wegmüller, U., Vecchia, A. Della, Guerriero, L., & Ferrazzoli, P. (2006). C-band polarimetric indexes for maize monitoring based on a validated radiative transfer model. *IEEE Transactions on Geoscience and Remote Sensing*, *44*(4), 791–799. https://doi.org/10.1109/TGRS.2005.860969

Bogner, C., Seo, B., Rohner, D., & Reineking, B. (2018). Classification of rare land cover types: Distinguishing annual and perennial crops in an agricultural catchment in South Korea. *PLOS ONE*, *13*(1), 1–22. Retrieved from https://doi.org/10.1371/journal.pone.0190476

Bouman, B. A. M., & van Kasteren, H. W. J. (1990a). Ground-based X-band (3-cm wave) radar backscattering of agricultural crops. I. Sugar beet and potato; backscattering and crop growth. *Remote Sensing of Environment*, *34*(2), 93–105. https://doi.org/10.1016/0034-4257(90)90101-Q

Bouman, B. A. M., & van Kasteren, H. W. J. (1990b). Ground-based X-band (3-cm wave) radar backscattering of agricultural crops. II. Wheat, barley, and oats; the impact of canopy structure. *Remote Sensing of Environment*, *34*(2), 107–119. https://doi.org/10.1016/0034-4257(90)90102-R

Brink, L., Bus, C. B., Groten, J. A. M., Lotz, L. A. P., Timmer, R. D., & Wiel, C. C. M. van de. (2008). *Crop and cultivation description of sugar beet, maize and potato in relation to the distribution of genetic material*. Retrieved from https://library.wur.nl/WebQuery/wurpubs/fulltext/1015

Carfagna, E., & Gallego, F. J. (2005). Using Remote Sensing for Agricultural Statistics. *International Statistical Review*, *73*(3), 389–404. https://doi.org/10.1111/j.1751-5823.2005.tb00155.x

Chen, J., Jönsson, P., Tamura, M., Gu, Z., Matsushita, B., & Eklundh, L. (2004). A simple method for reconstructing a high-quality NDVI time-series data set based on the Savitzky-Golay filter. *Remote Sensing of Environment*, *9*, 332–344. https://doi.org/10.1016/j.rse.2004.03.014

Cheng, T. Y., Chu, C. Y., Chen, K. S., Yamaguchi, Y., & Lee, J. Sen. (2012). Time series SAR polarimetric analysis of rice crop based on four-component scattering decomposition. *IEEE Antennas and Propagation Society, AP-S International Symposium (Digest)*, 620–623.

Choi, H. R., & Kim, T. (2018). Modified Dynamic Time Warping Based on Direction Similarity for Fast Gesture Recognition. *Mathematical Problems in Engineering*, *2018*. https://doi.org/10.1155/2018/2404089

Cloude, S. R., & Pottier, E. (1997). An entropy based classification scheme for land applications of polarimetric SAR. *IEEE Transactions on Geoscience and Remote Sensing*, *35*(1), 68–78. https://doi.org/10.1109/36.551935

Comaniciu, D., & Meer, P. (2002). Mean shift: A robust approach toward feature space analysis. *IEEE Transactions on Pattern Analysis and Machine Intelligence*, *24*(5), 603–619. https://doi.org/10.1109/34.1000236

Congalton, R. G. (1991). A review of assessing the accuracy of classifications of remotely sensed data. *Remote Sensing of Environment*, *37*(1), 35–46. https://doi.org/10.1016/0034-4257(91)90048-B

Csillik, O., Belgiu, M., Asner, G. P., & Kelly, M. (2019). Object-based time-constrained dynamic time warping classification of crops using Sentinel-2. *Remote Sensing*, *11*(10). https://doi.org/10.3390/rs11101257

Czuchlewski, K. R., Weissel, J. K., & Kim, Y. (2003). Polarimetric synthetic aperture radar study of the Tsaoling landslide generated by the 1999 Chi-Chi earthquake, Taiwan. *Journal of Geophysical Research: Earth Surface*, *108*(F1), n/a-n/a. https://doi.org/10.1029/2003jf000037

Danilla, C., Persello, C., Tolpekin, V., & Bergado, J. R. (2017). Classification of multitemporal SAR images using convolutional neural networks and Markov random fields. *International Geoscience and Remote Sensing Symposium (IGARSS)*, *2017-July*, 2231–2234. https://doi.org/10.1109/IGARSS.2017.8127432

Darwinkel, A., & Zwanepol, S. (1997). *Cultivation of winter wheat*. Retrieved from https://library.wur.nl/WebQuery/wurpubs/fulltext/216595

Dau, H. A., Silva, D. F., Petitjean, F., Forestier, G., Bagnall, A., Mueen, A., & Keogh, E. (2018). Optimizing dynamic time warping's window width for time series data mining applications. *Data Mining and Knowledge Discovery*, *32*(4), 1074–1120. https://doi.org/10.1007/s10618-018-0565-y

De Zan, F., & Guarnieri, A. M. (2006). TOPSAR: Terrain observation by progressive scans. *IEEE Transactions on Geoscience and Remote Sensing*, *44*(9), 2352–2360. https://doi.org/10.1109/TGRS.2006.873853

Delrue, J., Bydekerke, L., Eerens, H., Gilliams, S., Piccard, I., & Swinnen, E. (2013). Crop mapping in countries with small-scale farming: A case study for West Shewa, Ethiopia. *International Journal of Remote Sensing*, *34*(7), 2566–2582.

DLR. (2020). *TerraSAR-X dataset.* Germany.

Dobbie, M. J., Henderson, B. L., & Stevens, D. L. (2008). Sparse sampling: Spatial design for monitoring stream networks. *Statistics Surveys*, *2*, 113–153. https://doi.org/10.1214/07-SS032

El-Darymli, K., McGuire, P., Gill, E., Power, D., & Moloney, C. (2014). Understanding the significance of radiometric calibration for synthetic aperture radar imagery. *2014 IEEE 27th Canadian Conference on Electrical and Computer Engineering (CCECE)*, 1–6. https://doi.org/10.1109/CCECE.2014.6901104

El Hajj, M., Baghdadi, N., Bazzi, H., & Zribi, M. (2019). Penetration analysis of SAR signals in the C and L bands for wheat, maize, and grasslands. *Remote Sensing*, *11*(1). https://doi.org/10.3390/rs11010031

ESA. (2013). *Sentinel-1 User handbook* (p. 80). p. 80. European Space Agency.

ESA. (2017). Sentinel-1 speeds up crop insurance payouts. Retrieved June 1, 2019, from www.esa.int/Our_Activities/Observing_the_Earth/Copernicus/Sentinel-1/Sentinel-1_speeds_up_crop_insurance_payouts

ESA. (2018). *SNAP - ESA Sentinel Application Platform*. Retrieved from http://step.esa.int

Ferrazzoli, P., Paloscia, S., Pampaloni, P., Schiavon, G., Solimini, D., & Coppo, P. (1992). Sensitivity of Microwave Measurements to Vegetation Biomass and Soil Moisture Content: A Case Study. *IEEE Transactions on Geoscience and Remote Sensing*, *30*(4), 750–756. https://doi.org/10.1109/36.158869

Filipponi, F. (2019). Sentinel-1 GRD Preprocessing Workflow. *Proceedings*, *18*(1). https://doi.org/10.3390/ecrs-3-06201

Forkuor, G., Conrad, C., Thiel, M., Ullmann, T., & Zoungrana, E. (2014). Integration of Optical and Synthetic Aperture Radar Imagery for Improving Crop Mapping in Northwestern Benin, West Africa. *Remote Sensing*, *6*(7), 6472–6499. https://doi.org/10.3390/rs6076472

Gao, Q., Zribi, M., Escorihuela, M. J., Baghdadi, N., & Segui, P. Q. (2018). Irrigation mapping using Sentinel-1 time series at field scale. *Remote Sensing*, *10*(1495). https://doi.org/10.3390/rs10091495

Ghazaryan, G., Dubovyk, O., Löw, F., Lavreniuk, M., Kolotii, A., Schellberg, J., & Kussul, N. (2018). A rule-based approach for crop identification using multi-temporal and multi-sensor phenological metrics. *European Journal of Remote Sensing*, *51*(1), 511–524. https://doi.org/10.1080/22797254.2018.1455540

Górecki, T., & Łuczak, M. (2014). Non-isometric transforms in time series classification using DTW. *Knowledge-Based Systems*, *61*, 98–108. https://doi.org/10.1016/j.knosys.2014.02.011

Górecki, T., & Łuczak, M. (2015). Multivariate time series classification with parametric derivative dynamic time warping. *Expert Systems with Applications*, *42*(5), 2305–2312. https://doi.org/10.1016/j.eswa.2014.11.007

Guan, X., Liu, G., Huang, C., Meng, X., Liu, Q., Wu, C., … Wang, Q. (2018). An open-boundary locally weighted dynamic time warping method for cropland mapping. *ISPRS International Journal of Geo-Information*, *7*(2). https://doi.org/10.3390/ijgi7020075

Hall, O., Dahlin, S., Marstorp, H., Archila Bustos, M., Öborn, I., & Jirström, M. (2018). Classification of Maize in Complex Smallholder Farming Systems Using UAV Imagery. *Drones*, *2*(3), 22. https://doi.org/10.3390/drones2030022

Heupel, K., Spengler, D., & Itzerott, S. (2018). A Progressive Crop-Type Classification Using Multitemporal Remote Sensing Data and Phenological Information. *PFG - Journal of Photogrammetry, Remote Sensing and Geoinformation Science*, *86*(2), 53–69. https://doi.org/10.1007/s41064-018-0050-7

Hütt, C., & Waldhoff, G. (2018). Multi-data approach for crop classification using multitemporal, dual-polarimetric TerraSAR-X data, and official geodata. *European Journal of Remote Sensing*, *51*(1), 62–74. https://doi.org/10.1080/22797254.2017.1401909

Inglada, J., Arias, M., Tardy, B., Hagolle, O., Valero, S., Morin, D., … Koetz, B. (2015). Assessment of an operational system for crop type map production using high temporal and spatial resolution satellite optical imagery. *Remote Sensing*, *7*(9), 12356–12379. https://doi.org/10.3390/rs70912356

Itakura, F. (1975). Minimum Prediction Residual Principle Applied to Speech Recognition. *IEEE Transactions on Acoustics, Speech, and Signal Processing*, *23*(1), 67–72. https://doi.org/10.1109/TASSP.1975.1162641

Jain, M., Mondal, P., DeFries, R. S., Small, C., & Galford, G. L. (2013). Mapping cropping intensity of smallholder farms: A comparison of methods using multiple sensors. *Remote Sensing of Environment*, *134*, 210–223. https://doi.org/10.1016/j.rse.2013.02.029

Jeong, Y.-S., Jeong, M. K., & Omitaomu, O. A. (2011). Weighted dynamic time warping for time series classification. *Pattern Recognition*, *44*(9), 2231–2240. https://doi.org/10.1016/J.PATCOG.2010.09.022

Ji, K., & Wu, Y. (2015). Scattering mechanism extraction by a modified Cloude-Pottier decomposition for dual polarization SAR. *Remote Sensing*. https://doi.org/10.3390/rs70607447

Jiao, X., Kovacs, J. M., Shang, J., McNairn, H., Walters, D., Ma, B., & Geng, X. (2014). Object-oriented crop mapping and monitoring using multi-temporal polarimetric RADARSAT-2 data. *ISPRS Journal of Photogrammetry and Remote Sensing*, *96*, 38–46. https://doi.org/10.1016/j.isprsjprs.2014.06.014

Jin, Z., Azzari, G., Burke, M., Aston, S., & Lobell, D. B. (2017). Mapping smallholder yield heterogeneity at multiple scales in eastern Africa. *Remote Sensing*, *9*(9). https://doi.org/10.3390/rs9090931

Joseph, A. T., van der Velde, R., O'Neill, P. E., Lang, R., & Gish, T. (2010). Effects of corn on C- and L-band radar backscatter: A correction method for soil moisture retrieval. *Remote Sensing of Environment*, *114*(11), 2417–2430. https://doi.org/10.1016/j.rse.2010.05.017

Kenduiywo, B. K., Bargiel, D., & Soergel, U. (2016). Crop Type Mapping From A Sequence Of Terrasar-X Images With Dynamic Conditional Random Fields. *ISPRS Annals of the Photogrammetry, Remote Sensing and Spatial Information Sciences*, 59–66. https://doi.org/10.5194/isprs-annals-III-7-59-2016

Keogh, E., & Pazzani, M. (2001). Derivative Dynamic Time Warping. *First SIAM International Conference on Data Mining*, 1–11. https://doi.org/10.1137/1.9781611972719.1

Keogh, E., & Ratanamahatana, C. A. (2005). Exact indexing of dynamic time warping. *Knowledge and Information Systems*, *7*(3), 358–386. https://doi.org/10.1007/s10115-004-0154-9

Khabbazan, S., Vermunt, P., Steele-Dunne, S., Arntz, L. R., Marinetti, C., van der Valk, D., … van der Sande, C. (2019). Crop monitoring using Sentinel-1 data: A case study from The Netherlands. *Remote Sensing*, *11*(16). https://doi.org/10.3390/rs11161887

Kropatsch, W. G., & Strobl, D. (1990). The Generation of SAR Layover and Shadow Maps From Digital Elevation Models. *IEEE Transactions on Geoscience and Remote Sensing*, *28*(1), 98–107. https://doi.org/10.1109/36.45752

Kumar, V., Mandal, D., Bhattacharya, A., & Rao, Y. S. (2020). Crop characterization using an improved scattering power decomposition technique for compact polarimetric SAR data. *International Journal of Applied Earth Observation and Geoinformation*, *88*, 102052. https://doi.org/10.1016/j.jag.2020.102052

Kussul, N., Lemoine, G., Gallego, F. J., Skakun, S. V., Lavreniuk, M., & Shelestov, A. Y. (2016). Parcel-Based Crop Classification in Ukraine Using Landsat-8 Data and Sentinel-1A Data. *IEEE Journal of Selected Topics in Applied Earth Observations and Remote Sensing*, *9*(6), 2500–2508. https://doi.org/10.1109/JSTARS.2016.2560141

Lambert, M. J., Traoré, P. C. S., Blaes, X., Baret, P., & Defourny, P. (2018). Estimating smallholder crops production at village level from Sentinel-2 time series in Mali's cotton belt. *Remote Sensing of Environment*, *216*, 647–657. https://doi.org/10.1016/j.rse.2018.06.036

Lee, J. Sen, Grunes, M. R., & Pottier, E. (2001). Quantitative comparison of classification capability: Fully polarimetric versus dual and single-polarization SAR. *IEEE Transactions on Geoscience and Remote Sensing*, *39*(11), 2343–2351. https://doi.org/10.1109/36.964970

Lee, J. Sen, Lee, J. Sen, Wen, J. H., Ainsworth, T. L., Chen, K. S., & Chen, A. J. (2009). Improved Sigma Filter for Speckle Filtering of SAR Imagery. *IEEE Transactions on Geoscience and Remote Sensing*, *47*(1), 202–213. https://doi.org/10.1109/TGRS.2008.2002881

Li, M., & Bijker, W. (2019). Vegetable classification in Indonesia using Dynamic Time Warping of Sentinel-1A dual polarization SAR time series. *International Journal of Applied Earth Observation and Geoinformation*, *78*, 268–280. https://doi.org/10.1016/j.jag.2019.01.009

Liu, Chang, Chen, Z. X., Shao, Y., Chen, J. S., Hasi, T., & Pan, H. Z. (2019). Research advances of SAR remote sensing for agriculture applications: A review. *Journal of Integrative Agriculture*, *18*(3), 506–525. https://doi.org/10.1016/S2095-3119(18)62016-7

Liu, Chen, Shang, J., Vachon, P. W., & McNairn, H. (2013). Multiyear crop monitoring using polarimetric RADARSAT-2 data. *IEEE Transactions on Geoscience and Remote Sensing*, *51*(4), 2227–2240. https://doi.org/10.1109/TGRS.2012.2208649

Lopez-Sanchez, J. M., Ballester-Berman, J. D., & Hajnsek, I. (2011). First Results of Rice Monitoring Practices in Spain by Means of Time Series of TerraSAR-X Dual-Pol Images. *IEEE Journal of Selected Topics in Applied Earth Observations and Remote Sensing*, *4*(2), 412–422. https://doi.org/10.1109/JSTARS.2010.2047634

Lowder, S. K., Skoet, J., & Raney, T. (2016). The Number, Size, and Distribution of Farms, Smallholder Farms, and Family Farms Worldwide. *World Development*, *87*, 16–29. https://doi.org/10.1016/j.worlddev.2015.10.041

Lu, D., & Weng, Q. (2007). A survey of image classification methods and techniques for improving classification performance. *International Journal of Remote Sensing*, *28*(5), 823–870. https://doi.org/10.1080/01431160600746456

Lussem, U., Hütt, C., & Waldhoff, G. (2016). Combined analysis of Sentinel-1 and RapidEye data for improved crop type classification: An early season approach for rapeseed and cereals. *International Archives of the Photogrammetry, Remote Sensing and Spatial Information Sciences - ISPRS Archives*, 959–963. https://doi.org/10.5194/isprsarchives-XLI-B8-959-2016

Macelloni, G., Paloscia, S., Pampaloni, P., Marliani, F., & Gai, M. (2001). The relationship between the backscattering coefficient and the biomass of narrow and broad leaf crops. *IEEE Transactions on Geoscience and Remote Sensing*, *39*(4), 873–884. https://doi.org/10.1109/36.917914

Mandal, D., Kumar, V., Bhattacharya, A., Rao, Y. S., Siqueira, P., & Bera, S. (2018). Sen4Rice: A processing chain for differentiating early and late transplanted rice using time-series sentinel-1 SAR data with google earth engine. *IEEE Geoscience and Remote Sensing Letters*, *15*(12), 1947–1951. https://doi.org/10.1109/LGRS.2018.2865816

Maus, V., Câmara, G., Appel, M., & Pebesma, E. (2019). dtwSat : Time-Weighted Dynamic Time Warping for Satellite Image Time Series Analysis in R. *Journal of Statistical Software*, *88*(5), 1–31. https://doi.org/10.18637/jss.v088.i05

Maus, V., CĂmara, G., Cartaxo, R., Sanchez, A., Ramos, F. M., & De Queiroz, G. R. (2016). A Time-Weighted Dynamic Time Warping Method for Land-Use and Land-Cover Mapping. *IEEE Journal of Selected Topics in Applied Earth Observations and Remote Sensing*, *9*(8), 3729–3739. https://doi.org/10.1109/JSTARS.2016.2517118

Mc Nairn, H., & Brisco, B. (2004). The application of C-band polarimetric SAR for agriculture: A review. *Canadian Journal of Remote Sensing*, *30*(3), 525–542. https://doi.org/10.5589/m03-069

Mc Nairn, H., Duguay, C., Boisvert, J., Huffman, E., & Brisco, B. (2001). Defining the sensitivity of multi-frequency and multi-polarized radar backscatter to post-harvest crop residue. *Canadian Journal of Remote Sensing*, *27*(3), 247–263. https://doi.org/10.1080/07038992.2001.10854941

Miranda, N., & Meadows, P. J. (2015). Radiometric Calibration of S-1 Level-1 Products Generated by the S-1 IPF. In *Technical Note*. https://doi.org/10.1007/s00011-010-0303-4

Nakamura, T., Taki, K., Nomiya, H., Seki, K., & Uehara, K. (2013). A shape-based similarity measure for time series data with ensemble learning. *Pattern Analysis and Applications*, *16*(4), 535–548. https://doi.org/10.1007/s10044-011-0262-6

Nasirzadehdizaji, R., Sanli, F. B., Abdikan, S., Cakir, Z., Sekertekin, A., & Ustuner, M. (2019). Sensitivity analysis of multi-temporal Sentinel-1 SAR parameters to crop height and canopy coverage. *Applied Sciences (Switzerland)*, *9*(4). https://doi.org/10.3390/app9040655

Ndikumana, E., Minh, D. H. T., Baghdadi, N., Courault, D., & Hossard, L. (2018). Deep recurrent neural network for agricultural classification using multitemporal SAR Sentinel-1 for Camargue, France. *Remote Sensing*, *10*(2117). https://doi.org/10.3390/rs10081217

Oliphant, A. J., Thenkabail, P. S., Teluguntla, P., Xiong, J., Gumma, M. K., Congalton, R. G., & Yadav, K. (2019). Mapping cropland extent of Southeast and Northeast Asia using multi-year time-series Landsat 30-m data using a random forest classifier on the Google Earth Engine Cloud. *International Journal of Applied Earth Observation and Geoinformation*, *81*, 110–124. https://doi.org/10.1016/j.jag.2018.11.014

Osman, A. M., Bueren,   van den B., Berg, R. C. F. M. van den B. van den, & Van, E. T. L. (2005). *Rassenonderzoek voor BiologischeBedrijfssystemen2001-2004*. Retrieved from http://www.louisbolk.org/downloads/1459.pdf

Panagos, P., Borrelli, P., Meusburger, K., Alewell, C., Lugato, E., & Montanarella, L. (2015). Estimating the soil erosion cover-management factor at the European scale. *Land Use Policy*, *48*, 38–50. https://doi.org/10.1016/j.landusepol.2015.05.021

Periasamy, S. (2018). Significance of dual polarimetric synthetic aperture radar in biomass retrieval: An attempt on Sentinel-1. *Remote Sensing of Environment*, *217*, 537–549. https://doi.org/10.1016/j.rse.2018.09.003

Persello, C., Tolpekin, V. A., Bergado, J. R., & de By, R. A. (2019). Delineation of agricultural fields in smallholder farms from satellite images using fully convolutional networks and combinatorial grouping. *Remote Sensing of Environment*, *231*. https://doi.org/10.1016/j.rse.2019.111253

Petitjean, F., Inglada, J., & Gancarski, P. (2012). Satellite Image Time Series Analysis Under Time Warping. *IEEE Transactions on Geoscience and Remote Sensing*, *50*(8), 3081–3095. https://doi.org/10.1109/TGRS.2011.2179050

Ricciardi, V., Ramankutty, N., Mehrabi, Z., Jarvis, L., & Chookolingo, B. (2018). How much of the world's food do smallholders produce? *Global Food Security*, Vol. 17, pp. 64–72. https://doi.org/10.1016/j.gfs.2018.05.002

Roth, A. (2003). TerraSAR-X: A new perspective for scientific use of high resolution spaceborne SAR data. *2nd GRSS/ISPRS Joint Workshop on Remote Sensing and Data Fusion over Urban Areas, URBAN 2003*, 4–7. https://doi.org/10.1109/DFUA.2003.1219947

Ruud, T., Gerard, W. K., & Leendert, M. (n.d.). *Teelthandleiding groenbemesters : winterrogge*. Retrieved from https://www.researchgate.net/publication/283223971_Teelthandleiding_groenbemesters_winterrogge

Sakoe, H., & Chiba, S. (1978). Dynamic Programming Algorithm Optimization for Spoken Word Recognition. *IEEE Transactions on Acoustics, Speech, and Signal Processing*, *ASSP-26*(1), 43–49. https://doi.org/10.1109/TASSP.1978.1163055

Sakurai, Y., Faloutsos, C., & Yamamuro, M. (2007). Stream monitoring under the time warping distance. *Proceedings - International Conference on Data Engineering*, 1046–1055. https://doi.org/10.1109/ICDE.2007.368963

Salvador, S., & Chan, P. (2004). FastDTW: Toward Accurate Dynamic Time Warping in Linear Time and Space. *KDD 3rd Workshop on Mining Temporal and Sequential Data*.

Samberg, L. H., Gerber, J. S., Ramankutty, N., Herrero, M., & West, P. C. (2016). Subnational distribution of average farm size and smallholder contributions to global food production. *Environmental Research Letters*, *11*(12). https://doi.org/10.1088/1748-9326/11/12/124010

Santos, C. L. M. de O., Lamparelli, R. A. C., Figueiredo, G. K. D. A., Dupuy, S., Boury, J., Luciano, A. C. dos S., … le Maire, G. (2019). Classification of crops, pastures, and tree plantations along the season with multi-sensor image time series in a subtropical agricultural region. *Remote Sensing*, *11*. https://doi.org/10.3390/rs11030334

Savitzky, A., & Golay, M. J. E. (1964). Smoothing and Differentiation of Data by Simplified Least Squares Procedures. *Analytical Chemistry*, *36*(8), 1627–1639. https://doi.org/10.1021/ac60214a047

Shan, Z., Wang, C., Zhang, H., & Chen, J. (2011). H-α decomposition and alternative parameters for dual polarization SAR data. *Progress in Electromagnetics Research Symposium*, 1386–1390. Suzhou, China.

Skriver, H., Svendsen, M. T., & Thomsen, A. G. (1999). Multitemporal C- and L-band polarimetric signatures of crops. *IEEE Transactions on Geoscience and Remote Sensing*, *37*(5 II), 2413–2429. https://doi.org/10.1109/36.789639

Son, N. T., Chen, C. F., Chen, C. R., & Minh, V. Q. (2018). Assessment of Sentinel-1A data for rice crop classification using random forests and support vector machines. *Geocarto International*, *33*(6), 587–601. https://doi.org/10.1080/10106049.2017.1289555

Sonobe, R. (2019). Parcel-based crop classification using multi-temporal TerraSAR-X dual polarimetric data. *Remote Sensing*, *11*(10). https://doi.org/10.3390/rs11101148

Sonobe, R., Tani, H., Wang, X., Kobayashi, N., & Shimamura, H. (2014). Winter wheat growth monitoring using multi-temporal TerraSAR-X dual-polarimetric data. *Japan Agricultural Research Quarterly*, *48*(4), 471–476. https://doi.org/10.6090/jarq.48.471

Stratoulias, D., Tolpekin, V., de By, R. A., Zurita-Milla, R., Retsios, V., Bijker, W., … Vermote, E. (2017). A workflow for automated satellite image processing: From raw VHSR data to object-based spectral information for smallholder agriculture. *Remote Sensing*, Vol. 9. https://doi.org/10.3390/rs9101048

Sweeney, S., Ruseva, T., Estes, L., & Evans, T. (2015). Mapping cropland in smallholder-dominated savannas: Integrating remote sensing techniques and probabilistic modeling. *Remote Sensing*, *7*(11), 15295–15317. https://doi.org/10.3390/rs71115295

Tan, C. P., Ewe, H. T., & Chuah, H. T. (2011). Agricultural crop-type classification of multi-polarization SAR images using a hybrid entropy decomposition and support vector machine technique. *International Journal of Remote Sensing*, *32*(22), 7057–7071. https://doi.org/10.1080/01431161.2011.613414

Teke, M., & Yardımcı, Y. (2019). *Multi-Year Vector Dynamic Time Warping Based Crop Mapping*. Retrieved from http://arxiv.org/abs/1909.04930

Torres, R., Snoeij, P., Geudtner, D., Bibby, D., Davidson, M., Attema, E., … Rostan, F. (2012). GMES Sentinel-1 mission. *Remote Sensing of Environment*, *120*, 9–24. https://doi.org/10.1016/j.rse.2011.05.028

Tsiligirides, T. A. (1998). Remote sensing as a tool for agricultural statistics: A case study of area frame sampling methodology in Hellas. *Computers and Electronics in Agriculture*, *20*(1), 45–77. https://doi.org/10.1016/S0168-1699(98)00011-8

Tso, B., & Mather, P. M. (1999). Crop discrimination using multi-temporal SAR imagery. *International Journal of Remote Sensing*, *20*(12), 2443± 2460. https://doi.org/10.1080/014311699212119

Ulaby, F. T. (1975). Radar Response to Vegetation. *IEEE Transactions on Antennas and Propagation*, *23*(1), 36–45. https://doi.org/10.1109/TAP.1975.1140999

Uppala, D., Venkata, R. K., Poloju, S., Rama, V. S. S., & Dadhwal, V. K. M. (2016). Discrimination of maize crop with hybrid polarimetric RISAT1 data. *International Journal of Remote Sensing*, *37*(11), 2641–2652. https://doi.org/10.1080/01431161.2016.1184353

Useya, J., & Chen, S. (2019). Exploring the Potential of Mapping Cropping Patterns on Smallholder Scale Croplands Using Sentinel-1 SAR Data. *Chinese Geographical Science*, *29*(4), 626–639. https://doi.org/10.1007/s11769-019-1060-0

Useya, J., Chen, S., & Murefu, M. (2019). Cropland Mapping and Change Detection: Toward Zimbabwean Cropland Inventory. *IEEE Access*, *7*, 53603–53620. https://doi.org/10.1109/ACCESS.2019.2912807

Ustuner, M., Sanli, F. B., & Abdikan, S. (2016). Balanced vs imbalanced training data: Classifying rapid-eye data with support vector machines. *International Archives of the Photogrammetry, Remote Sensing and Spatial Information Sciences - ISPRS Archives*, *41*, 379–384. https://doi.org/10.5194/isprsarchives-XLI-B7-379-2016

Valcarce-Diñeiro, R., Arias-Pérez, B., Lopez-Sanchez, M. J., & Sánchez, N. (2019). Multi-Temporal Dual- and Quad-Polarimetric Synthetic Aperture Radar Data for Crop-Type Mapping. *Remote Sensing*, *11*(13). https://doi.org/10.3390/rs11131518

van den Brink, A., & Molema, M. (2008). The origins of Dutch rural planning: A study of the early history of land consolidation in the Netherlands. *Planning Perspectives*, *23*(4), 427–453. https://doi.org/10.1080/02665430802319005

van den Noort, P. C. (1987). Land consolidation in the Netherlands. *Land Use Policy*, *4*(1), 11–13. https://doi.org/10.1016/0264-8377(87)90004-4

van der Wal, T., Abma, B., Viguria, A., Prévinaire, E., Zarco-Tejada, P. J., Serruys, P., … Van Der Voet, P. (2013). Fieldcopter: Unmanned aerial systems for crop monitoring services. *Precision Agriculture 2013 - Papers Presented at the 9th European Conference on Precision Agriculture, ECPA 2013*, 169–175.

Van Niel, T. G., & McVicar, T. R. (2004). Determining temporal windows for crop discrimination with remote sensing: A case study in south-eastern Australia. *Computers and Electronics in Agriculture*, *45*(1–3), 91–108. https://doi.org/10.1016/j.compag.2004.06.003

Van Zyl, J. J. (1993). The effect of topography on radar scattering from vegetated areas. *IEEE Transactions on Geoscience and Remote Sensing*, *31*(1), 153–161. https://doi.org/10.1109/IGARSS.1992.578363

Vanlauwe, B., Coyne, D., Gockowski, J., Hauser, S., Huising, J., Masso, C., … Van Asten, P. (2014). Sustainable intensification and the African smallholder farmer. *Current Opinion in Environmental Sustainability*, Vol. 8, pp. 15–22. https://doi.org/10.1016/j.cosust.2014.06.001

Vreugdenhil, M., Wagner, W., Bauer-Marschallinger, B., Pfeil, I., Teubner, I., Rüdiger, C., & Strauss, P.

(2018). Sensitivity of Sentinel-1 backscatter to vegetation dynamics: An Austrian case study. *Remote Sensing*, *10*(9). https://doi.org/10.3390/rs10091396

Waldner, F., Fritz, S., Di Gregorio, A., & Defourny, P. (2015). Mapping priorities to focus cropland mapping activities: Fitness assessment of existing global, regional, and national cropland maps. *Remote Sensing*, *7*, 7959–7986. https://doi.org/10.3390/rs70607959

Wang, H., Magagi, R., & Goita, K. (2016). Polarimetric Decomposition for Monitoring Crop Growth Status. *IEEE Geoscience and Remote Sensing Letters*, *13*(6), 870–874. https://doi.org/10.1109/LGRS.2016.2551377

Wang, S., Sun, J., Phillips, P., Zhao, G., & Zhang, Y. (2018). Polarimetric synthetic aperture radar image segmentation by convolutional neural network using graphical processing units. *Journal of Real-Time Image Processing*, *15*, 631–642. https://doi.org/10.1007/s11554-017-0717-0

Whelen, T., & Siqueira, P. (2018). Time-series classification of Sentinel-1 agricultural data over North Dakota. *Remote Sensing Letters*, *9*(5), 411–420. https://doi.org/10.1080/2150704X.2018.1430393

Xie, B., Zhang, H. K., & Xue, J. (2019). Deep convolutional neural network for mapping smallholder agriculture using high spatial resolution satellite image. *Sensors (Switzerland)*, *19*(10). https://doi.org/10.3390/s19102398

Xu, L., Zhang, H., Wang, C., Zhang, B., & Liu, M. (2019). Crop classification based on temporal information using Sentinel-1 SAR time-series data. *Remote Sensing*, *11*(1). https://doi.org/10.3390/rs11010053

Yang, Z., & Boryan, C. G. (2019). Impact of Non-Proportional Training Sampling of Imbalanced Classes on Land Cover Classification Accuracy with See5 Decision Tree. *International Geoscience and Remote Sensing Symposium (IGARSS)*, 9466–9469. https://doi.org/10.1109/IGARSS.2019.8897985

Zhang, X., Xiong, Q., Di, L., Tang, J., Yang, J., Wu, H., … Zhou, W. (2018). Phenological metrics-based crop classification using HJ-1 CCD images and Landsat 8 imagery. *International Journal of Digital Earth*, *11*(12), 1219–1240. https://doi.org/10.1080/17538947.2017.1387296

APPENDIX 1: Supplementary information

Appendix 1A: Specific sensing dates of utilized images

12/01/2018	20180226	06/04/2018	14/05/2018	23/06/2018	04/08/2018	15/10/2018
18/01/2018	01/03/2018	11/04/2018	18/05/2018	05/07/2018	21/08/2018	21/10/2018
24/01/2018	07/03/2018	12/04/2018	24/05/2018	08/07/2018	22/08/2018	27/10/2018
30/01/2018	09/03/2018	22/04/2018	25/05/2018	11/07/2018	03/09/2018	
05/02/2018	13/03/2018	24/04/2018	30/05/2018	17/07/2018	12/09/2018	
11/02/2018	19/03/2018	30/04/2018	05/06/2018	19/07/2018	21/09/2018	
15/02/2018	25/03/2018	03/05/2018	11/06/2018	23/07/2018	27/09/2018	
17/02/2018	31/03/2018	06/05/2018	16/06/2018	29/07/2018	03/10/2018	
23/02/2018	31/03/2018	12/05/2018	17/06/2018	30/07/2018	09/10/2018	

Key

TerraSAR-X sensing date

Sentinel-1 Sensing Date

Appendix 1B: Reference crop polygons from PDOK

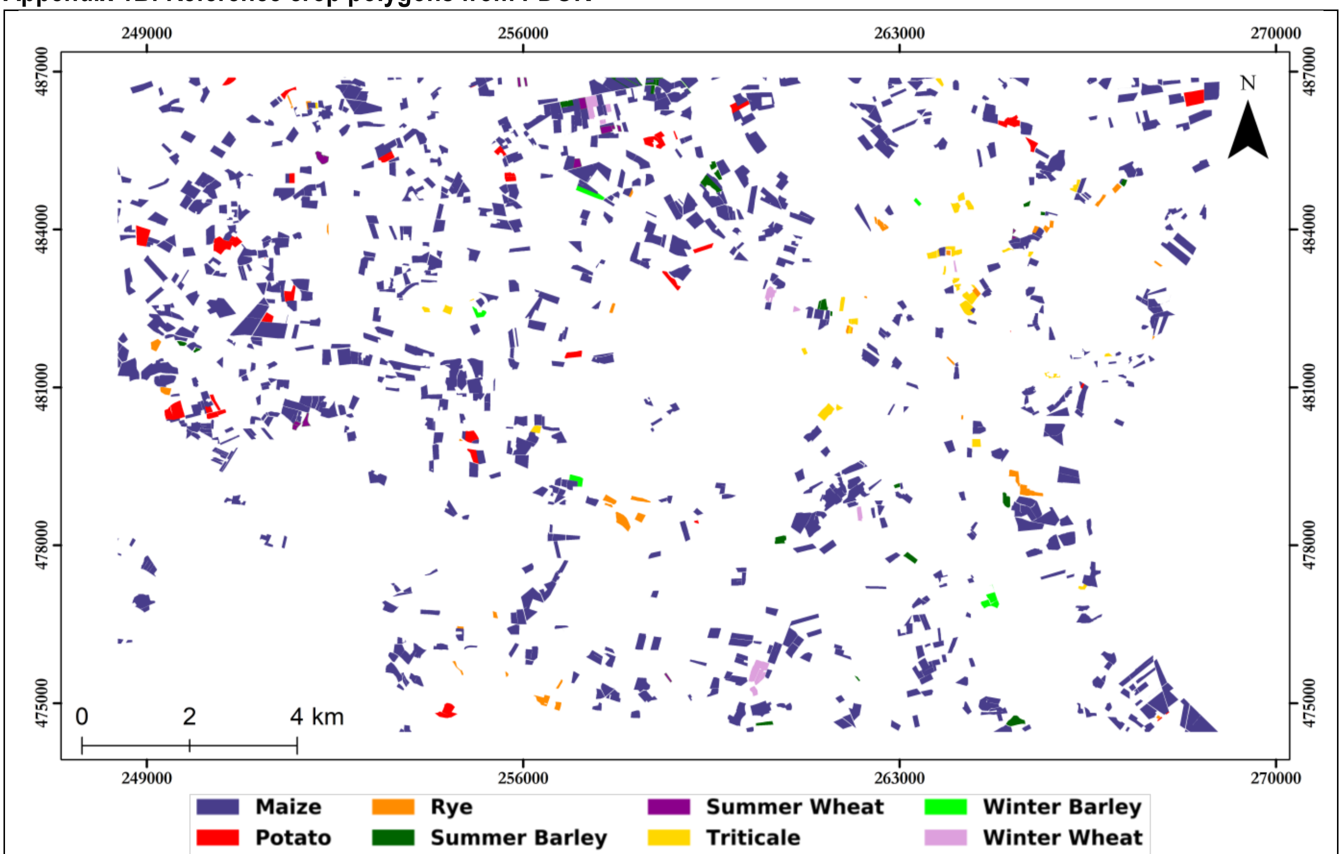

Appendix 1C: Distribution of sampling points within a polygon

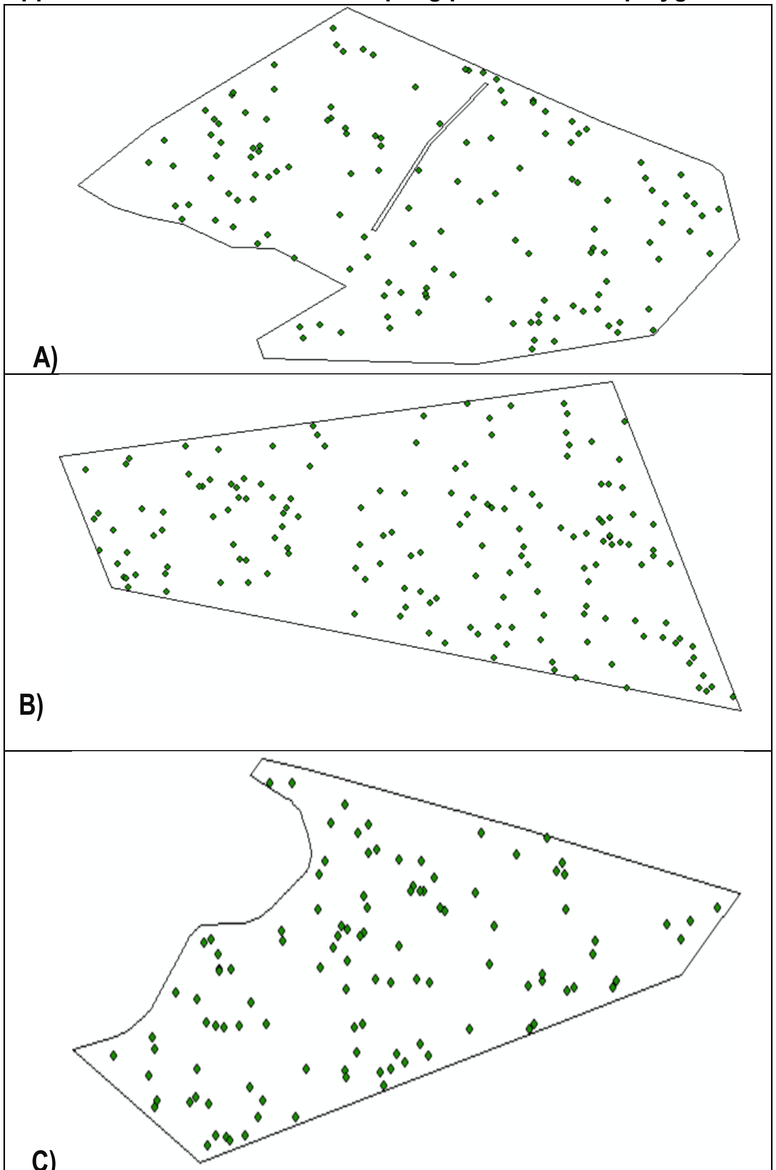

Distribution of samples within training polygons (A) Potato, (B) Potato (C) Summer barley

Note: These maps are just to show how well the points were distributed in training polygons. Polygons are just picked from sample polygons selected for training and are not a representation of the whole set of training points used in the study.

APPENDIX 2: Algorithms

Appendix 2A. Algorithmic Procedures for Sampling and Temporal Profile Generation

Algorithm 1: Sample Spliting and Temporal Profile Generation

```
Input   : Reference crop polygon (parcel boundary) (Ref);
          Satellite Image Tme Series(SITS)
Output  : Training set, Validation set and Temporal profile(TPF)
Require:  A column Cname from Ref that contain crop name;
          n which is number of samples from each crop used for Training;
Ensure  : Ref is with projected coordinate system
begin
    Generate Croplist which is unique crop names in Cname;
    for Crop ∈ Croplist do
        subset = all samples in Ref where Column value equal Crop name;
        for each crop sample ∈ subset do
            Compute Distance to all points in a subset;
            Record Minimum from distances with crop;
        sort subset using computed minimum distance in descending order;
        pick the first n% of samples from subset and record to Trainning;
Validation = Centroids of all polygons in Ref;
Generate Croplist which is unique crop names in Column in Ref;
for crop ∈ Croplist do
    TPF_crop ;                    // empty dictionary for saving crop temporal profile
    subset = all samples in Training where Column value equal Crop name;
    for Polygon ∈ subset do
        Points;  // empty geodataframe to save sampled points within polygon per crop
        compute X_min, X_max ,Y_min ,Y_max for a Polygon;
        lon = generate n random points within X_min and X_max;
        lat = generate n random points within Y_min and Y_max;
        feature = generate points using lon and lat;
        samples = pick feature only within Polygon;
        append samples in Points;
        for observable ∈ SITS do
            P = extract using Points;
            P_a = aggregate using median statistic;
            P_as = smooth P_a using Savitzky − Golayfilter;
            Record P_as in TPF_crop
    Record TPF_crop in TPS
end
```

Appendix 2B. Algorithmic Implementation for twDTW

Algorithm 2: Time weighted Dynamic Time warping

Input : $SITS_{(V,L,C,R)}$, $DOY_{(L,)}$, $TPF_{key:(L,V)}$, β

Output: $Classified_{(R,C)}$, $Distances_{key:(R,C)}$;

where subscripts indicate dimensions as number of variables(V) in $SITS$, layers per variable(L), rows per layer (R), and columns per layer(C);

$SITS$: A 4-D array of Satellite Image Time Series;

TPS: Dictionary with crops as *key* and a 2-D temporal profile for a crop with given dimension;

Classified: 2-D array of categorical map indicating specific crop type;

β: A maximum allowable time lag to search for warping;

Distances: A dictionary with crop as key and a 2-D array of minimum warping distances per crop as *value*;

```
begin
    for i ←1 to R do
        for j ←1 to C do
            SITS_sub = SITS[:, :, i, j] ;
            Crop list = All keys of TPS;
            WD(Crop:dist) ;                          // dist is minimum warping distance
            for Crop in Croplist do
                TPS_crop = pick from TPS;
                Ensure: dimensions of SITS_sub & TPS_crop = LxV;
                D ;                                  // LxL distance matrix
                M ;                                  // LxL commulative cost distance matrix
                w ;                                  // logistic time weight
                for i ← 1 to L do
                    for j ← 1 to L do
                        Δt = |DOY_i − DOY_j| ;       // Date diference
                        if Δt ≤ β then
                            w(i,j) = Compute using Eq(12);
                            D(i,j) = Compute based on Eq(11);
                            M(i,j) = Compute based on Eq(13)& Eq(14);
                        else
                            M(i,j) = ∞
                Record Crop and M(L,L) in WD;
            for warping distances in WD do
                value = minimum of warping distances in WD;
                class = Crop corresponding with value;
                Classified(i,j) = class;
                Distances(Crop:dist(i,j)) = value;
end
```

Appendix 2C: Implementation Procedures for vtwDTW

Algorithm 3: Variable Time Dynamic Time Warping

Input : $SITS_{(V,L,C,R)}$, $DOY_{(L,)}$, $TPF_{key:(L,V)}$, T_{lag}
Output: $Classified_{(R,C)}$, $Distances_{key:(R,C)}$
where subscripts indicate dimensions as number of variables(V) in $SITS$, layers per variable(L), rows per layer (R), and columns per layer(C)
SITS: A 4-D array of Satellite Image Time Series
TPS: Dictionary with crops as *key* and a 2-D temporal profile for a crop with given dimension
Classified: 2-D array of categorical map indicating specific crop type
T_{lag}: A dictionary containing crop and respective temporal lag
Distances: A dictionary with crop as key and a 2-D array of minimum warping distances per crop as *value*

```
begin
    for i ← 1 to R do
        for j ← 1 to C do
            SITS_sub = SITS[:, :, i, j]
            Crop list = All keys of TPS
            WD_(Crop:dist)                          // dist is minimum warping distance
            for Crop in Croplist do
                TPS_crop = pick from TPS
                Ensure: dimensions of SITS_sub & TPS_crop = LxV
                D                                   // LxL distance matrix
                M                                   // LxL commulative cost distance matrix
                w                                   // logistic time weight
                for i ← 1 to L do
                    for j ← 1 to L do
                        β = pick from T_lag
                        Δ_t = |DOY_i − DOY_j|       // Date diference
                        if Δ_t ≤ β then
                            w_(i,j) = Compute using Eq(15)
                            D_(i,j) = Compute based on Eq(6)
                            M_(i,j) = Compute based on Eq(13)& Eq(14)
                        else
                            M_(i,j) = ∞
                Record Crop and M_(L,L) in WD
            for warping distances ∈ WD do
                value = minimum of warping distances in WD
                class = Crop corresponding with value
                Classified_(i,j) = class
                Distances_(Crop:dist(i,j)) = value
end
```

Appendix 2D: Implementation procedures for AMSS

Algorithm 4: Angular Metric for Shape Simmilarity

Input : $SITS_{(V,L,C,R)}$, $DOY_{(L,)}$, $TPF_{key:(L,V)}$, T_{lag}

Output: $Classified_{(R,C)}$, $Distances_{key:(R,C)}$

where subscripts indicate dimensions as number of variables(V) in $SITS$, layers per variable(L), rows per layer (R), and columns per layer(C)

SITS: A 4-D array of Satellite Image Time Series

TPS: Dictionary with crops as *key* and a 2-D temporal profile for a crop with given dimension

Classified: 2-D array of categorical map indicating specific crop type

T_{lag}: A dictionary containing crop and respective temporal lag

Distances: A dictionary with crop as key and a 2-D array of minimum warping distances per crop as *value*

```
begin
    for i ←1 to R do
        for j ←1 to C do
            SITS_sub = SITS[:, :, i, j]
            Crop list = All keys of TPS
            WD_(Crop:dist)                          // dist is minimum warping distance
            for Crop in Croplist do
                TPS_crop = pick from TPS
                Ensure: dimensions of SITS_sub & TPS_crop = LxV
                for i ← 1 to L do
                    for j ← 1 to L do
                        PV& SV = Compute using Eq(16) // vectors
                        AS                              // Cosine distance matrix
                        AM                              // commulative cost distance matrix
                        for i ← 1 to (L − 1) do
                            for j ← 1 to (L − 1) do
                                AS_(i,j) = Compute by Eq(17)
                                AM_(i,j) = Compute by Eq(19)
                        Record Crop and M_(L−1,L−1) in WD
            for warping distances in WD do
                value = minimum of warping distances in WD
                class = Crop corresponding with value
                Classified_(i,j) = class
                Distances_(Crop:dist(i,j)) = value
end
```

APPENDIX 3: Supplementary analysis results for discussion

Appendix 3A: Spatial uncertainty of classification from Sentinel 1(VV, VH) twDTW

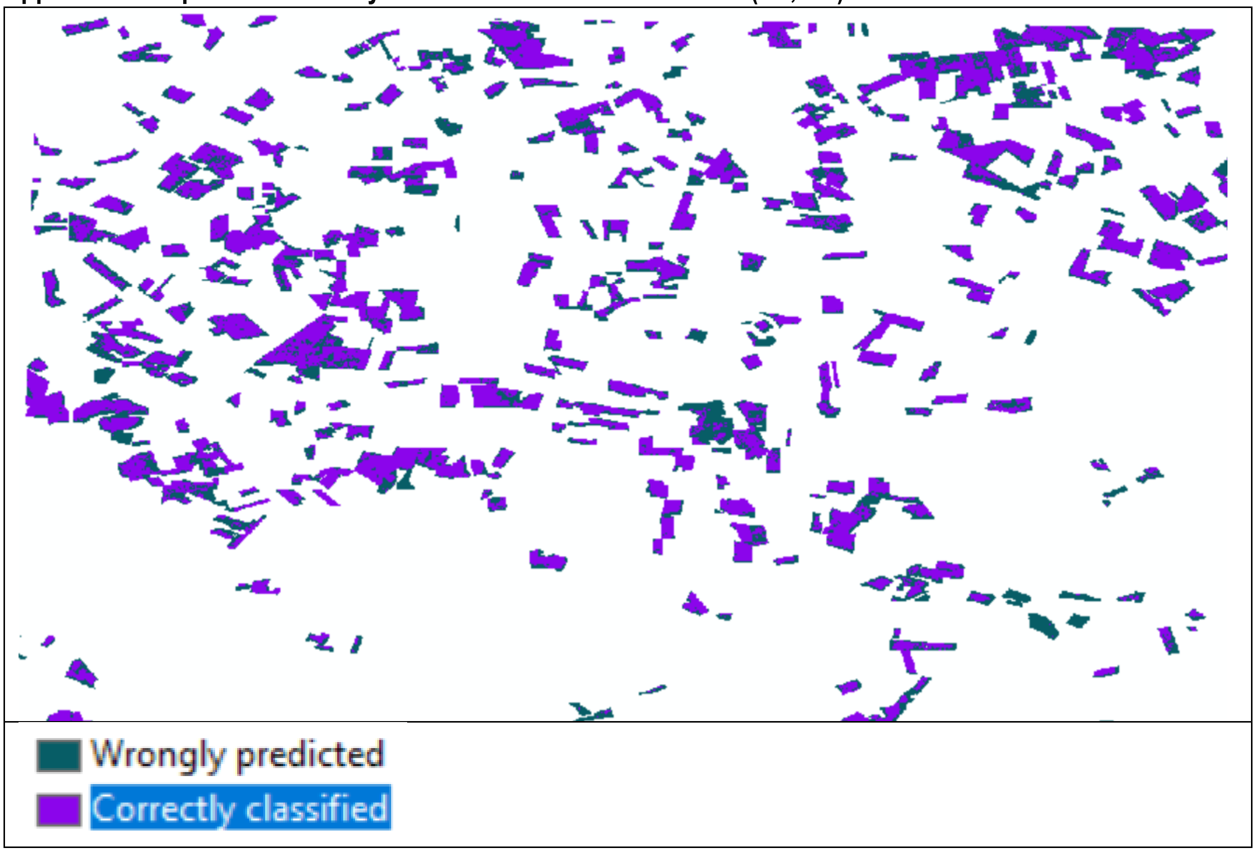

Appendix 3B: Backscattering Maize and Potato Within Plots of Diferent Orientation Angle

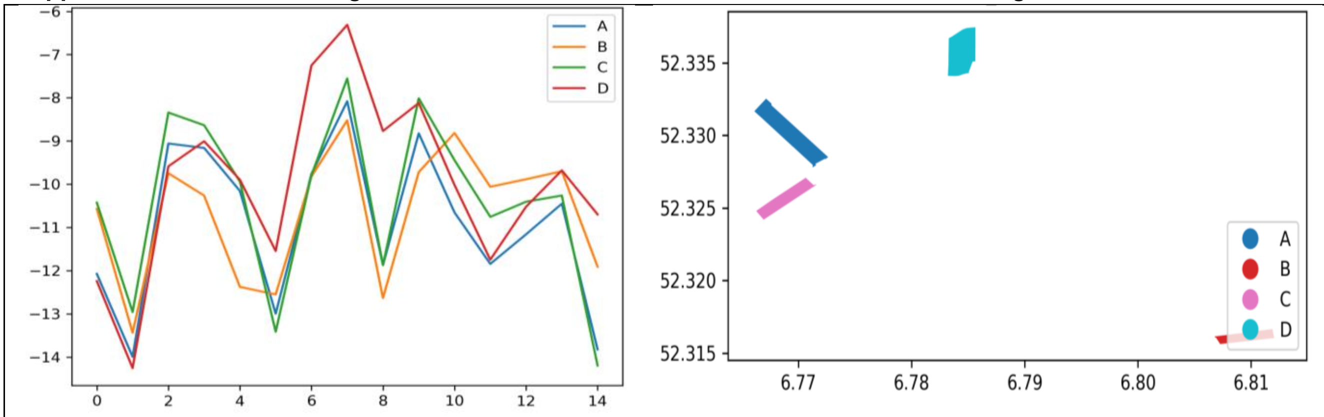

A)

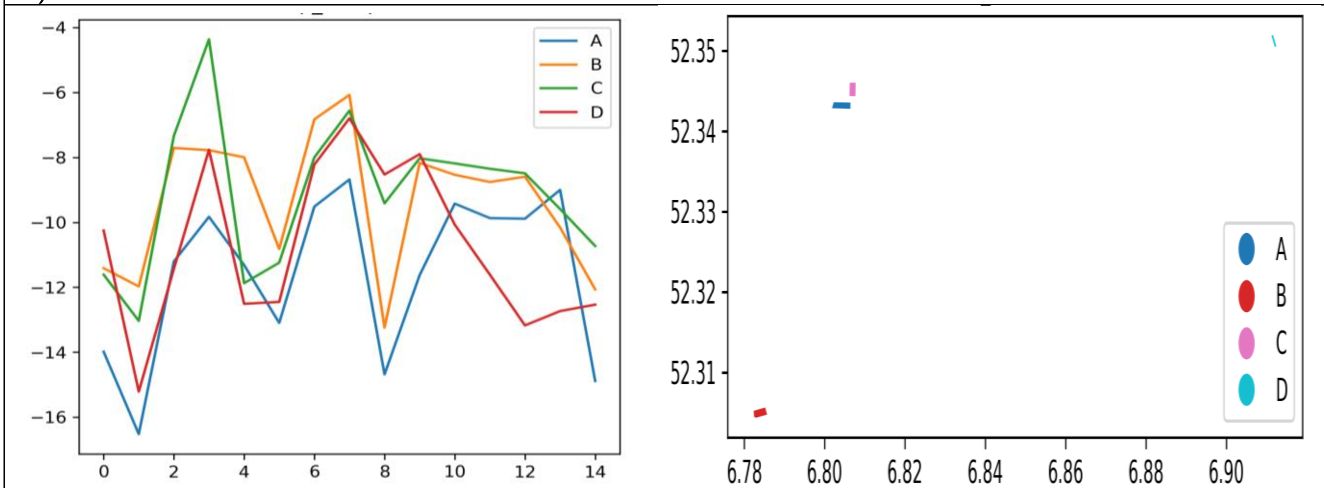

B)

Backscatter characteristics of crops within plots that have different orientation angle

A) Backscatter of Maize and its respective plots
B) Backscatter of potato and its respective plots

Appendix 3C: Classification maps from twDTW using segmentation TerraSAR-X Images

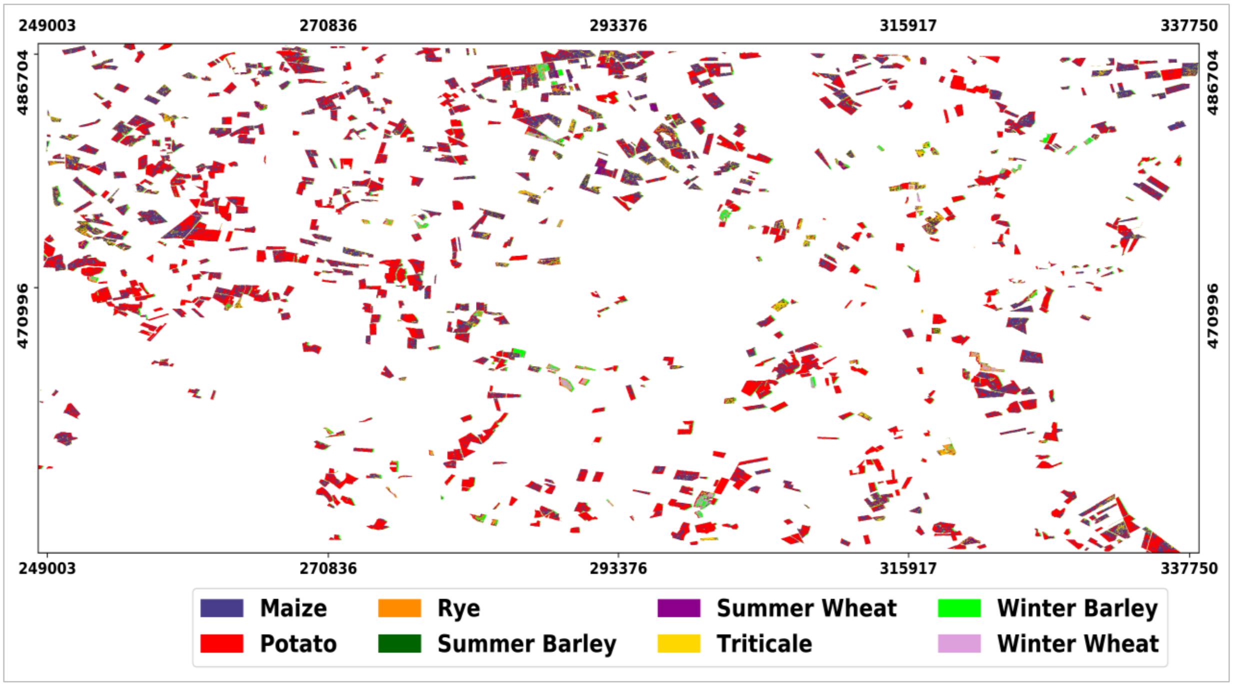

From Mean Shift Segmentation

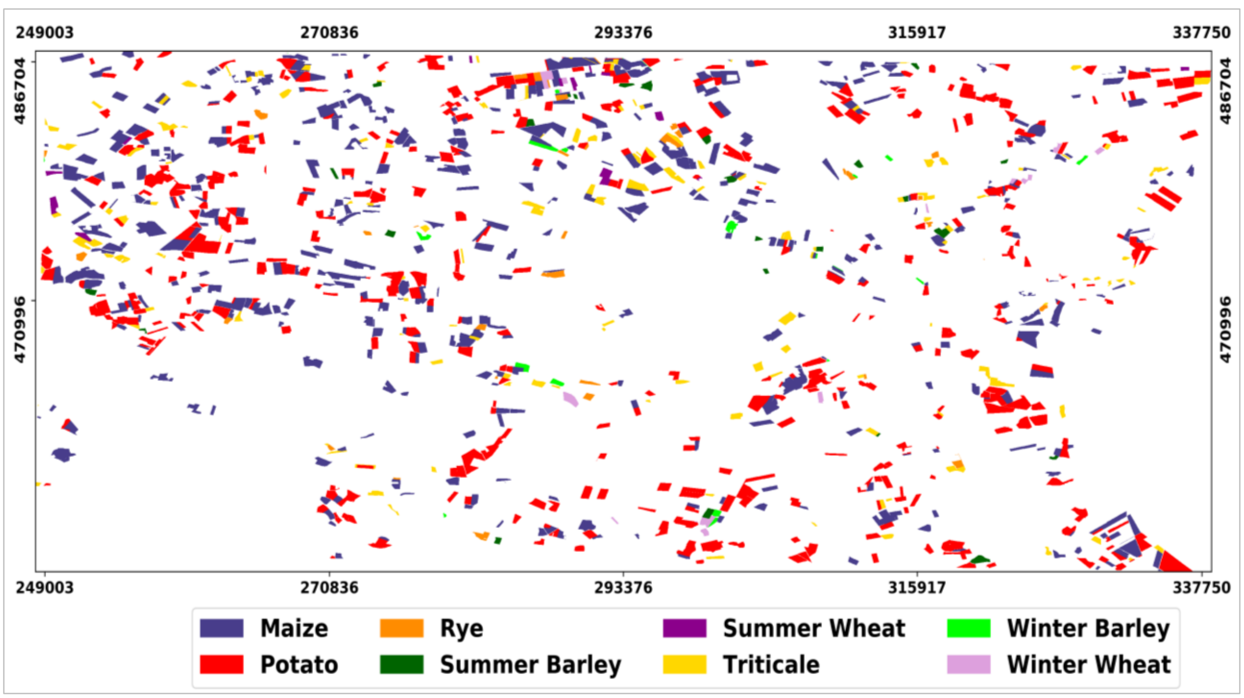

From Polygon based segmentation

Appendix 3D: Accuracy report segmentation of TerraSAR-X with twDTW

From Mean Shift Segmentation

	Reference									
Crop	Maize	Potato	Rye	Summer Barley	Summer Wheat	Triticale	Winter Barley	Winter Wheat	Sum	UA
Maize	427	16	4	8	1	10	0	0	466	91.63
Potato	555	34	2	2	2	1	0	0	596	5.70
Rye	10	1	7	5	2	4	2	2	33	21.21
Summer Barley	21	0	3	3	3	3	0	0	33	9.09
Summer Wheat	12	0	4	6	1	1	0	1	25	4.00
Triticale	41	0	6	9	3	11	0	0	70	15.71
Winter Barley	4	0	7	1	1	4	2	6	25	8.00
Winter Wheat	2	0	8	1		1	3	7	22	31.82
Sum	1072	51	41	35	13	35	7	16	1270	
PA	39.83	66.67	17.07	8.57	7.69	31.43	28.57	43.75		
Overall accuracy		38.74								

Polygon based Segmentation

Crop	Maize	Potato	Rye	Summer Barley	Summer Wheat	Triticale	Winter Barley	Winter Wheat	Sum	UA
Maize	475	12	2	5	2	10	0	0	506	93.87
Potato	462	34	2	2	0	0	0	0	500	6.80
Rye	7	1	11	5	4	5	1	1	35	31.43
Summer Barley	8	0	2	3	3	7	0	2	25	12.00
Summer Wheat	13	0	0	0	1	0	0	0	14	7.14
Triticale	101	4	13	18	2	11	2	0	151	7.28
Winter Barley	5	0	6	2	0	0	4	5	22	18.18
Winter Wheat	1	0	5	0	1	2	0	8	17	47.06
Sum	1072	51	41	35	13	35	7	16	1270	
PA	44.31	66.67	26.83	8.57	7.69	31.43	57.14	50.00		
Overall accuracy		43.07								

Appendix 3E: Accuracy report after balancing infrequent classes

Random Over Sampling (SOS)										
	Reference									
Crop	Maize	Potato	Rye	Summer Barley	Summer Wheat	Triticale	Winter Barley	Winter Wheat	Sum	UA
Maize	789	200	70	106	0	0	0	136	1301	60.65
Potato	135	796	0	105	71	32	0	0	1139	69.89
Rye	18	0	25	35	0	59	0	0	137	18.25
Summer Barley	58	33	27	210	89	151	0	0	568	36.97
Summer Wheat	14	0	27	113	165	35	0	71	425	38.82
Triticale	23	20	177	151	68	155	0	0	594	26.09
Winter Barley	23	23	192	90	246	262	615	0	1451	42.38
Winter Wheat	12	0	554	262	433	378	457	865	2961	29.21
Sum	1072	1072	1072	1072	1072	1072	1072	1072	8576	
PA	73.6	74.25	2.33	19.59	15.39	14.46	57.37	80.69		
Overall accuracy			42.21							
Geometric accuracy			26.69							

Synthetic Minority Oversampling (SMOTE)										
Crop	Maize	Potato	Rye	Summer Barley	Summer Wheat	Triticale	Winter Barley	Winter Wheat	Sum	UA
Maize	789	224	45	123	0	0	0	38	1219	64.73
Potato	135	784	23	127	26	10	0	16	1121	69.94
Rye	18	20	38	18	33	80	0	12	219	17.35
Summer Barley	58	24	19	186	67	183	0	15	552	33.7
Summer Wheat	14	4	22	127	159	12	0	31	369	43.09
Triticale	23	13	211	173	103	143	0	27	693	20.63
Winter Barley	23	3	190	59	254	285	643	32	1489	43.18
Winter Wheat	12	0	524	259	430	359	429	901	2914	30.92
Sum	1072	1072	1072	1072	1072	1072	1072	1072	8576	
PA	73.6	73.13	3.54	17.35	14.83	13.34	59.98	84.05		
Overall accuracy			42.5							
Geometric accuracy			27.53							

Adaptive Synthetic Minority Oversampling (ADASYN)										
Reference										
Crop	Maize	Potato	Rye	Summer Barley	Summer Wheat	Triticale	Winter Barley	Winter Wheat	Sum	UA
Maize	789	250	49	129	0	0	0	42	1259	62.67
Potato	135	750	23	136	23	14	0	16	1097	68.37
Rye	18	28	35	16	46	72	0	21	236	14.83
Summer Barley	58	24	32	212	67	211	0	24	628	33.76
Summer Wheat	14	5	30	121	132	23	0	20	345	38.26
Triticale	23	14	234	154	104	112	0	32	673	16.64
Winter Barley	23	14	133	68	264	286	628	19	1435	43.76
Winter Wheat	12	0	525	236	430	360	443	900	2906	30.97
Sum	1072	1085	1061	1072	1066	1078	1071	1074	8579	
PA	73.6	69.12	3.3	19.78	12.38	10.39	58.64	83.8		
Overall accuracy			41.47							
Geometric accuracy			26.02							

SMOTE and cleaning using Tomek links (SMOTETomek)										
Crop	Maize	Potato	Rye	Summer Barley	Summer Wheat	Triticale	Winter Barley	Winter Wheat	Sum	UA
Maize	789	210	38	113	0	0	0	40	1190	66.3
Potato	135	783	11	120	9	5	0	7	1070	73.18
Rye	18	7	14	11	15	56	0	6	127	11.02
Summer Barley	58	15	11	173	40	148	0	8	453	38.19
Summer Wheat	14	5	9	102	120	10	0	11	271	44.28
Triticale	23	9	174	153	62	119	0	19	559	21.29
Winter Barley	23	3	195	45	212	266	583	14	1341	43.48
Winter Wheat	12	0	548	258	414	402	403	880	2917	30.17
Sum	1072	1032	1000	975	872	1006	986	985	7928	
PA	73.6	75.87	1.4	17.74	13.76	11.82	59.12	89.34		
Overall accuracy			43.66							
Geometric accuracy			24.24							

Appendix 3F: Accuracy results from Non-Isometric DDTW using TerraSAR-X images

Non-Isometric Derivative Dynamic Time Warping (2D case)										
				Reference						
Crop	Maize	Potato	Rye	Summer Barley	Summer Wheat	Triticale	Winter Barley	Winter Wheat	Sum	UA
Maize	313	10	10	4	0	5	0	0	342	91.52
Potato	415	30	3	2	2	4	0	0	456	6.58
Rye	165	6	5	3	4	2	0	2	187	2.67
Summer Barley	14	0	3	2	1	3	0	1	24	8.33
Summer Wheat	46	2	10	8	3	6	4	6	85	3.53
Triticale	104	2	5	6	1	10	1	3	132	7.58
Winter Barley	11		2	10	2	4	2	3	34	5.88
Winter Wheat	4	1	3	0	0	1	0	1	10	10.00
Sum	1072	51	41	35	13	35	7	16	1270	
PA	29.20	58.82	12.20	5.71	23.08	28.57	28.57	6.25		
Overall accuracy		28.82								

Non-Isometric Derivative Dynamic Time Warping (3D case)										
Crop	Maize	Potato	Rye	Summer Barley	Summer Wheat	Triticale	Winter Barley	Winter Wheat	Sum	UA
Maize	299	10	10	4	0	7	0	0	330.00	90.61
Potato	430	29	3	2	2	4	0	0	470.00	6.17
Rye	77	4	3	1	2	0	0	1	88.00	3.41
Summer Barley	27	0	1	4	1	4	0	1	38.00	10.53
Summer Wheat	61	4	10	11	5	7	4	7	109.00	4.59
Triticale	172	4	9	8	2	10	1	4	210.00	4.76
Winter Barley	3	0	3	5	1	2	2	2	18.00	11.11
Winter Wheat	3	0	2	0	0	1	0	1	7.00	14.29
Sum	1072.00	51.00	41.00	35.00	13.00	35.00	7.00	16.00	1270.00	
PA	27.89	56.86	7.32	11.43	38.46	28.57	28.57	6.25		
Overall accuracy		27.80								